Synthesis of Novel Higher-Nuclearity Heterometallic Sulfide Clusters by a Building Block Method

Seiji Ogo

DOCTOR OF PHILOSOPHY

Department of Structural Molecular Science
School of Mathematical and Physical Science
The Graduate University for Advanced Studies

1995

Contents

Abstract

The purposes of this thesis are to develop a systematically synthetic method of higher-nuclearity heterometallic sulfide clusters, to investigate interactions of M-S-M' (M and M' = Rh, W, or Cu) groups in the newly prepared clusters, and to find an interesting reactivity of the M-S-M' groups in the clusters toward small molecules (e.g. H_2O and H_2S) from view points of a basic cluster chemistry.

Most clusters prepared in this research have been obtained by a unique building block method as a rationally synthetic approach in which an organorhodium group ($Cp^*RhP(OEt)_3$, $Cp^* = \eta^5$-C_5Me_5) plays an important role to prevent from polymerizing of the products and to construct the higher-nuclearity heterometallic sulfide clusters soluble in common organic solvents.

In Chapter 1 the building-block approach toward a stepwise synthesis, $[Cp^*RhP(OEt)_3Cl_2]$ (**1**) → $[Cp^*RhP(OEt)_3WS_4]$ (**2**) → $[Cp^*RhP(OEt)_3(\mu$-$WS_4)CuCl]$ (**3**) → $[\{Cp^*RhP(OEt)_3(\mu$-$WS_4)(CuCl)Cu\}_2(\mu$-$Cl)_2]$ (**4**), and as well as **1** → $[\{Cp^*RhP(OEt)_3\}_2(\mu$-$WS_4)][BPh_4]_2$ (**5**·$[BPh_4]_2$), is demonstrated. The structures of **1**, **2**, **3**, **4**, and **5**·$[BPh_4]_2$ were confirmed by X-ray diffraction analysis. The formation and structures of **3** and **4** have the following characteristics: the trinuclear sulfide cluster **3** possesses a linear sequence of Rh, W, and Cu atoms with octahedral, tetrahedral, and trigonal planar coordination geometries, respectively. Although there are three presumed geometrical isomers for **3** based on the difference in the binding site of CuCl on the WS_4 core, the reaction between **2** and CuCl gave specifically **3** in nearly quantitative yield because the specific formation of **3** is due to the strong coordination ability of the terminal S atoms in **2** (see Scheme 1). The linear-type framework of **3** is preserved in dichloromethane and acetonitrile solutions.

Scheme 1

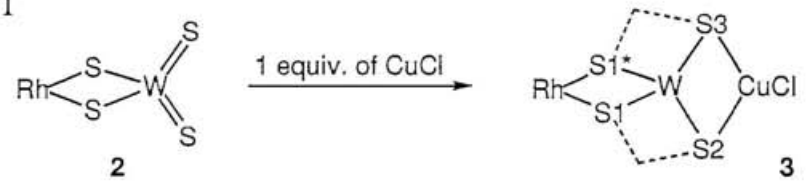

2 **3**

Cluster **4** has an octanuclear framework (Rh···W···Cu1···Cu1*···W*···Rh*) with a

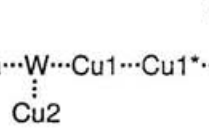

crystallographic inversion center, and the eight metal atoms are arranged in a branched configuration in which Rh···W···Cu1 is almost linear (172.43°) and Rh···W···Cu2 is an approximately right angle (90.73°). The X-ray results indicate that cluster **3** performs a regiospecific CuCl-addition at S1 (or S1*) and S2 atoms to form **4**. This regiospecific addition is attributed mainly to a steric demand of the Cp* and $P(OEt)_3$ ligands. In dichloromethane cluster **4** exists as a tetranuclear species, [{Cp*RhP$(OEt)_3$ (μ-WS_4)$(CuCl)_2$], however, in acetonitrile exists as **3** and the freed CuCl.

In Chapter 2 a unique conversion of a bridging S atom of **4** to a terminal O atom of [Cp*RhP$(OEt)_3$(μ-WOS_3)(CuCl)Cu}$_2$(μ-$Cl)_2$] (**8**) by the water saturated in dichloromethane is described. This is the first example of the conversion of the bridging S atom in the M-S-M' groups into the terminal O atom without releasing the metal atoms. The use of the water saturated in dichloromethane is essential, because the several attempts to obtain **8** from **4** by using aqueous acetonitrile, basic conditions in common solvents, and two-phase conditions of water and dichloromethane which gave **1**, **3**, [Cp*RhP$(OEt)_3$(μ-WOS_3)(CuCl)] (**7**), and other unidentified products were not successful. On the other hand, clusters **2** and **3** are little reacted with the water saturated in dichloromethane or water under two-phase conditions of water and dichloromethane in contrast to **4**. It seems that the specific reactivity of the W-S-Cu groups of **4** is dependent on differences in electron densities of the S atoms and steric effects of the Cp* and $P(OEt)_3$ groups. A tentative mechanism of the transformation reaction, **4** $\rightarrow$ **8**, can be assumed as follows: water molecule interacts with the W atom and the S atom that has the high electron density in the four S atoms of the μ-WS_4 group of **4** to give an intermediary species that has W-O-H and Cu-S-H groups, and then the species is transformed to **8**.

Cluster **8** was also obtained by a stepwise synthesis using $[WOS_3]^{2-}$ as a tungsten source: **1** $\rightarrow$ [Cp*RhP$(OEt)_3$(μ-$S)_2$WOS] (**6a**) $\rightarrow$ **7** $\rightarrow$ **8**. Cluster **6a** is one

of two possible geometrical isomers of [Cp*RhP(OEt)$_3$(μ-S)$_2$WOS]. The structures of **7** and **8** were determined by X-ray analysis. In addition the reactions of **4**, **7**, and **8** with hydrogen sulfide to give **3** as the only major product are studied in Chapter 2.

In Chapter 3 it was investigated whether fast atom bombardment mass spectrometry (FAB-MS) provides useful information about higher-nuclearity sulfide clusters, which may be synthesized by a direct synthetic method. The FAB mass spectrum of the linear trinuclear sulfide cluster **3** shows many ions heavier than the molecular ion. One envelope corresponds to a pentanuclear sulfide cluster, [{Cp*RhP(OEt)$_3$(μ-WS$_4$)}$_2$Cu]$^+$ ([**B**]$^+$). It was synthesized by the reaction between cluster **2** and Cu$^+$ in a 2:1 molar ratio to yield the compound, [{Cp*RhP(OEt)$_3$(μ-WS$_4$)}$_2$Cu][PF$_6$] (**9**·[PF$_6$]). The structure was determined by a combination of single-crystal X-ray diffraction analysis, Extended X-ray absorption fine structure (EXAFS), and IR measurements. The FAB mass spectrum of **9**·[PF$_6$] showed that the cationic

Scheme 2

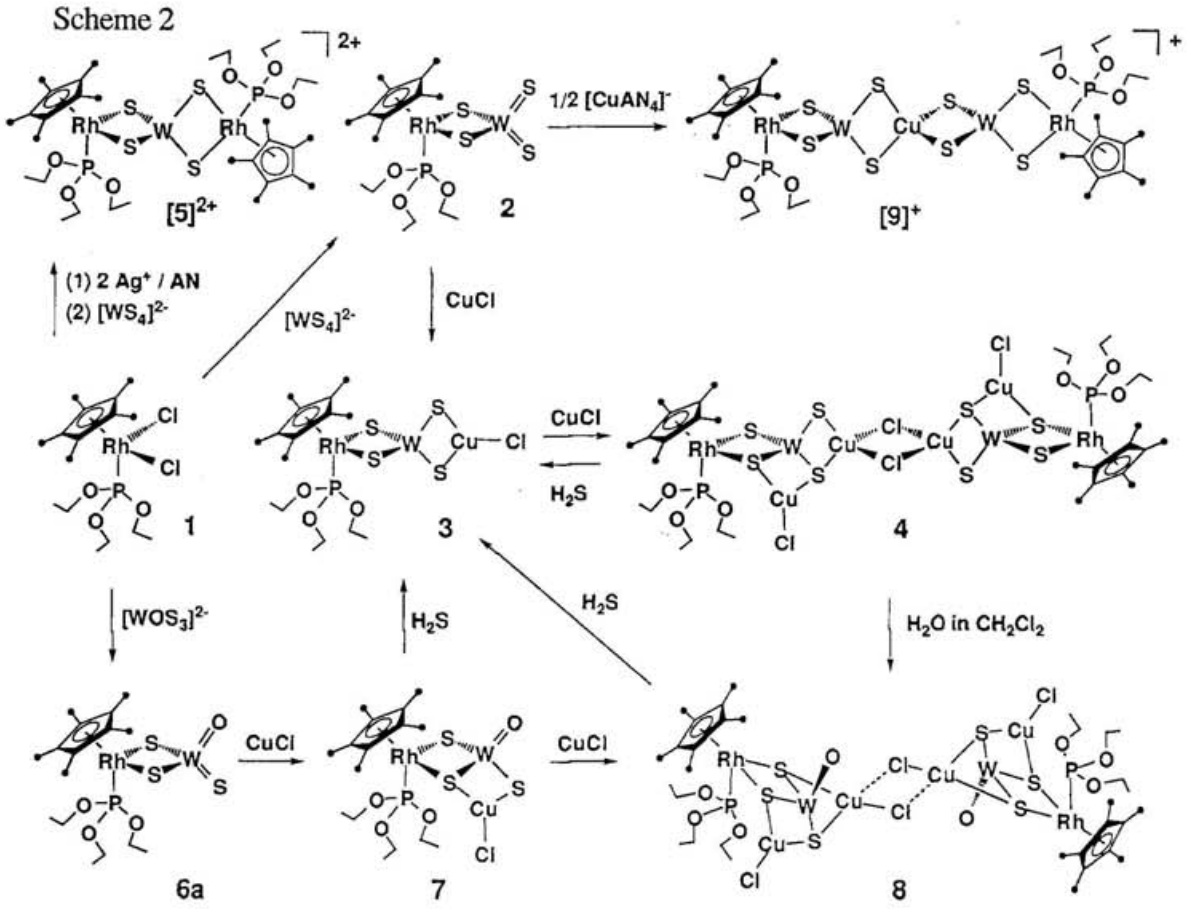

cluster $[9]^+$ is identical with $[\mathbf{B}]^+$ found in the FAB mass spectrum of **3**. Thus this result suggests that the FAB-MS technique provides useful guiding principal for synthesis of higher nuclearity clusters.

Scheme 2 is presented for easily understanding of this thesis.

Abbreviations

AN	acetonitrile
Cp*	η^5-pentamethylcyclopentadienyl
cymene	isopropylmethylbenzene
DMF	*N*,*N*-dimethylformamide
eq.	equation
equiv.	equivalent
Et	ethyl
EXAFS	extended X-ray absorption fine structure
FAB-MS	fast atom bombardment mass spectrometry
HDS	hydrodesulfurization
Me	methyl
NBA	*m*-nitrobenzylalcohol
NMR	nuclear magnetic resonance
Ph	phenyl
TMS	tetramethylsilane
D_x	calculated density
F(000)	sum of atomic numbers in the unit cell
μ	linear absorption coefficient
Z	number of asymmetric units in the unit cell

Chapter 1

Stepwise synthesis of higher-nuclearity heterometallic sulfide clusters by a building-block method using an organorhodium group ($Cp^*RhP(OEt)_3$, $Cp^* = \eta^5$-C_5Me_5)

1-1 Introduction

The chemistry of heterometallic sulfide clusters is interested in their geometrical structures of the active site of nitrogenase enzymes (Fe-S-Mo cluster),[1] in the models for hydrodesulfurization (HDS) catalysts (e.g. Rh-S-Mo complex),[2] and in the interaction of trace elements in animals as seen in the molybdenum-copper antagonism (the interaction between $[MoO_mS_{4-m}]^{2-}$ (m = 0, 1, or 2) and Cu^I),[3] because the interactions of the heterometallic centers and S atoms seem to play an important role in these processes. However molecular level studies for such interactions and the reactivity of the M-S-M' groups (M and M' = transition metal atoms) in these processes have not been developed effectively. Thus the purposes of this thesis are to develop a systematically synthetic method of higher-nuclearity heterometallic sulfide clusters, to investigate interactions of M-S-M' (M and M' = Rh, W, or Cu) groups, and to find an interesting reactivity of the M-S-M' groups from view points of a basic cluster chemistry. The reason why thiotungstate ($[WS_4]^{2-}$) is used for preparation of the heterometallic sulfide clusters is that intermediary species from $[WS_4]^{2-}$ are much more stabilized than that those from other $[MS_4]^{2-}$.[4]

It is difficult to construct frameworks of desired sulfide clusters, in other words, the employed conditions could not necessarily have afforded clusters of predictable structure.[5] In order to overcome the lack of control, this research uses a unique synthetic method in which a terminal building-block with an organorhodium group ($Cp^*RhP(OEt)_3$, $Cp^* = \eta^5$-C_5Me_5) having two reaction sites plays an important role to prevent from polymerizing of the products and to construct stepwise higher-nuclearity

heterometallic sulfide clusters soluble in common organic solvents.

An example of preparation of a trinuclear sulfide cluster having a Rh-WS_4-Rh framework based on the above concept is shown in Figure 1-1. The reaction of $[WS_4]^{2-}$ with two equivalents of $[Cp^*Rh(NCMe)_3]^{2+}$ gave many kinds of reaction products because this Rh compound does not have an appropriate number of acetonitrile ligands as reaction points for the $[WS_4]^{2-}$ group. In contrast, the reaction of $[WS_4]^{2-}$ with two equivalents of $[Cp^*RhP(OEt)_3(NCMe)_2]^{2+}$ that has a triethylphosphite group gave $[\{Cp^*RhP(OEt)_3\}_2(\mu\text{-}WS_4)]^{2+}$ ($[\mathbf{5}]^{2+}$) under similar conditions. In this reaction the number of the reaction sites of the Rh complex as a building-block is controlled by introductions of Cp* and triethylphosphite groups.

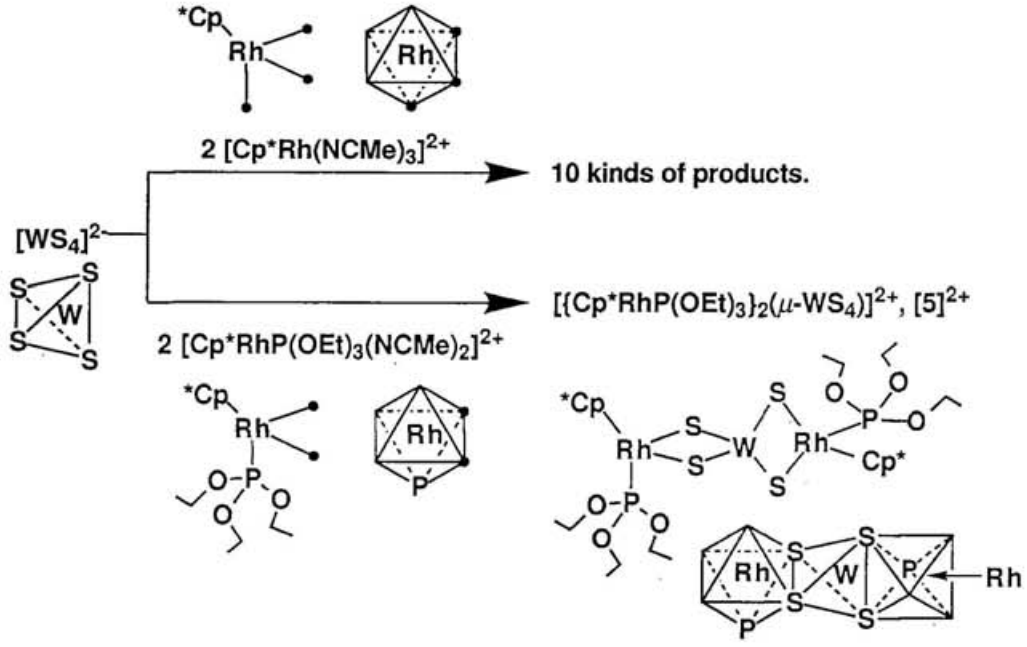

Figure 1-1. An example of preparation of a trinuclear sulfide cluster, $[\mathbf{5}]^{2+}$, having Rh-WS_4-Rh framework by controlling the number of acetonitrile ligand (= •) as the reaction sites of the Rh complex.

Why the building-blocks with the $Cp^*RhP(OEt)_3$ group is so important for above purposes are as follows. First, the Cp^*Rh group is fairly soluble in both organic solvents and water and very stable for atmospheric oxygen and water.[6] Second, the Cp^* and triethylphosphite ligands can stabilize unstable species both electronically and geometrically. The reasons why triethylphosphite is used among many tertiary phosphines (PR_3) and phosphites ($P(OR)_3$) are as follows. (1) Triethylphosphite has considerably smaller cone angle ($\theta = 109°$) than that of triethylphosphine ($\theta = 132°$) or triphenylphosphine ($\theta = 145°$) in order to facilitate cluster formation due to its less steric hindrance.[7] (2) Trialkylphsphite has fairly stronger back donation from Rh atom than trialkylphosphine to stabilize the organometallic group.[8] (3) Trialkylphosphite is much more stable to air atmosphere than trialkylphosphine. (4) Triethylphosphite has better solubility in organic solvents than trimethylphosphite. Therefore use of the building-blocks including the $Cp^*RhP(OEt)_3$ group as the terminal ones has some advantages for preparations and isolation of such higher nuclearity heterometallic sulfide clusters soluble in common organic solvents as discrete molecules and investigation of the their reactivity with water under moisture conditions.

In Chapter 1, the building block approach toward a stepwise synthesis of a novel branched-type heterometallic octanuclear sulfide cluster, $[\{Cp^*RhP(OEt)_3(\mu\text{-}WS_4)(CuCl)Cu\}_2(\mu\text{-}Cl)_2]$ (**4**), which has early- and 6th- (W^{VI}), middle- and 5th- (Rh^{III}), and late-transition metals[9] and 4th-periods (Cu^I) shown in Figure 1-2 is demonstrated. In addition, in this Chapter, $[\{Cp^*RhP(OEt)_3\}_2(\mu\text{-}WS_4)][BPh_4]_2$ (**5**·$[BPh_4]_2$) in which $[WS_4]^{2-}$ functions as a bridging bidentate ligand to two $Cp^*RhP(OEt)_3$ is prepared as an example of Rh-W-Rh dimetallic trinuclear sulfide cluster.[10]

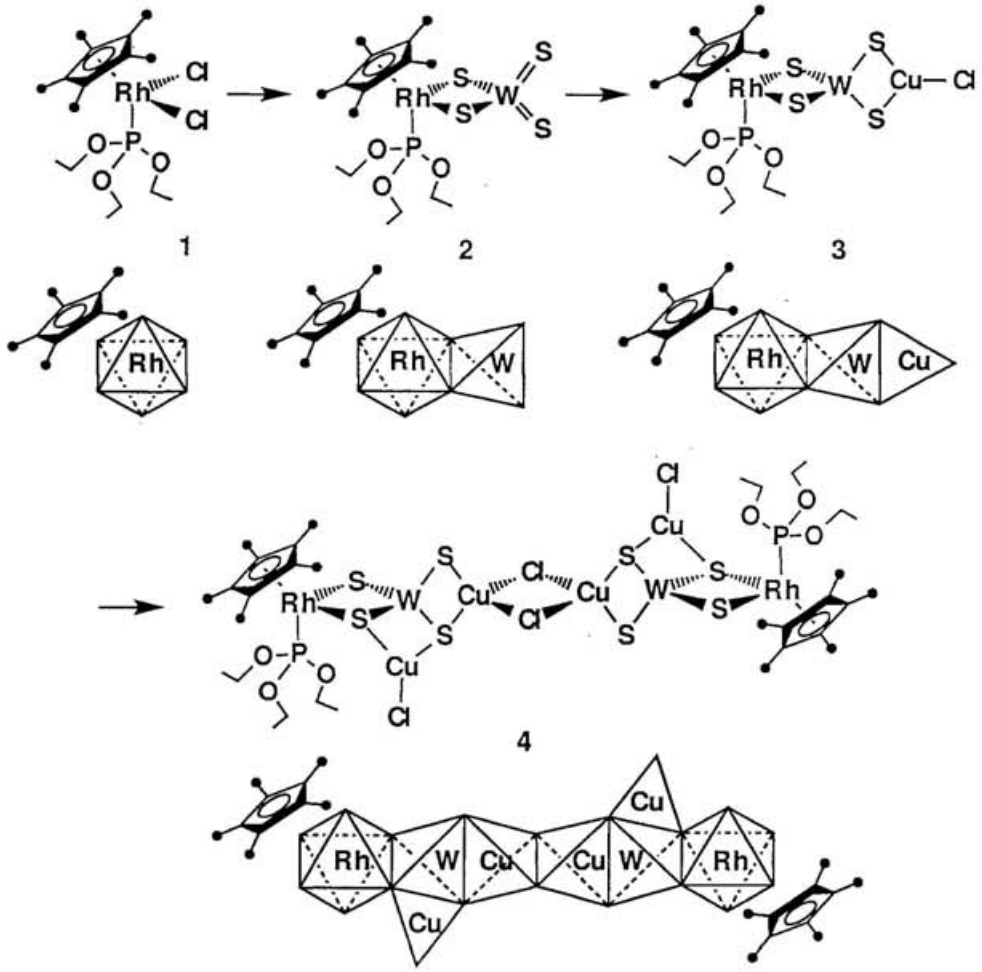

Figure 1-2. Stepwise synthesis of higher-nuclearity heterometallic sulfide clusters by a unique building-block method. The terminal blocks with the organorhodium ($Cp^*RhP(OEt)_3$, $Cp^* = \eta^5\text{-}C_5Me_5$) group prevent from polymerizing of compounds.

1-2 Experimental section

1-2-1 Methods and materials

All preparative procedures were routinely carried out under an argon atmosphere because compounds $[Cp^*RhP(OEt)_3Cl_2]$ (**1**), $[Cp^*RhP(OEt)_3WS_4]$ (**2**), $[Cp^*RhP(OEt)_3(\mu\text{-}WS_4)CuCl]$ (**3**), $[\{Cp^*RhP(OEt)_3(\mu\text{-}WS_4)(CuCl)Cu\}_2(\mu\text{-}Cl)_2]$ (**4**), and $[\{Cp^*RhP(OEt)_3\}_2(\mu\text{-}WS_4)][BPh_4]_2$ (**5**·$[BPh_4]_2$) are stable to dried air, but not to moisture. Toluene, acetone, acetonitrile, and DMF were distilled from calcium hydride. Methanol was distilled from magnesium turnings and iodine. Diethyl ether was distilled from lithium aluminum hydride. Organorhodium complex, $[(Cp^*RhCl)_2(\mu\text{-}Cl)_2]$, was prepared by the methods described in the literature.[11] The thiometalate, $[Ph_4P]_2[WS_4]$, was prepared by a method similar to that for $[PPh_4]_2[MoS_4]$.[12] Triethylphosphite and copper(I) chloride were purchased from Wako Pure Chemical Industries, Ltd. $AgPF_6$ was purchased from Aldrich Chemicals. $NaBPh_4$ was purchased from Nacalai Tesque, Inc.

1-2-2 Physical measurements

^1H NMR spectroscopy

^1H NMR spectra were recorded on JEOL 270 and 400MHz spectrometers (JNM-EX270 and 400) and reported in ppm versus TMS.

Infrared spectroscopy

IR spectra of solid compounds in mineral oil (Merck Paraffin flüssig) were measured on a Hitachi 270-30 Infrared spectrophotometer, and those in dichloromethane or acetonitrile were measured by using KBr cell for liquid on a Perkin-Elmer 1600 Series FTIR spectrometer.

Vapor Pressure Osmometry

The values of molecular weights of compounds were obtained by a Knauer Vapor Pressure Osmometer and calibrated with dichloromethane solutions of benzil.

X-ray photoelectron spectroscopy

X-ray photoelectron spectra were measured on a VG Scientific ESCALAB MK II electron spectrometer by use of Mg-K_α radiation. The binding energies are corrected by assuming C 1s binding energy of the carbon atoms of the ligand in specimens as 284.6 eV.[13]

1-2-3 Preparations

1-2-3-1 Preparation of $[Cp^*RhP(OEt)_3Cl_2]$ (1)

The mononuclear complex, $[Cp^*RhP(OEt)_3Cl_2]$ (**1**), was prepared from $[(Cp^*RhCl)_2(\mu\text{-}Cl)_2]$. To a suspension of **1** (10.6 g, 17.1 mmol) in toluene (250 cm^3) was added triethylphosphite (6.08 g, 36.6 mmol) at room temperature, and the mixture was stirred for 2 h giving a deep red solution. On evaporation of the solvent red crystals of $[Cp^*Rh\{P(OEt)_3\}Cl_2]$ (**2**) were obtained and dried in vacuo (15.9 g, 98% yield). Anal. Found: C, 40.31; H, 6.08%. Calcd for $C_{16}H_{30}Cl_2O_3PRh$: C, 40.44; H, 6.36%. ^1H NMR ($CDCl_3$, 23 °C, TMS) : δ 1.30 (t, $^3J_{H,H}$=7.0 Hz, 9H, $-CH_2CH_3$), 1.66 (d, $^4J_{P,H}$=5.2 Hz, 15H, $-CH_3(Cp^*)$), 4.25 (dq, $^3J_{P,H}$=7.0 Hz, $^3J_{H,H}$=7.0 Hz, 6H, $-CH_2-$).

1-2-3-2 Preparation of $[Cp^*RhP(OEt)_3WS_4]$ (2)

The dinuclear sulfide cluster, $[Cp^*RhP(OEt)_3WS_4]$ (**2**), was prepared by addition of a methanol solution (50 cm^3) of $[Cp^*RhP(OEt)_3Cl_2]$ (**1**, 2.00 g, 4.21 mmol) to a methanol solution (1.2×10^3 cm^3) of $[PPh_4]_2[WS_4]$ (4.17 g, 4.21 mmol) at room temperature. The mixture was stirred for 12 h to yield a red precipitate of **2**, which was collected by filtration, washed with methanol (3×50 cm^3) and diethyl ether

(3×20 cm^3), and dried in vacuo. Further crystals of **2** were obtained by evaporating the filtrate to ca. 100 cm^3 below 30 °C. Total yield : 2.72 g (91%). Anal. Found: C, 26.89; H, 4.04%. Calcd for $C_{16}H_{30}O_3PRhS_4W$: C, 26.83; H, 4.22%. ^{1}H NMR : ($CDCl_3$, 23 °C, TMS) δ 1.27 (t, $^3J_{H,H}$=7.0 Hz, 9H, -CH_2CH_3), 2.02 (d, $^4J_{P,H}$=5.2 Hz, 15H, -CH_3(Cp*)), 4.04 (dq, $^3J_{P,H}$=7.0 Hz, $^3J_{H,H}$=7.0 Hz, 6H, -CH_2-).

1-2-3-3 Preparation of [Cp*RhP(OEt)$_3$(μ-WS$_4$)CuCl] (3)

The trinuclear sulfide cluster, [Cp*RhP(OEt)$_3$(μ-WS$_4$)CuCl] (**3**), was obtained from a reaction of **2** (1.00 g, 1.40 mmol) and CuCl (0.140 g, 1.40 mmol) in acetonitrile (100 cm^3). After stirring for 12 h at room temperature, the mixture was concentrated to 30 cm^3 giving red crystals, which were collected by filtration, washed with a small amount of diethyl ether, and dried in vacuo (1.04 g, 91% yield).
Anal. Found: C, 23.36; H, 3.48%. Calcd for $C_{16}H_{30}ClCuO_3PRhS_4W$: C, 23.57; H, 3.71%. ^{1}H NMR : (CD_2Cl_2, 23 °C, TMS) δ 1.33 (t, $^3J_{H,H}$=7.0 Hz, 9H, -CH_2CH_3), 2.05 (d, $^4J_{P,H}$=5.2 Hz, 15H, -CH_3(Cp*)), 4.05 (dq, $^3J_{P,H}$=7.0 Hz, $^3J_{H,H}$=7.0 Hz, 6H, -CH_2-).

1-2-3-4 Preparation of [{Cp*RhP(OEt)$_3$(μ-WS$_4$)(CuCl)Cu}$_2$(μ-Cl)$_2$] (4)

The octanuclear sulfide cluster, [{Cp*RhP(OEt)$_3$(μ-WS$_4$)(CuCl)Cu}$_2$(μ-Cl)$_2$] (**4**), was prepared from **3**. A reaction of trinuclear cluster **3** with an equimolar amount of CuCl in acetonitrile at room temperature gave immediately a precipitate of [{Cp*RhP(OEt)$_3$(μ-WS$_4$)(CuCl)Cu}$_2$(μ-Cl)$_2$] (**4**), which was recrystallized from DMF/diethyl ether to give red crystals (97% yield). Anal. Found: C, 20.76; H, 3.10%. Calcd for $C_{32}H_{60}Cl_4Cu_4O_6P_2Rh_2S_8W_2$: C, 21.02; H, 3.31%. ^{1}H NMR (CD_2Cl_2, 23°C): δ 1.34 (t, $^3J_{H,H}$ = 7.0 Hz, 18H, -CH_2CH_3), 2.09 (d, $^4J_{P,H}$ = 5.2 Hz, 30H, -CH_3(Cp*)), 4.02 (dq, $^3J_{P,H}$ = 7.0 Hz, $^3J_{H,H}$ = 7.0 Hz, 12H, -CH_2-).

1-2-3-5 Preparation of $[\{Cp^*RhP(OEt)_3\}_2(\mu\text{-}WS_4)](BPh_4)_2$ ($\mathbf{5}\cdot[BPh_4]_2$)

To a solution of $[Cp^*RhP(OEt)_3Cl_2]$ (**1**, 0.95 g, 2.00 mmol) in acetonitrile (30 cm^3) was added $AgPF_6$ (1.01 g, 4.00 mmol). The reaction mixture was stirred at ambient temperature for 6 h, and filtered. A solution of $[PPh_4]_2[WS]_4$ (0.99 g, 1.00 mmol) in acetonitrile (80 cm^3) was added to the filtrate (acetonitrile solution of $[Cp^*RhP(OEt)_3(NCMe)_2][PF_6]_2$) and after stirring for 6 h at room temperature, the solvent was evaporated to leave a orange-red solid. Then it was stirred in dichloromethane, and filtered to remove $[PPh_4][PF_6]$. The resulting filtrate was evaporated in vacuo to give $[\{Cp^*RhP(OEt)_3\}_2(\mu\text{-}WS_4)][PF_6]_2$, $\mathbf{5}\cdot[PF_6]_2$, (Yield: 90% based on **1**). $[\{Cp^*RhP(OEt)_3\}_2(\mu\text{-}WS_4)][BPh_4]_2$, $\mathbf{5}\cdot[BPh_4]_2$, which was used for elemental analysis, NMR measurements, and X-ray analysis, was obtained by adding of appropriate amount of $NaBPh_4$ to the acetonitrile solution of $\mathbf{5}\cdot[PF_6]_2$ (Yield: 87% based on **1**). Anal. Found: C, 54.41; H, 5.87%. Calcd for $C_{80}H_{100}B_2O_6P_2Rh_2S_4W$: C, 54.62; H, 5.73%. ^1H NMR : (CD_2Cl_2, 23 °C, TMS) δ 1.34 (t, $^3J_{H,H}$=7.0 Hz, 18H, $-CH_2CH_3$), 1.96 (d, $^4J_{P,H}$=5.2 Hz, 30H, $-CH_3(Cp^*)$), 3.97 (dq, $^3J_{P,H}$=7.0 Hz, $^3J_{H,H}$=7.0 Hz, 12H, $-CH_2-$), 6.85 (t, $^3J_{H,H}$=7.3 Hz, 8H, $-H_{para}$), 7.01 (dd, $^3J_{H,H}$=7.3 Hz, $^3J_{H,H}$=7.3 Hz, 16H, $-H_{meta}$), (m, 16H, $-H_{ortho}$).

1-2-4 X-ray crystallographic studies of 1, 2, 3, 4, and $5\cdot[BPh_4]_2$

Crystallographic data, experimental conditions, and refinement details of X-ray analysis for $[Cp^*RhP(OEt)_3Cl_2]$ (**1**), $[Cp^*RhP(OEt)_3WS_4]$ (**2**), $[Cp^*RhP(OEt)_3(\mu\text{-}WS_4)CuCl]$ (**3**), $[\{Cp^*RhP(OEt)_3(\mu\text{-}WS_4)(CuCl)Cu\}_2(\mu\text{-}Cl)_2]$ (**4**), and $[\{Cp^*RhP(OEt)_3\}_2(\mu\text{-}WS_4)][BPh_4]_2$ ($\mathbf{5}\cdot[BPh_4]_2$) are collected in Tables 1-1, -2, -3, -4 and -5, respectively.

Table 1-1. Crystallographic data, experimental conditions, and refinement details of X-ray analysis for $[Cp^*RhP(OEt)_3Cl_2]$ (**1**)

Crystal data	
Compound	$[(\eta^5\text{-}C_5Me_5)Rh\{P(OC_2H_5)_3\}Cl_2]$
Chemical formula	$C_{16}H_{30}Cl_2O_3PRh$
Formula weight	475.20
Solvent for crystallization	Acetone/diethyl ether
Color of crystal	Red
Shape of crystal	Prism
Size of specimen / mm^3	0.50 x 0.36 x 0.30
Crystal mount	Glass fiber
Crystal system	Orthorhombic
Laue group	*mmm*
Systematic absence	*h0l*: l = odd
	hk0: $h+k$ = odd
Possible space group	$P2_1cn$, *Pmcn*
Space group (number)	$P2_1cn$ (No. 33)
No. and range (/ °) of reflections used in the least-squares refinement of cell dimensions	25 and $20 < 2\theta < 25$
Lattice constants	
a / Å	8.988(3)
b / Å	28.591(5)
c / Å	8.276(3)
α/ °	90
β/ °	90
γ/ °	90
Unit-cell volume, V / $Å^3$	2127(1)
Number of asymmetric units in the unit cell, Z	4
Calculated density, D_x / g cm^{-3}	1.484
Linear absorption coefficient, μ(Mo K_α) / cm^{-1}	11.4
F(000)	975.9

Table 1-1. (Continued)

Data collection	
Instrument	AFC-5
(voltage, current)	(50 kV, 30 mA)
X-ray tube	Normal-focus
Radiation (wave length, λ / Å)	Mo K_α (0.71073)
Monochromator	Graphite
Collimator diameter / mm	1.0
Temperature / °C	23
Scan method	ω
Scan width / °	$0.68 + 0.5\tan\theta$
Scan speed (in θ) / ° min^{-1}	4
2θ range / °	$2\theta < 60$
Range of h, k, l	$0 \le h \le 13$
	$0 \le k \le 40$
	$0 \le l \le 12$
No. of reflections collected	3287
No. of independent reflections	3287
R_{int}	0
No. and frequency of standard reflections	3 and 150
Variation in standard reflections ($\Sigma(\lvert F_o \rvert / \lvert F_o \rvert_{initial})/n$)	1.002 - 0.994
Data reduction	
Lorentz and polarization corrections	Yes
Corrections for decay	No
Absorption corrections method	Gaussian[14]
Transmission factor, A	0.690 - 0.744

Table 1-1. (Continued)

Structure analysis	
Method used in structure solution	Patterson
Total no. of hydrogen atoms	30
No. of H atoms located in difference Fourier maps	30
Were these positions and thermal parameters refined?	Yes, both
No. of H atoms calculated	0
No. of parameters refined	327
2θ limit used for calculation / °	60
Cutoff criteria	$\|F_o\| > 3\sigma(\|F_o\|)$
No. of independent reflections used for calculation	1952
Atoms refined anisotropically	all non-H
Atoms refined isotropically	H
Weighting scheme	$w^{-1} = \sigma 2(\|F_o\|) + (0.025\|F_o\|)^2$
R[15]	0.049
R_w[16]	0.053
S[17]	1.305
Matrix type	Full
Final scale factor	0.709(2)
Extinction parameter refined ?	No
Anomalous dispersion corrections for which atoms	None
$(\Delta/\sigma)_{max}$ for non-hydrogen atoms	0.037
$(\Delta/\sigma)_{av}$ for non-hydrogen atoms	0.0032
$(\Delta\rho)_{min}$, $(\Delta\rho)_{max}$ / eÅ^{-3}	-0.74, 0.50
Scattering factors used	Ref. [18]
Computer	Fujitsu S-4/IX
Computational program	*Xtal3.2*[19]

Table 1-2. Crystallographic data, experimental conditions, and refinement details of X-ray analysis for [Cp*RhP(OEt)$_3$WS$_4$] (**2**)

Crystal data	
Compound	[(η^5-C_5Me_5)Rh{P(OC_2H_5)$_3$}(μ-S)$_2$$WS_2$]
Chemical formula	$C_{16}H_{30}O_3PRhS_4W$
Formula weight	716.41
Solvent for crystallization	Acetonitrile/diethyl ether
Color of crystal	Red
Shape of crystal	Prism
Size of specimen / mm^3	0.34 x 0.30 x 0.30
Crystal mount	Glass fiber
Crystal system	Monoclinic
Laue group	*2/m*
Systematic absence	*h0l*: $h+l$ = odd
	0k0: k = odd
Possible space group	$P2_1/n$
Space group (number)	$P2_1/n$ (No.14)
No. and range (/ °) of reflections used in the least-squares refinement of cell dimensions	25 and $22 < 2\theta < 26$
Lattice constants	
a / Å	14.633(2)
b / Å	15.191(2)
c / Å	11.490(1)
α/ °	90
β/ °	104.97(1)
γ/ °	90
V / Å^3	2467.3(5)
Z	4
D_x / g cm^{-3}	1.929
μ(Mo Kα) / cm^{-1}	58.2
F(000)	1392

Table 1-2. (Continued)

Data collection	
Instrument	Enraf-Nonius CAD4
(voltage, current)	(50 kV, 26 mA)
X-ray tube	Sealed tube (long fine focus)
Radiation (wave length, λ / Å)	Mo K_α (0.71073)
Monochromator	Graphite
Collimator diameter / mm	0.8
Temperature / °C	23
Scan method	θ - 2θ
Scan width / °	$0.8 + 0.35\tan\theta$
Scan speed (in θ) / ° min^{-1}	variable (1.6 - 5.0)
2θ range / °	$2\theta < 60$
Range of h, k, l	$0 \le h \le 20$
	$0 \le k \le 21$
	$-16 \le l \le 16$
No. of reflections collected	7656
No. of independent reflections	7133
R_{int}	0.044
No. and frequency of standard reflections	3 and every 2 h
Variation in standard reflections ($\Sigma(\lvert F_o \rvert / \lvert F_o \rvert_{initial})/n$)	< 0.01
Data reduction	
Lorentz and polarization corrections	Yes
Corrections for decay	No
Absorption corrections method	Empirical (ψ-scan)[20]
Transmission factor, A	1.000 - 0.914

Table 1-2. (Continued)

Structure analysis	
Method used in structure solution	Patterson
Total no. of hydrogen atoms	30
No. of H atoms located in difference Fourier maps	30
Were these positions and thermal parameters refined?	Refine xyz
No. of H atoms calculated	0
No. of parameters refined	325
2θ limit used for calculation / °	60
Cutoff criteria	$\|Fo\| > 3\sigma(\|Fo\|)$
No. of independent reflections used for calculation	4407
Atoms refined anisotropically	All non-H
Atoms refined isotropically	H (fixed at B=8.0)
Weighting scheme	$w^{-1} = \sigma^2(\|Fo\|) + (0.030\ \|Fo\|)^2$
R[21]	0.040
R_w[22]	0.053
S[23]	1.160
Matrix type	Block-diagonal
Extinction parameter refined ?	No
Anomalous dispersion corrections for which atoms	All non-H (f')
$(\Delta/\sigma)_{max}$ for non-hydrogen atoms	0.1
$(\Delta\rho)_{min}$, $(\Delta\rho)_{max}$ / eÅ^{-3}	-1.3, 0.9
Scattering factors used	Ref. [24]
Computer	HITACHI M680H
Computational program	*UNICS III* [25]

Table 1-3. Crystallographic data, experimental conditions, and refinement details of X-ray analysis for [Cp*RhP(OEt)$_3$(μ-WS$_4$)CuCl] (**3**)

Crystal data	
Compound	[(η^5-C_5Me_5)Rh{P(OC_2H_5)$_3$}(μ-S)$_2$W(μ-S)$_2$CuCl]
Chemical formula	$C_{16}H_{30}ClCuO_3PRhS_4W$
Formula weight	815.40
Solvent for crystallization	Dimethylformamide/diethyl ether
Color of crystal	Red
Shape of crystal	Prism
Size of specimen / mm^3	0.34 x 0.28 x 0.20
Crystal mount	Glass fiber
Crystal system	Monoclinic
Laue group	*2/m*
Systematic absence	*0k0: k* = odd
Possible space group	$P2_1$, $P2_1/m$
Space group (number)	$P2_1/m$ (No.11)
No. and range (/ °) of reflections used in the least-squares refinement of cell dimensions	25 and $25 < 2\theta < 30$
Lattice constants	
a / Å	10.221(2)
b / Å	11.943(2)
c / Å	10.809(1)
α / °	90
β / °	94.40(1)
γ / °	90
V / Å^3	1315.6(3)
Z	2
D_x / g cm^{-3}	2.058
μ(Mo Kα) / cm^{-1}	62.8
F(000)	787.8

Table 1-3. (Continued)

Data collection	
Instrument	AFC-5R
(voltage, current)	(50 kV, 120 mA)
X-ray tube	Normal-focus
Radiation (wave length, λ / Å)	Mo K_α (0.71073)
Monochromator	Graphite
Collimator diameter / mm	1.0
Temperature / °C	23
Scan method	$\theta - 2\theta$
Scan width / °	$1.6 + 0.5\tan\theta$
Scan speed (in θ) / ° min^{-1}	6
2θ range / °	$2\theta < 60$
Range of h, k, l	$0 \le h \le 14$
	$0 \le k \le 17$
	$-15 \le l \le 15$
No. of reflections collected	4221
No. of independent reflections	4022
R_{int}	0.030
No. and frequency of standard reflections	3 and 150
Variation in standard reflections ($\Sigma(\lvert F_o \rvert / \lvert F_o \rvert_{initial})/n$)	1.000 - 0.957
Data reduction	
Lorentz and polarization corrections	Yes
Corrections for decay	No
Absorption corrections method	Gaussian[26]
Transmission factor, A	0.169 - 0.333

Table 1-3. (Continued)

Structure analysis	
Method used in structure solution	Patterson
Total no. of hydrogen atoms	16
No. of H atoms located in difference Fourier maps	16
Were these positions and thermal parameters refined?	Yes, both
No. of H atoms calculated	0
No. of parameters refined	207
2θ limit used for calculation / °	60
Cutoff criteria	$\|F_o\| > 3\sigma(\|F_o\|)$
No. of independent reflections used for calculation	3168
Atoms refined anisotropically	All non-H
Atoms refined isotropically	H
Weighting scheme	$w^{-1} = \sigma^2(\|F_o\|) + (0.015\|F_o\|)^2$
R[27]	0.045
R_w[28]	0.052
S[29]	1.925
Matrix type	Full
Final scale factor	2.061(4)
Extinction parameter refined ?	No
Anomalous dispersion corrections for which atoms	None
$(\Delta/\sigma)_{max}$ for non-hydrogen atoms	0.022
$(\Delta/\sigma)_{av}$ for non-hydrogen atoms	0.0021
$(\Delta\rho)_{min}$, $(\Delta\rho)_{max}$ / eÅ^{-3}	-2.3, 1.1
Scattering factors used	Ref. [30]
Computer	Fujitsu S-4/IX
Computational program	*Xtal3.2*[31]

Table 1-4. Crystallographic data, experimental conditions, and refinement details of X-ray analysis for [{Cp*RhP(OEt)$_3$(μ-WS$_4$)(CuCl)Cu}$_2$(μ- Cl)$_2$] (**4**)

Crystal data	
Compound	[{η^5-C$_5$Me$_5$)RhP(OEt)$_3$(μ-WS$_4$)(CuCl)Cu}$_2$(μ-Cl)$_2$]
Chemical formula	$C_{32}H_{60}Cl_4Cu_4O_6P_2Rh_2S_8W_2$
Formula weight	1828.81
Solvent for crystallization	Dimethylformamide / diethyl ether
Color of crystal	Red
Shape of crystal	Prism
Size of specimen / mm^3	0.24 × 0.20 × 0.18
Crystal mount	Glass fiber
Crystal system	Monoclinic
Laue group	*2/m*
Systematic absence	*h0l; h+l* = odd, *0k0; k* = odd
Possible space group	$P2_1/n$
Space group (number)	$P2_1/n$ (No. 14)
No. and range (/ °) of reflections used in the least-squares refinement of cell dimensions	25 $25 < 2\theta < 30$
Lattice constants	
a / Å	10.170(3)
b / Å	14.495(3)
c / Å	19.411(3)
α/ °	90
β/ °	104.42(1)
γ/ °	90
V / Å^3	2771.5(8)
Z	2
D_x / g cm^{-3}	2.192
μ(Mo K$_\alpha$) / cm^{-1}	67.5
F(000)	1760

Table 1-4. (Continued)

Data collection	
Instrument	AFC5R
(voltage, current)	(50 kV, 180 mA)
X-ray tube	Normal-focus
Radiation (wave length, λ / Å)	Mo K_α (0.71073)
Monochromator	Graphite
Collimator diameter / mm	1.0
Temperature / °C	23
Scan method	θ-2θ
Scan width / °	1.3 + 0.5tanθ
Scan speed (in θ) / ° min^{-1}	4
2θ range / °	$2\theta \leq 60$
Range of h, k, l	$0 \leq h \leq 14$, $0 \leq k \leq 20$, $-27 \leq l \leq 27$
No. of reflections collected	8796
No. of independent reflections	8085
R_{int}	0.037
No. and frequency of standard reflections	3 and 150
Variation in standard reflections ($\Sigma(\lvert F_o \rvert / \lvert F_o \rvert_{initial})/n$)	0.987 - 1.003
Data reduction	
Lorentz and polarization corrections	Yes
Corrections for decay	No
Absorption corrections method	Empirical (ψ-scan)[32]
Transmission factor, A	0.932 - 1.000

Table 1-4. (Continued)

Structure analysis	
Method used in structure solution	Usual heavy-atom method
Total no. of hydrogen atoms	30
No. of H atoms located in difference Fourier maps	30
Were these positions and thermal parameters refined?	Yes, both
No. of parameters refined	391
2θ limit used for calculation / °	60
Cutoff criteria	$\|F_o\| > 3\sigma(\|F_o\|)$
No. of independent reflections used for calculation	5504
Atoms refined anisotropically	All non-H
Atoms refined isotropically	H
Weighting scheme	$w^{-1} = \sigma^2(\|F_o\|) + (0.015\|F_o\|)^2$
R[33]	0.043
R_w[34]	0.043
S[35]	1.418
Matrix type	Full
Final scale factor	0.4422(5)
Extinction parameter refined ?	No
$(\Delta/\sigma)_{max}$ for non-hydrogen atoms	0.0068
$(\Delta/\sigma)_{av}$ for non-hydrogen atoms	0.00060
$(\Delta\rho)_{min}$, $(\Delta\rho)_{max}$ / eÅ^{-3}	-0.98, 1.61
Scattering factors used	Ref. [36]
Computer	Fujitsu S-4/IX
Computational program	*Xtal3.2*[37]

Table 1-5. Crystallographic data, experimental conditions, and refinement details of X-ray analysis for [{Cp*RhP(OEt)$_3$}$_2$(μ-WS$_4$)][BPh$_4$]$_2$ (**5**·[BPh$_4$]$_2$)

Crystal data	
Compound	[{(η^5-C$_5$Me$_5$)Rh(P(OC$_2$H$_5$)$_3$)}$_2$(μ-WS$_4$)][BPh$_4$]$_2$
Chemical formula	$C_{80}H_{100}B_2O_6P_2Rh_2S_4W$
Formula weight	1759.16
Solvent for crystallization	acetonitrile
Color of crystal	Red
Shape of crystal	Prism
Size of specimen / mm^3	0.36 × 0.28 × 0.26
Crystal mount	Glass fiber
Crystal system	Orthorhombic
Laue group	*mmm*
Systematic absence	*0kl; h+l* = odd, *h0l; h* = odd, *hk0; k* = odd
Possible space group	*Pnab*
Space group (number)	*Pnab* (No. 60)
No. and range (/ °) of reflections used in the least-squares refinement of cell dimensions	25 $20 < 2\theta < 25$
Lattice constants	
a / Å	16.451(2)
b / Å	16.477(4)
c / Å	29.390(5)
α / °	90
β / °	90
γ / °	90
V / Å^3	7967(3)
Z	4
D_x / g cm^{-3}	1.467
μ(Mo Kα) / cm^{-1}	20.4
F(000)	3584

Table 1-5. (Continued)

Data collection	
Instrument	AFC5R
(voltage, current)	(50 kV, 150 mA)
X-ray tube	Normal-focus
Radiation (wave length, λ / Å)	Mo K_α (0.71073)
Monochromator	Graphite
Collimator diameter / mm	1.0
Temperature / °C	23
Scan method	ω
Scan width / °	$1.0 + 0.5\tan\theta$
Scan speed (in θ) / ° min^{-1}	6
2θ range / °	$2\theta \leq 50$
Range of h, k, l	$0 \leq h \leq 23$, $0 \leq k \leq 23$, $0 \leq l \leq 41$
No. of reflections collected	8925
No. of independent reflections	7023
R_{int}	0
No. and frequency of standard reflections	3 and 150
Variation in standard reflections ($\Sigma(\lvert F_o \rvert / \lvert F_o \rvert_{initial})/n$)	0.995 - 1.005
Data reduction	
Lorentz and polarization corrections	Yes
Corrections for decay	No
Absorption corrections method	Gaussian[38]
Transmission factor, A	0.5649 - 0.6226

Table 1-5. (Continued)

Structure analysis	
Method used in structure solution	Patterson
Total no. of hydrogen atoms	30
No. of H atoms located in difference Fourier maps	30
Were these positions and thermal parameters refined?	Yes, both
No. of parameters refined	638
2θ limit used for calculation / °	50
Cutoff criteria	$\|F_o\| > 3\sigma(\|F_o\|)$
No. of independent reflections used for calculation	4101
Atoms refined anisotropically	All non-H
Atoms refined isotropically	H
Weighting scheme	$w^{-1} = \sigma^2(\|F_o\|) + (0.015\|F_o\|)^2$
R[39]	0.055
R_w[40]	0.057
S[41]	1.882
Matrix type	Full
Final scale factor	0.4481(9)
Extinction parameter refined ?	No
$(\Delta/\sigma)_{max}$ for non-hydrogen atoms	0.03284
$(\Delta/\sigma)_{av}$ for non-hydrogen atoms	0.001780
$(\Delta\rho)_{min}$, $(\Delta\rho)_{max}$ / eÅ^{-3}	-2.18, 1.02
Scattering factors used	Ref. [42]
Computer	Fujitsu S-4/IX
Computational program	*Xtal3.2*[43]

1-3 Results and discussion

1-3-1 Structures of 1, 2, 3, 4, and 5·[PF_6] in the solid state

1-3-1-1 X-ray crystallography

The molecular structures of [Cp*RhP(OEt)$_3$Cl$_2$] (**1**), [Cp*RhP(OEt)$_3$WS$_4$] (**2**), [Cp*RhP(OEt)$_3$(μ-WS$_4$)CuCl] (**3**), [{Cp*RhP(OEt)$_3$(μ-WS$_4$)(CuCl)Cu}$_2$(μ- Cl)$_2$] (**4**), and [{Cp*RhP(OEt)$_3$}$_2$(μ-WS$_4$)](BPh$_4$)$_2$ (**5**·[PF_6]) determined by single-crystal X-ray analyses are shown in Figures 1-3, -4, -5, -6, and -7, respectively. The fractional coordinates and equivalent isotropic thermal parameters of non-hydrogen atoms of **1**, **2**, **3**, **4**, and **5**·[BPh$_4$]$_2$ are collected in Tables 1-6, -8, -10, -12, and -14, respectively, and bond lengths and angles of **1**, **2**, **3**, **4**, and **5**·[BPh$_4$]$_2$ in Tables 1-7, -9, -11, -13, and -15, respectively.

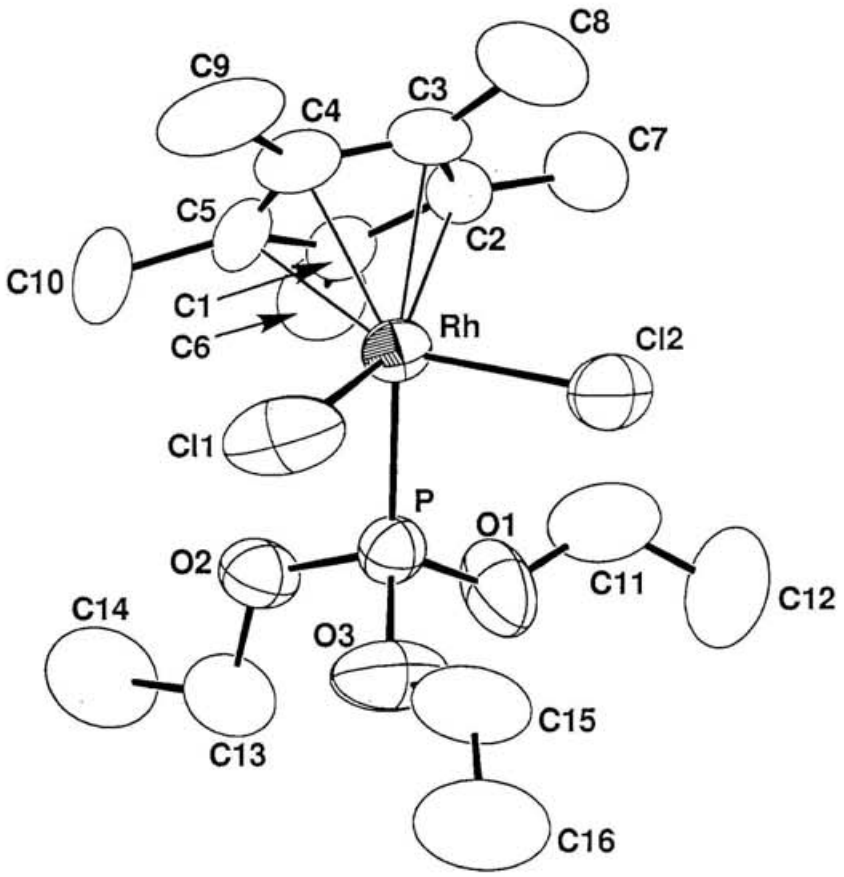

Figure 1-3. ORTEP drawing of [Cp*RhP(OEt)$_3$Cl$_2$] (**1**)

Table 1-6. Fractional coordinates and equivalent isotropic thermal parameters (U_{eq}[44]/ Å^2) of non-hydrogen atoms for [Cp*RhP(OEt)$_3$Cl$_2$] (**1**)

	x / *a*	**y / *b***	**z / *c***	***U*eq**
Rh	0.50000[45]	0.40743(2)	0.71485(8)	0.0473(2)
Cl1	0.5099(7)	0.3858(1)	0.9925(3)	0.101(1)
Cl2	0.7557(4)	0.4330(1)	0.7132(6)	0.083(1)
P	0.5713(4)	0.3336(1)	0.6519(4)	0.0504(8)
O1	0.654(1)	0.3244(3)	0.490(1)	0.095(4)
O2	0.433(1)	0.3002(3)	0.642(1)	0.066(3)
O3	0.670(1)	0.3038(3)	0.774(1)	0.100(4)
C1	0.329(1)	0.4129(3)	0.532(1)	0.051(3)
C2	0.427(1)	0.4519(3)	0.519(1)	0.047(3)
C3	0.416(1)	0.4791(3)	0.664(1)	0.057(4)
C4	0.317(2)	0.4568(4)	0.767(1)	0.061(4)
C5	0.265(1)	0.4145(5)	0.689(2)	0.063(4)
C6	0.287(2)	0.3801(7)	0.401(3)	0.077(7)
C7	0.509(3)	0.4672(5)	0.371(2)	0.079(5)
C8	0.503(4)	0.5245(5)	0.688(3)	0.095(8)
C9	0.265(3)	0.474(1)	0.931(2)	0.12(1)
C10	0.152(2)	0.382(1)	0.755(3)	0.101(9)
C11	0.700(2)	0.3543(8)	0.374(2)	0.097(8)
C12	0.852(4)	0.351(1)	0.326(5)	0.15(1)
C13	0.447(2)	0.2512(6)	0.607(4)	0.088(8)
C14	0.290(3)	0.2313(7)	0.588(4)	0.12(1)
C15	0.800(2)	0.3171(7)	0.849(4)	0.12(1)
C16	0.890(3)	0.286(1)	0.912(6)	0.16(2)

Table 1-7. Bond lengths (l / Å), angles (ϕ / °) of $[Cp^*RhP(OEt)_3Cl_2]$ (**1**)

Bond lengths	**(l / Å)**		
Rh-Cl1	2.381(3)	C1-C2	1.43(1)
Rh-Cl2	2.411(4)	C1-C5	1.42(2)
Rh-P	2.268(3)	C1-C6	1.49(2)
Rh-C1	2.16(1)	C2-C3	1.43(1)
Rh-C2	2.17(1)	C2-C7	1.49(2)
Rh-C3	2.22(1)	C3-C4	1.39(2)
Rh-C4	2.21(1)	C3-C8	1.53(3)
Rh-C5	2.14(1)	C4-C5	1.45(2)
P-O1	1.55(1)	C4-C9	1.51(3)
P-O2	1.570(9)	C5-C10	1.49(3)
P-O3	1.59(1)	C11-C12	1.42(4)
O1-C11	1.35(2)	C13-C14	1.53(3)
O2-C13	1.44(2)	C15-C16	1.32(4)
O3-C15	1.38(3)		
Bond Angles	**(ϕ / °)**		
Cl1-Rh-Cl2	92.8(2)	P-Rh-C2	117.4(3)
Cl1-Rh-P	88.2(1)	P-Rh-C3	155.5(3)
Cl2-Rh-P	90.7(1)	P-Rh-C4	148.3(3)
Cl1-Rh-C1	136.0(3)	P-Rh-C5	110.1(4)
Cl1-Rh-C2	152.6(3)	C1-Rh-C2	38.5(4)
Cl1-Rh-C3	115.9(3)	C1-Rh-C3	63.9(4)
Cl1-Rh-C4	90.3(3)	C1-Rh-C4	64.0(4)
Cl1-Rh-C5	99.1(4)	C1-Rh-C5	38.6(5)
Cl2-Rh-C1	130.7(3)	C2-Rh-C3	38.1(4)
Cl2-Rh-C2	96.2(3)	C2-Rh-C4	62.9(4)
Cl2-Rh-C3	92.4(3)	C2-Rh-C5	64.4(5)
Cl2-Rh-C4	121.1(3)	C3-Rh-C4	36.5(4)
Cl2-Rh-C5	156.2(4)	C3-Rh-C5	63.8(4)
P-Rh-C1	96.2(3)	C4-Rh-C5	39.0(5)

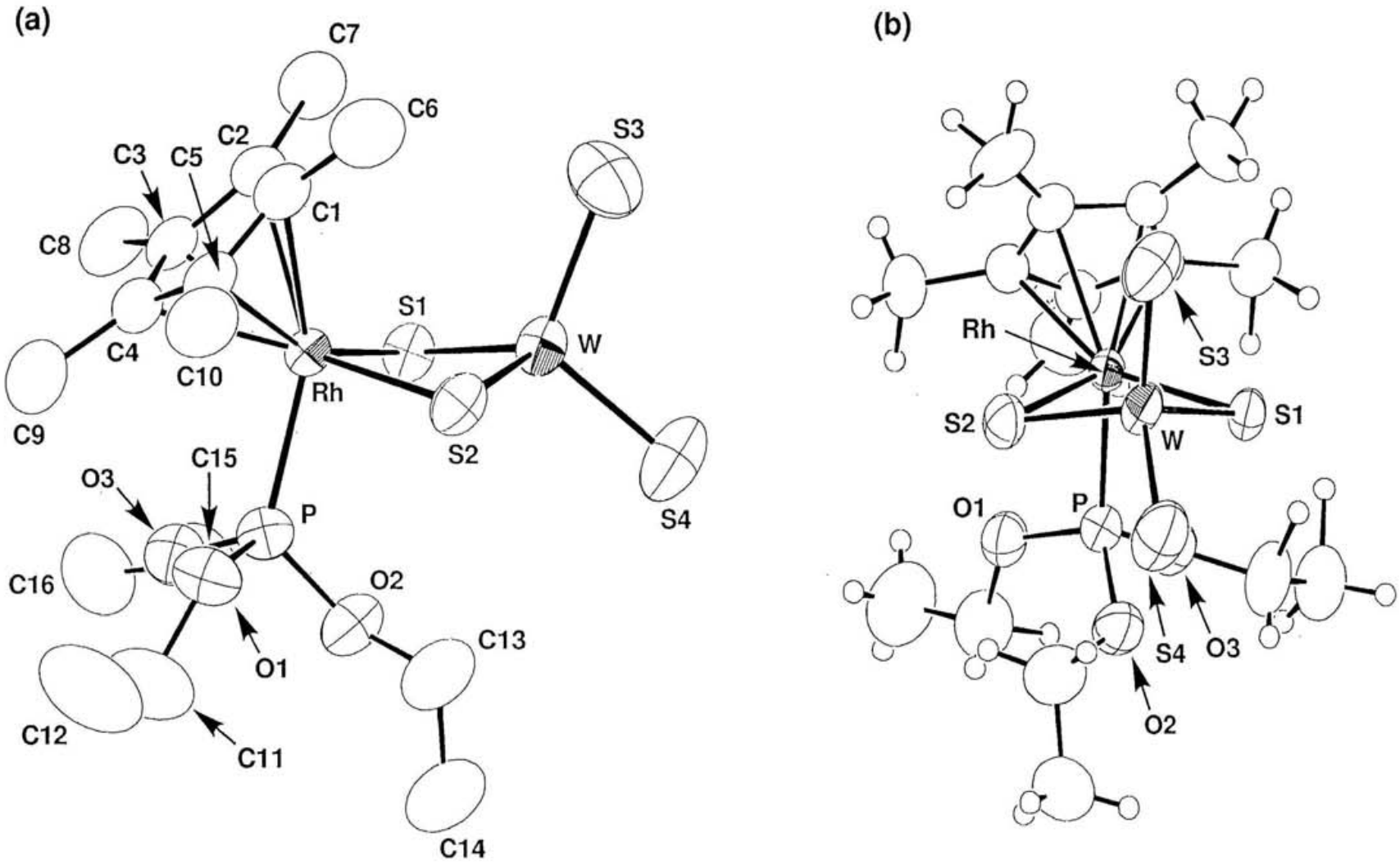

Figure 1-4. ORTEP drawings of $[Cp^*RhP(OEt)_3WS_4]$ (**2**)

Table 1-8. Fractional coordinates and equivalent isotropic thermal parameters (B_{eq}[46]/ Å^2) of non-hydrogen atoms for [Cp*RhP(OEt)$_3$WS$_4$] (**2**)

	x / *a*	y / *b*	z / *c*	B_{eq}
W	0.33892(2)	0.20067(2)	0.92943(3)	3.46(1)
Rh	0.35000(4)	0.33274(3)	0.75080(5)	2.54(1)
S 1	0.4497(1)	0.3063(1)	0.9497(2)	3.33(4)
S 2	0.2747(1)	0.1914(1)	0.7298(2)	3.95(5)
S 3	0.2342(2)	0.2357(2)	0.10232(2)	6.23(9)
S 4	0.4032(2)	0.772(2)	0.9958(3)	6.70(9)
P 1	0.4632(1)	0.2801(1)	0.6688(2)	3.28(5)
O 1	0.4192(4)	0.2725(4)	0.5280(5)	4.4(2)
O 2	0.5200(4)	0.1925(3)	0.7126(6)	4.5(2)
O 3	0.5499(4)	0.3450(4)	0.6786(5)	4.1(2)
C 1	0.2089(5)	0.4024(5)	0.7254(7)	3.8(2)
C 2	0.2783(5)	0.4502(5)	0.8092(6)	3.3(2)
C 3	0.3510(5)	0.4770(4)	0.7541(6)	3.2(2)
C 4	0.3234(5)	0.4490(4)	0.6321(6)	3.3(2)
C 5	0.2387(5)	0.3980(5)	0.6148(7)	3.5(2)
C 6	0.1200(6)	0.3627(7)	0.7458(10)	6.0(3)
C 7	0.2767(8)	0.4722(6)	0.9362(7)	5.8(3)
C 8	0.4332(6)	0.5364(6)	0.8080(9)	5.3(3)
C 9	0.3706(8)	0.4768(6)	0.5367(9)	6.1(3)
C10	0.1826(7)	0.3583(6)	0.4988(8)	5.5(3)
C11	0.4781(8)	0.2577(9)	0.4425(8)	7.0(4)
C12	0.4226(9)	0.2696(11)	0.3263(10)	9.9(6)
C13	0.4854(7)	0.1021(6)	0.6908(11)	6.3(4)
C14	0.5660(8)	0.481(7)	0.6698(10)	7.1(4)
C15	0.6295(7)	0.3503(8)	0.7843(9)	6.1(3)
C16	0.6943(7)	0.4210(8)	0.7704(9)	6.2(3)

Table 1-9. Bond lengths (l / Å), angles (ϕ / °), and selected contact distances (d / Å) of $[Cp^*RhP(OEt)_3WS_4]$ (**2**)

Bond lengths	(l / Å)		
W-S1	2.250 (2)	O1-C11	1.48 (1)
W-S2	2.248 (2)	O2-C13	1.46 (1)
W-S3	2.155 (3)	O3-C15	1.45 (1)
W-S4	2.148 (3)	C1-C2	1.41 (1)
Rh-S1	2.407 (2)	C2-C3	1.43 (1)
Rh-S2	2.397 (2)	C3-C4	1.42 (1)
Rh-P	2.253 (2)	C4-C5	1.43 (1)
Rh-C1	2.270(8)	C5-C1	1.45 (1)
Rh-C2	2.259(7)	C1-C6	1.51 (1)
Rh-C3	2.192(7)	C2-C7	1.50 (1)
Rh-C4	2.204(8)	C3-C8	1.51 (1)
Rh-C5	2.182(8)	C4-C9	1.50 (1)
P-O1	1.583 (6)	C5-C10	1.50 (1)
P-O2	1.581 (6)	C11-C12	1.39 (1)
P-O3	1.588 (6)	C13-C14	1.51 (2)
		C15-C16	1.47 (2)
Bond Angles	(ϕ / °)		
W-S1-Rh	77.09 (5)	O2-P-O3	99.0 (3)
W-S2-Rh	77.33 (6)	O1-C11-C12	108.9 (9)
S1-Rh-S2	95.52 (7)	O2-C13-C14	106.7 (8)
S1-Rh-P	90.40 (7)	O3-C15-C16	110.5 (8)
S2-Rh-P	90.47 (8)	C5-C1-C2	107.3 (7)
S1-W-S2	104.53 (7)	C1-C2-C3	109.3 (7)
S1-W-S3	111.01 (10)	C2-C3-C4	107.4 (6)
S1-W-S4	110.37 (9)	C3-C4-C5	108.3 (7)
S2-W-S3	111.22 (9)	C4-C5-C1	107.4 (6)
S2-W-S4	109.69 (10)	C5-C1-C6	126.1 (7)
S3-W-S4	109.91 (13)	C2-C1-C6	126.5 (8)
Rh-P-O1	107.7(3)	C1-C2-C7	126.0 (8)
Rh-P-O2	123.3 (3)	C3-C2-C7	124.7 (7)
Rh-P-O3	114.2 (2)	C2-C3-C8	126.4 (7)
P-O1-C11	122.5 (5)	C4-C3-C8	125.6 (8)
P-O2-C13	127.3 (5)	C3-C4-C9	124.8 (7)

Table 1-9. (Continued)

P-O3-C15	123.1 (6)	C5-C4-C9	126.7 (7)
O1-P-O2	107.8 (3)	C4-C5-C10	126.6 (8)
O1-P-O3	102.9 (3)	C1-C5-C10	125.4 (7)

Contact distance (d / Å)

Rh-W	2.9044(7)

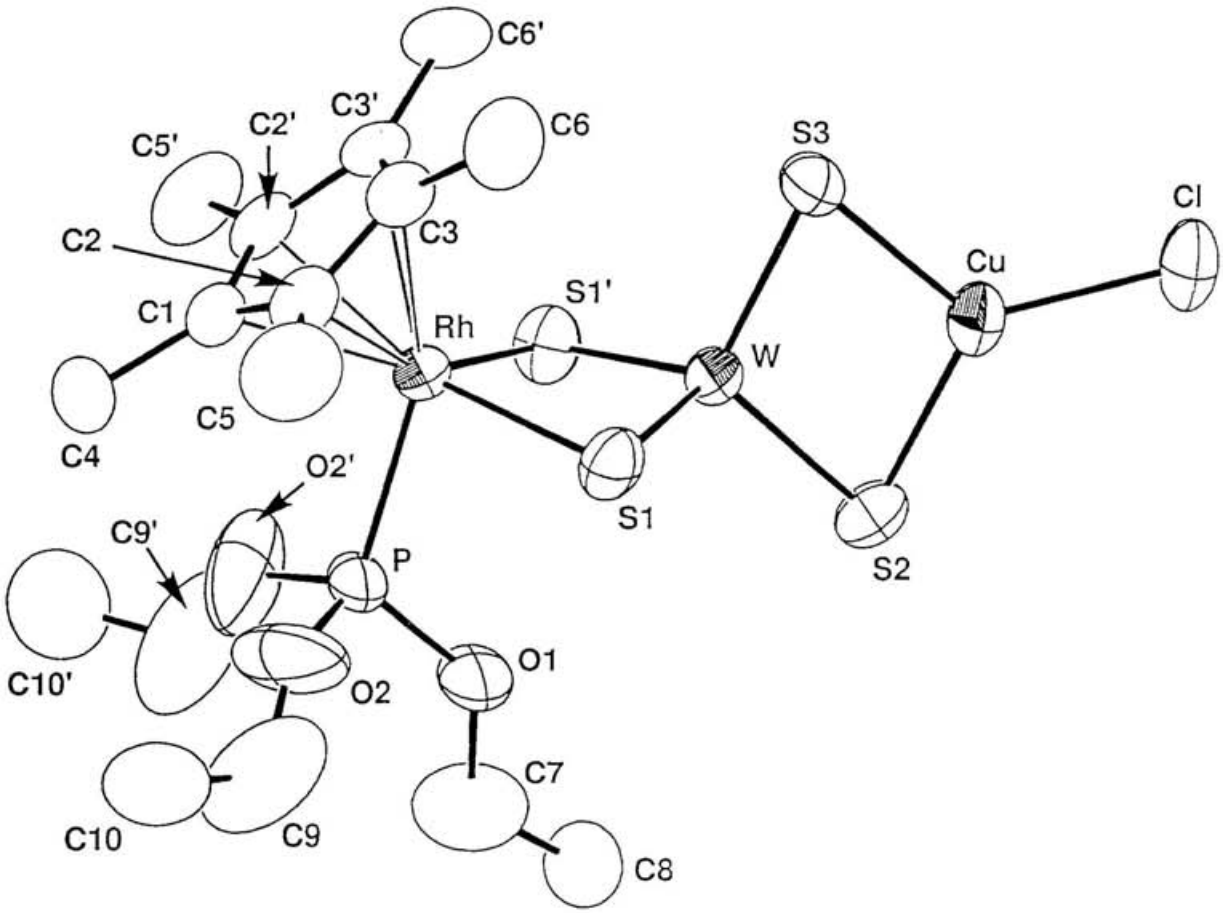

Figure 1-5. ORTEP drawing of [Cp*RhP(OEt)$_3$(μ-WS$_4$)CuCl] (3)

Table 1-10. Fractional coordinates and equivalent isotropic thermal parameters (U_{eq}[47]/ Å^2) of non-hydrogen atoms for [Cp*RhP(OEt)$_3$(μ-WS$_4$)CuCl] (**3**)

	x / *a*	y / *b*	z / *c*	U_{eq}
W	0.38818(4)	3/4[48]	0.11049(3)	0.0388(1)
Rh	0.65165(6)	3/4	0.23089(6)	0.0342(2)
Cu	0.1794(1)	3/4	-0.0478(1)	0.0503(4)
Cl	0.0134(3)	3/4	-0.1828(3)	0.066(1)
S1	0.4962(2)	0.6018(2)	0.1906(2)	0.0483(6)
S2	0.1825(3)	3/4	0.1588(3)	0.062(1)
S3	0.3896(3)	3/4	-0.0918(2)	0.062(1)
P	0.6129(3)	3/4	0.4328(2)	0.060(1)
O1	0.4621(8)	3/4	0.4635(7)	0.090(4)
O2	0.6780(8)	0.643(1)	0.5000(7)	0.162(5)
C1	0.8652(9)	3/4	0.2699(9)	0.046(3)
C2	0.8278(6)	0.6539(6)	0.1990(7)	0.046(2)
C3	0.7764(7)	0.6915(6)	0.0778(6)	0.047(2)
C4	0.945(1)	3/4	0.392(1)	0.065(5)
C5	0.854(1)	0.533(1)	0.233(1)	0.085(5)
C6	0.736(1)	0.615(1)	-0.027(1)	0.077(4)
C7	0.407(3)	3/4	0.573(3)	0.18(2)
C8	0.277(2)	3/4	0.574(2)	0.12(1)
C9	0.673(2)	0.580(2)	0.591(2)	0.16(1)
C10	0.788(2)	0.524(1)	0.633(1)	0.099(6)

Table 1-11. Bond lengths (l / Å), angles (ϕ / °), and selected contact distances (d / Å) of [Cp*RhP(OEt)$_3$(μ-WS$_4$)CuCl] (**3**)

Bond lengths	(l / Å)		
W-S1	2.226(2)	P-O1	1.601(8)
W-S2	2.205(3)	P-O2	1.59(1)
W-S3	2.187(3)	O1-C7	1.35(3)
Rh-S1	2.396(2)	O2-C9	1.24(3)
Rh-P	2.248(3)	C1-C2	1.416(9)
Rh-Cl	2.191(9)	C1-C4	1.50(2)
Rh-C2	2.184(7)	C2-C3	1.44(1)
Rh-C3	2.274(7)	C2-C5	1.51(1)
Rh-S1	2.396(2)	C3-C6	1.49(1)
Cu-Cl	2.151(3)	C3-C3'	1.40(1)
Cu-S2	2.231(3)	C7-C8	1.33(3)
Cu-S3	2.236(3)	C9-C10	1.40(3)
Bond Angles	(ϕ / °)		
Rh-W-Cu	166.17(4)	W-S2-Cu	72.8(1)
Cu-W-S1	127.34(5)	W-S3-Cu	72.99(9)
Cu-W-S2	54.08(8)	Rh-P-O1	116.4(3)
Cu-W-S3	54.35(8)	Rh-P-O2	110.1(3)
S1-W-S2	111.18(6)	O1-P-O2	106.3(4)
S1-W-S3	110.37(7)	O2-P-O2'	107.1(5)
S1-W-S1'	105.31(7)	P-O1-C7	131(1)
S2-W-S3	108.4(1)	P-O2-C9	143(1)
S1-Rh-P	90.71(7)	C2-C1-C4	125.7(4)
S1-Rh-S1	95.24(7)	C2-C1-C2'	108.2(7)
P-Rh-S1	90.71(7)	C1-C2-C3	107.6(6)
W-Cu-Cl	177.8(1)	C1-C2-C5	127.4(8)
W-Cu-S2	53.17(8)	C3-C2-C5	124.3(8)
W-Cu-S3	52.66(7)	C2-C3-C6	123.8(8)
Cl-Cu-S2	129.0(1)	C2-C3-C3'	108.1(6)
Cl-Cu-S3	125.2(1)	C6-C3-C3'	128.1(8)
S2-Cu-S3	105.8(1)	O1-C7-C8	120(2)
W-S1-Rh	77.63(6)	O2-C9-C10	118(2)

Table 1-11. (Continued)

Contact distances (d / Å)			
Rh-W	2.8996(9)	W-Cu	2.631(1)

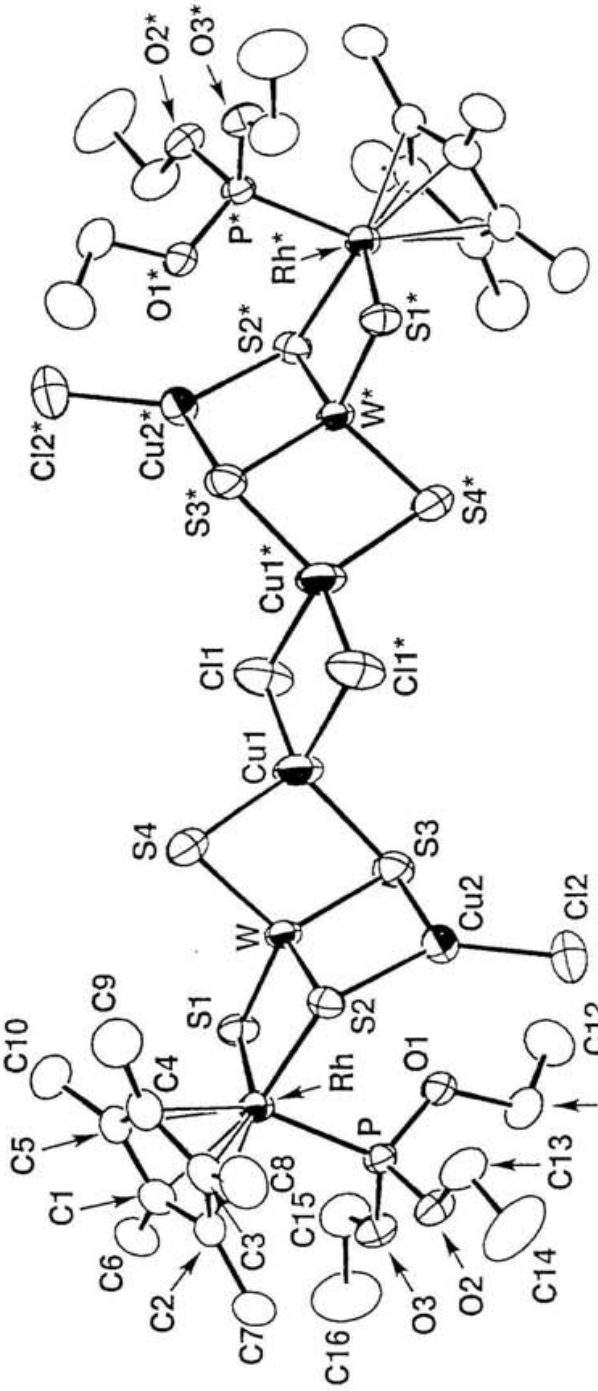

Figure 1-6. ORTEP drawing of $[\{Cp^*RhP(OEt)_3(\mu\text{-}WS_4)(CuCl)Cu\}_2(\mu\text{-}Cl)_2]$ (4)

Table 1-12. Fractional coordinates and equivalent isotropic thermal parameters (U_{eq}[49]/ Å^2) of non-hydrogen atoms for [{Cp*RhP(OEt)$_3$(μ-WS$_4$)(CuCl)Cu}$_2$(μ- Cl)$_2$] (**4**)

	x / *a*	y / *b*	z / *c*	U_{eq}
W	0.71236(3)	0.50473(2)	0.33663(1)	0.03328(8)
Rh	0.87737(5)	0.53010(4)	0.23472(3)	0.0310(1)
Cu1	0.5802(1)	0.49931(9)	0.44038(5)	0.0600(4)
Cu2	0.51495(9)	0.60371(7)	0.25637(5)	0.0428(3)
Cl1	0.5277(3)	0.3804(2)	0.5100(1)	0.066(1)
Cl2	0.3519(2)	0.6768(2)	0.1855(1)	0.0569(8)
P	0.7147(2)	0.5145(1)	0.13211(8)	0.0291(5)
S1	0.8021(2)	0.3932(1)	0.2843(1)	0.0373(6)
S2	0.7410(2)	0.6381(1)	0.28117(9)	0.0336(5)
S3	0.4902(2)	0.4783(1)	0.3205(1)	0.0458(7)
S4	0.8079(2)	0.5161(2)	0.4496(1)	0.0504(7)
O1	0.5710(4)	0.4935(3)	0.1461(2)	0.039(2)
O2	0.6951(5)	0.5978(3)	0.0775(2)	0.038(2)
O3	0.7398(5)	0.4386(3)	0.0776(2)	0.040(2)
C1	1.0678(7)	0.4722(5)	0.2209(4)	0.036(2)
C2	1.0384(6)	0.5554(5)	0.1791(4)	0.035(2)
C3	1.0363(7)	0.6300(5)	0.2265(4)	0.039(2)
C4	1.0754(7)	0.5934(6)	0.2992(4)	0.044(3)
C5	1.0942(6)	0.4976(6)	0.2952(4)	0.040(2)
C6	1.0899(9)	0.3783(6)	0.1949(5)	0.050(3)
C7	1.0261(9)	0.5650(7)	0.1020(5)	0.051(3)
C8	1.022(1)	0.7300(7)	0.2105(7)	0.065(5)
C9	1.095(1)	0.6495(7)	0.3660(6)	0.066(4)
C10	1.140(1)	0.4330(9)	0.3560(6)	0.058(4)
C11	0.4504(8)	0.4854(7)	0.0862(4)	0.050(3)
C12	0.346(1)	0.4311(8)	0.1123(6)	0.062(4)
C13	0.661(1)	0.6909(6)	0.0983(5)	0.052(3)
C14	0.644(2)	0.7512(8)	0.0364(7)	0.091(6)
C15	0.741(1)	0.3406(6)	0.0945(5)	0.053(3)
C16	0.773(2)	0.2911(8)	0.0335(7)	0.083(6)

Table 1-13. Bond lengths (l / Å), angles (ϕ / °), and selected contact distances (d / Å) of [{Cp*RhP(OEt)$_3$(μ-WS$_4$)(CuCl)Cu}$_2$(μ- Cl)$_2$] (**4**)

Bond lengths	**(l / Å)**		
Rh-P	2.261(1)	P-O1	1.581(5)
Rh-S1	2.412(2)	P-O2	1.587(5)
Rh-S2	2.410(2)	P-O3	1.591(5)
Rh-C1	2.189(7)	O1-C11	1.470(8)
Rh-C2	2.205(7)	O2-C13	1.47(1)
Rh-C3	2.205(7)	O3-C15	1.46(1)
Rh-C4	2.282(7)	C1-C2	1.44(1)
Rh-C5	2.274(6)	C1-C5	1.45(1)
W-S1	2.223(2)	C1-C6	1.49(1)
W-S2	2.267(2)	C2-C3	1.42(1)
W-S3	2.236(2)	C2-C7	1.48(1)
W-S4	2.173(2)	C3-C4	1.47(1)
Cu1-Cl1	2.332(3)	C3-C8	1.48(1)
Cu1-Cl1*	2.387(3)	C4-C5	1.41(1)
Cu1-S3	2.299(2)	C4-C9	1.50(1)
Cu1-S4	2.291(3)	C5-C10	1.49(1)
Cu2-Cl2	2.151(2)	C11-C12	1.50(1)
Cu2-S2	2.284(2)	C13-C14	1.46(2)
Cu2-S3	2.253(2)	C15-C16	1.49(2)
Bond Angles	**(ϕ / °)**		
S1-W-S2	106.70(7)	O1-P-O2	107.1(3)
S1-W-S3	109.05(7)	O1-P-O3	106.8(3)
S1-W-S4	112.69(8)	O2-P-O3	95.5(3)
S2-W-S3	108.96(7)	W-S1-Rh	77.93(6)
S2-W-S4	109.65(7)	W-S2-Rh	77.15(6)
S3-W-S4	109.69(8)	W-S2-Cu2	70.85(6)
P-Rh-S1	91.92(6)	Rh-S2-Cu2	114.95(8)
P-Rh-S2	91.81(6)	W-S3-Cu1	72.63(6)
S1-Rh-S2	96.67(7)	W-S3-Cu2	71.98(7)
Cl1-Cu1-S3	113.42(9)	Cu1-S3-Cu2	112.38(9)
Cl1-Cu1-S4	113.95(9)	W-S4-Cu1	73.95(6)
S3-Cu1-S4	103.49(8)	P-O1-C11	120.3(5)
Cl2-Cu2-S2	127.05(9)	P-O2-C13	120.8(5)

Table 1-13. (Continued)

Cl2-Cu2-S3	125.18(9)	P-O3-C15	121.2(5)
S2-Cu2-S3	107.77(7)	O1-C11-C12	107.1(7)
Rh-P-O1	111.9(2)	O2-C13-C14	108.1(8)
Rh-P-O2	117.0(2)	O3-C15-C16	106.4(9)
Rh-P-O3	116.9(2)		
Contact distances	**(*d* / Å)**		
Rh-W	2.9187(8)	W-Cu2	2.638(1)
W-Cu1	2.686(1)	Cu1-Cu1*	3.146(2)

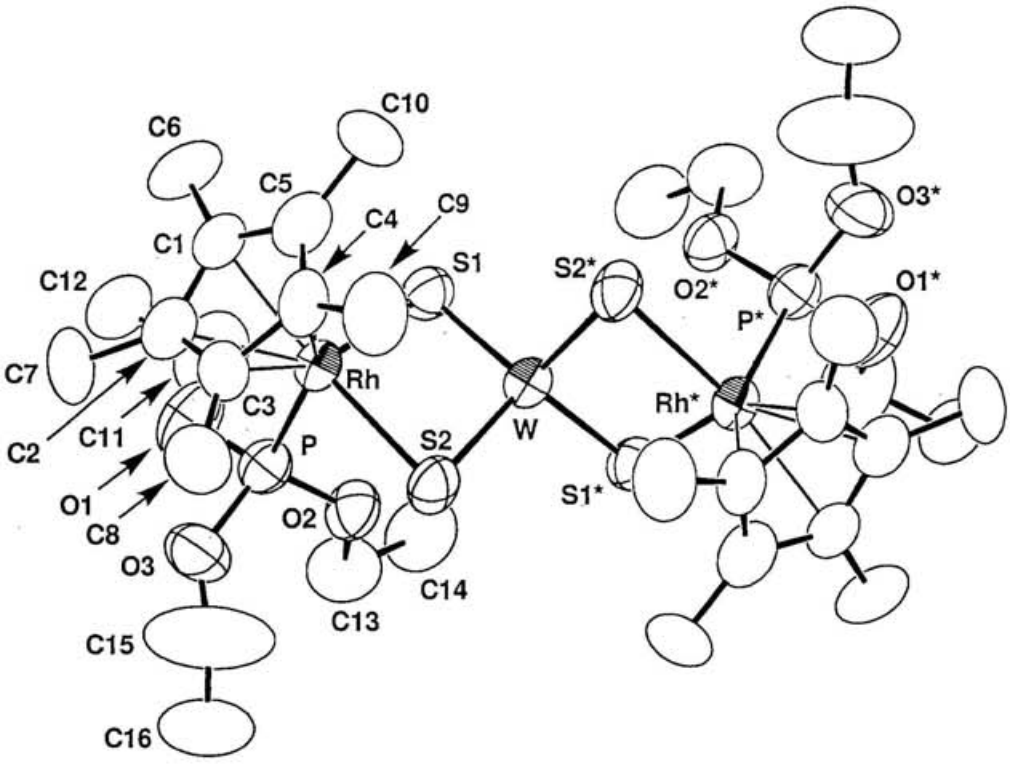

Figure 1-7. ORTEP drawing of $[\{Cp^*RhP(OEt)_3\}_2(\mu\text{-}WS_4)][BPh_4]_2$ (**5**·$[BPh_4]_2$)

Table 1-14. Fractional coordinates and equivalent isotropic thermal parameters (U_{eq}[50]/ Å^2) of non-hydrogen atoms for [{Cp*RhP(OEt)$_3$}$_2$(μ-WS$_4$)][BPh$_4$]$_2$ (**5**·[BPh$_4$]$_2$)

	x / *a*	y / *b*	z / *c*	U_{eq}
W	3/4[51]	0.75315(4)	1/2[52]	0.0498(2)
Rh	0.64876(5)	0.72615(5)	0.42167(3)	0.0482(3)
S(1)	0.6449(2)	0.8280(2)	0.4796(1)	0.056(1)
S(2)	0.7819(2)	0.6781(2)	0.4405(1)	0.063(1)
P	0.7020(2)	0.8197(2)	0.3737(1)	0.055(1)
O(1)	0.6384(5)	0.8821(5)	0.3532(3)	0.088(4)
O(2)	0.7719(4)	0.8695(5)	0.3969(3)	0.065(3)
O(3)	0.7348(6)	0.7854(6)	0.3273(3)	0.098(4)
B	1.1652(7)	0.7451(8)	0.3628(5)	0.054(5)
C(1)	0.5161(7)	0.7119(7)	0.4124(4)	0.059(4)
C(2)	0.5572(7)	0.6829(7)	0.3722(5)	0.064(5)
C(3)	0.6092(8)	0.6153(7)	0.3858(4)	0.062(5)
C(4)	0.5930(8)	0.6030(7)	0.4345(4)	0.064(5)
C(5)	0.5369(8)	0.6612(7)	0.4510(5)	0.067(5)
C(6)	0.4516(9)	0.777(1)	0.4137(7)	0.081(7)
C(7)	0.544(1)	0.709(1)	0.3232(5)	0.088(8)
C(8)	0.661(1)	0.561(1)	0.3561(7)	0.090(8)
C(9)	0.629(1)	0.5326(9)	0.4624(7)	0.088(8)
C(10)	0.504(1)	0.668(1)	0.4986(6)	0.076(6)
C(11)	0.603(1)	0.949(1)	0.3752(8)	0.12(1)
C(12)	0.529(1)	0.976(1)	0.3489(7)	0.080(7)
C(13)	0.813(1)	0.942(1)	0.3773(6)	0.088(7)
C(14)	0.822(1)	1.003(1)	0.4145(7)	0.091(8)
C(15)	0.800(2)	0.751(3)	0.313(1)	0.26(2)
C(16)	0.865(2)	0.781(2)	0.289(1)	0.14(1)
C(17)	1.2024(8)	0.8121(7)	0.3262(4)	0.056(5)
C(18)	1.147(1)	0.8578(8)	0.2997(4)	0.071(6)
C(19)	1.173(1)	0.9200(9)	0.2703(5)	0.084(7)
C(20)	1.257(1)	0.9381(9)	0.2672(5)	0.092(7)
C(21)	1.313(1)	0.894(1)	0.2928(6)	0.093(8)
C(22)	1.285(1)	0.8312(9)	0.3220(5)	0.074(6)
C(23)	1.1246(7)	0.7997(6)	0.4030(4)	0.054(4)

Table 1-14. (Continued)

C(24)	1.0420(9)	0.8170(8)	0.4045(5)	0.070(6)
C(25)	1.009(1)	0.867(1)	0.4383(6)	0.097(8)
C(26)	1.057(1)	0.902(1)	0.4717(7)	0.101(9)
C(27)	1.142(1)	0.8876(9)	0.4701(5)	0.089(7)
C(28)	1.175(1)	0.8361(8)	0.4362(5)	0.072(6)
C(29)	1.2363(6)	0.6827(6)	0.3814(4)	0.051(4)
C(30)	1.2881(8)	0.6441(8)	0.3494(6)	0.073(6)
C(31)	1.3467(9)	0.5859(8)	0.3643(6)	0.080(6)
C(32)	1.3550(9)	0.5664(8)	0.4099(6)	0.082(7)
C(33)	1.3030(8)	0.6030(8)	0.4420(6)	0.073(6)
C(34)	1.2447(8)	0.6618(7)	0.4277(5)	0.062(5)
C(35)	1.0990(7)	0.6854(7)	0.3384(4)	0.064(5)
C(36)	1.098(1)	0.6686(9)	0.2919(5)	0.082(7)
C(37)	1.044(1)	0.612(1)	0.2726(8)	0.109(9)
C(38)	0.987(1)	0.573(1)	0.2999(8)	0.12(1)
C(39)	0.986(1)	0.588(1)	0.3457(8)	0.116(9)
C(40)	1.0420(9)	0.6424(8)	0.3651(6)	0.083(6)

Table 1-15. Bond lengths (l / Å) and angles (ϕ / °) of [{Cp*RhP(OEt)$_3$}$_2$(μ-WS$_4$)][BPh$_4$]$_2$ (**5**·[BPh$_4$]$_2$)

Bond lengths	(l / Å)		
W-S1	2.207(3)	O3-C15	1.28(4)
W-S2	2.205(3)	C1-C2	1.44(2)
Rh-S1	2.390(3)	C1-C5	1.45(2)
Rh-S2	2.394(3)	C1-C6	1.51(2)
Rh-P	2.265(3)	C2-C3	1.46(2)
Rh-C1	2.21(1)	C2-C7	1.52(2)
Rh-C2	2.21(1)	C3-C4	1.47(2)
Rh-C3	2.21(1)	C3-C8	1.51(2)
Rh-C4	2.26(1)	C4-C5	1.42(2)
Rh-C5	2.30(1)	C4-C9	1.54(2)
P-O1	1.586(9)	C5-C10	1.51(2)
P-O2	1.568(8)	C11-C12	1.51(3)
P-O3	1.57(1)	C13-C14	1.49(3)
O1-C11	1.40(2)	C15-C16	1.37(4)
O2-C13	1.48(2)		
Bond Angles	(ϕ / °)		
S1-W-S2	106.5(1)	Rh-P-O3	115.3(4)
S1-W-S1*	112.1(1)	O1-P-O2	108.1(4)
S1-W-S2*	110.0(1)	O1-P-O3	97.4(5)
S2-W-S2*	111.8(1)	O2-P-O3	108.3(5)
S1-Rh-S2	95.3(1)	P-O1-C11	127(1)
S1-Rh-P	88.6(1)	P-O2-C13	125.6(9)
S2-Rh-P	90.9(1)	P-O3-C15	137(2)
W-S1-Rh	77.34(9)	O1-C11-C12	110(2)
W-S2-Rh	77.3(1)	O2-C13-C14	108(1)
Rh-P-O1	115.0(4)	O3-C15-C16	132(4)
Rh-P-O2	111.7(3)		
Contact distance	(d / Å)		
Rh-W	2.8764(9)		

As shown in Figure 1-8, the distances between Rh atom and carbons of the Cp* ring of $[Cp^*RhP(OEt)_3Cl_2]$ (**1**) in the solid state are not equivalent. The distances (av. 2.22Å) of Rh-C_3 and Rh-C_4 trans to the $P(OEt)_3$ ligand are longer than the distances (av. 2.16Å) of Rh-C_1, Rh-C_2, and Rh-C_5 trans to the Cl ligands. This result indicates that the $P(OEt)_3$ ligand has a greater trans influence than the Cl ligands for the Cp* ring. Therefore the C_3-C_4 bond distance (1.39Å) is shorter than other C-C bond distances (av. 1.43Å) of the Cp* ring, and has double bond character in higher extend. The ^{13}C NMR spectrum of **1** in dichloromethane, however, has one kind of the $^1J_{Rh,C}$ and $^2J_{P,C}$ values because the Cp* ring should rotate in solution. The same situation applies to other compounds in this study (see Figure 1-13). Figure 1-9 shows distances between the Rh metal atoms and the centroids of the Cp* of $[(Cp^*RhCl)_2Cl_2]$ (**A'**), **1**, $[Cp^*RhP(OEt)_3WS_4]$ (**2**), $[Cp^*RhP(OEt)_3(\mu\text{-}WS_4)CuCl]$ (**3**), and $[\{Cp^*RhP(OEt)_3(\mu\text{-}WS_4)(CuCl)Cu\}_2(\mu\text{-}Cl)_2]$ (**4**), namely, 1.755, 1.811, 1.860, 1.857, and 1.865Å, respectively. From this result the abilities of trans influences of ligands for the Cp* ring are ordered in strength as follows. **$P(OEt)_3$ > S > Cl ligands**

As depicted in Figure 1-4 the W-S(terminal) bond distances (av. 2.152 Å) of **2**, which are considerably shorter than the W-S(bridge) distances (av. 2.249 Å), correspond to a double bond character.[53] The Rh-W-S3 angle (111°) is smaller than Rh-W-S4 (139°) by a steric influence of the triethylphosphite group.

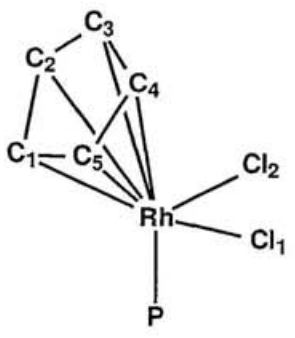

Rh-C1 = 2.16(1)
Rh-C2 = 2.17(1)
Rh-C5 = 2.14(1)
} av. 2.16

Rh-C3 = 2.22(1)
Rh-C4 = 2.21(1)
} av. 2.22

C1-C2 = 1.43(1)
C2-C3 = 1.43(1)
C3-C4 = 1.39(2)
C4-C5 = 1.45(2)
C5-C1 = 1.42(2)

Rh-Cl1 = 2.381(3)
Rh-Cl2 = 2.411(4)
Rh-P = 2.268(3)

The dihedral angle between C2C1C5 and C2C3C5 is 3.2°.
The dihedral angle between C2C1C5 and C2C4C5 is 3.7°.
The dihedral angle between C2C1C5 and C2C3C4C5 is 3.4°.

Figure 1-8. Distances (Å) between the Rh metal atom and carbons of the Cp* ring of $[Cp^*RhP(OEt)_3Cl_2]$ (**1**).

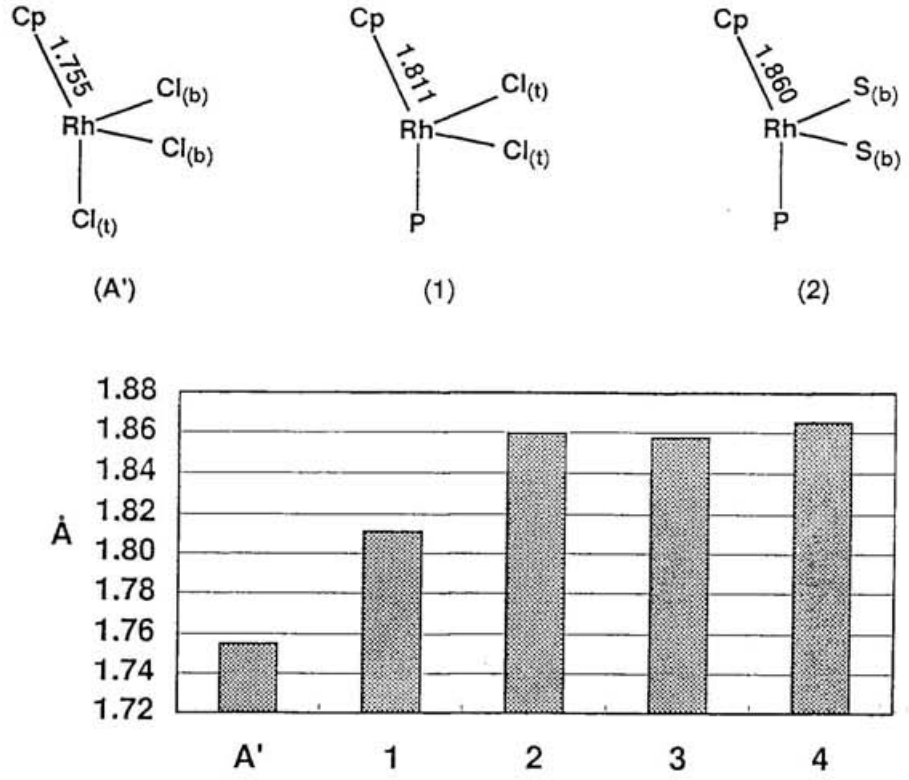

Figure 1-9. Distances (Å) between the Rh metal atoms and the centroids of the Cp* of $[(Cp^*RhCl)_2Cl_2]$ (A'), **1**, **2**, **3**, and **4**.
(Subscript (b) = bridging, (t) = terminal.)

The similar heterodimetallic framework is found in the *p*-cymene ruthenium complex of $[(p\text{-cymene})RuPPh_3WS_4]$[54] which has the Ru-W distance of 2.934(1) Å, the W-S (terminal) bond distances (av. 2.153 Å), and the W-S(bridge) distances (av. 2.237 Å).

Although vast majority of the known heterometallic trinuclear sulfide clusters have nonlinear-type configurations, $[Cp^*RhP(OEt)_3(\mu\text{-}WS_4)CuCl]$ (**3**) has a linear-type one as shown in Figure 1-10. As depicted in Figure 1-5, $[Cp^*RhP(OEt)_3(\mu\text{-}WS_4)CuCl]$ (**3**) possesses a crystallographic plane of symmetry. The Cu atom is chelated by two terminal S atoms of **2** forming a trigonal planar coordination geometry. Hence, the three metal ions are arranged in a linear fashion (Rh-W-Cu = 166.17(4)°) and all of S atoms in **3** have a μ_2-coordination mode. The S2-W-S3 angle (108.4(1)°) is larger than the S1-W-S1' angle (105.31(7)°).

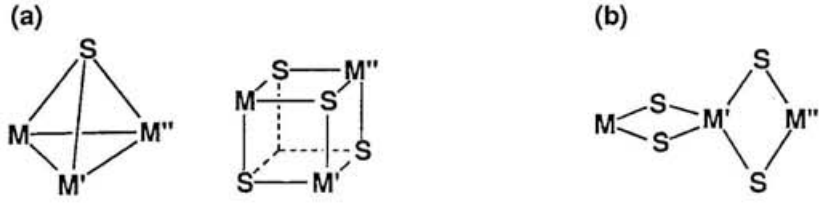

Figure 1-10. Examples of geometrical configurations of heterometallic trinuclear sulfide clusters of (a) nonlinear-type and (b) linear-type.

The Cu-S bond distances (av. 2.234 Å) correspond well to those in [{CuCl(μ-S)$_2$}$_2$W] (av. 2.237 Å).[55] The W-S(-Cu) bonds in **3** (av. 2.196 Å) are considerably elongated from the W-S(terminal) bonds in **2**, suggesting that the bonds have a single bond character. The W-S(-Rh) bonds in **3** (2.226(2) Å) are slightly longer than the W-S(-Cu) bonds, suggesting that the rhodium atom has a stronger affinity for the sulfur atoms than does the copper atom. These W-S bonds in **3** are, however, shorter compared to the W-S(bridge) bonds in **2** (av. 2.249 Å). As mentioned later these differences in W-S bonds of **2** and **3** agree with shifts of $\nu_{W\text{-}S}$ bands in the infrared spectra. Although there are three presumed geometrical isomers for **3** based on the difference in the binding site of CuCl on the WS_4 core, the reaction between **2** and CuCl gave specifically **3** with the above structure in nearly quantitative yield because the specific formation of **3** is due to the strong coordination ability of the terminal S atoms in **2**.

Cluster **3** performs a regiospecific CuCl-addition at S1 (or S1*) and S2 atoms to form [{Cp*RhP(OEt)$_3$(μ-WS$_4$)(CuCl)Cu}$_2$(μ- Cl)$_2$] (**4**), but not at other sets of S atoms. This regiospecific addition is attributed mainly to the steric demands of the Cp* and P(OEt)$_3$ ligands. As shown in Figure 1-6, cluster **4** has an octanuclear framework with a crystallographic inversion center. Rh-W-Cu1 is almost linear (172.43(3)°) and Rh-W-Cu2 is an approximately right angle (90.73(3)°), and hence the eight metals are arranged in a branched configuration. The Rh and W atoms are octahedrally and tetrahedrally coordinated, respectively, similarly to those of **3**. The Cu2 atom has a trigonal planar geometry, but the Cu1 atom a slightly distorted tetrahedral one as shown

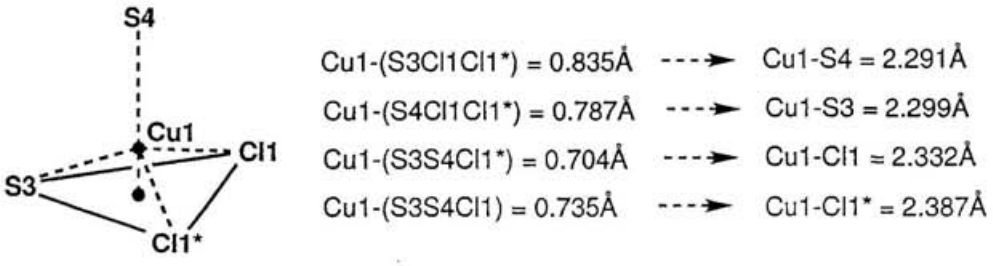

Figure 1-11. A slightly distorted tetrahedral coordination geometry of Cu1 of **4**. For example, if S3S4Cl1Cl1* is a regular tetrahedron: Cu1-(S3Cl1Cl1*) = 1/3 (Cu1-S4).

in Figure 1-11. The two different coordination geometries around Cu atoms in a discrete molecule are also found in $[\{MS_4(CuCl)_3Cu\}_2(\mu\text{-}Cl)_2]^{4-}$ (M = W,[56] Mo[57]). The distance of Cu1-Cl1* (2.387(3) Å) is almost same as Cu1-Cl1 (2.332(3) Å) in the bridging 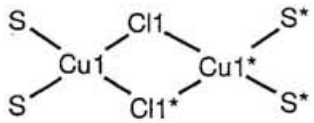 system in **4**, indicating that Cu1 and Cl1* atoms have a bonding interaction to stabilize the octanuclear structure of **4** in the solid state.

Dimerization of two tetranuclear species, $[Cp^*RhP(OEt)_3(\mu\text{-}WS_4)(CuCl)_2]$, takes place upon crystallization to form **4**. In contrast, dimerization of cluster **3** does not occur even in the solid state. It is recognized that this difference in the dimerization abilities depends on a strength of positive charges of the Cu atoms, because in order to cause such dimerization, the Cu atoms need the positive charges enough to attract the lone pairs of electrons of the Cl atoms of the approaching other molecules. The difference in the positive charges of the Cu atoms of clusters **3** and **4** is dependent on the difference in the strength of donations of the lone pairs of electrons from the S atoms. This view is supported by the investigation of binding energies for X-ray photoelectron spectra of **3** and **4** (see Figure 1-16). The reason the dimerization in cluster **4** does not take place at the Cu2Cl2 (or Cu2*Cl2*) group is due to a steric hindrance of the $P(OEt)_3$ groups.

Figure 1-12 shows a manner of stepwise additions of the CuCl groups to **2** and

3 with changes of metal-sulfur bond distances. An attempt to add the further CuCl group to **4** was not successful, even under conditions of reflux in dichloromethane or acetonitrile solutions for several hours.

As shown in Figure 1-5, $[\{Cp^*RhP(OEt)_3\}_2(\mu\text{-}WS_4)][BPh_4]_2$ (**5**·$[BPh_4]_2$) has a trinuclear framework with a crystallographic inversion center. The three metal atoms are arranged in a linear configuration and the two coordination geometries around the Rh atoms are twisted at 90° to each other through the Rh···W···Rh* axis. The similar framework is found in $[\{Cp^*RhCl\}_2(\mu\text{-}WS_4)]$.[58]

The bond distances between metal atoms and adjacent atoms of **1**, **2**, **3**, **4**, and **5**·$[BPh_4]_2$ are summarized in Figure 1-13.

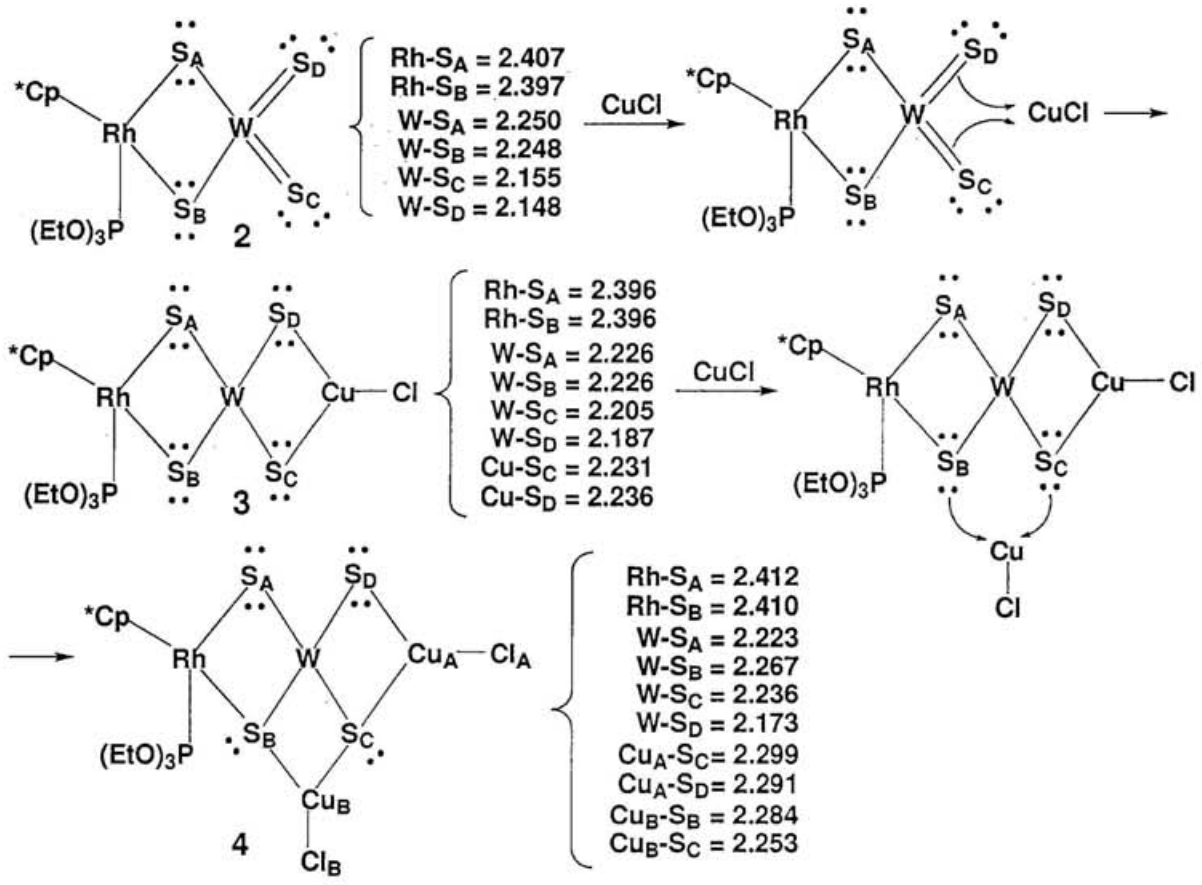

Figure 1-12. Additions of CuCl to **2** and **3** with changes of metal-sulfur bond distances (Å).

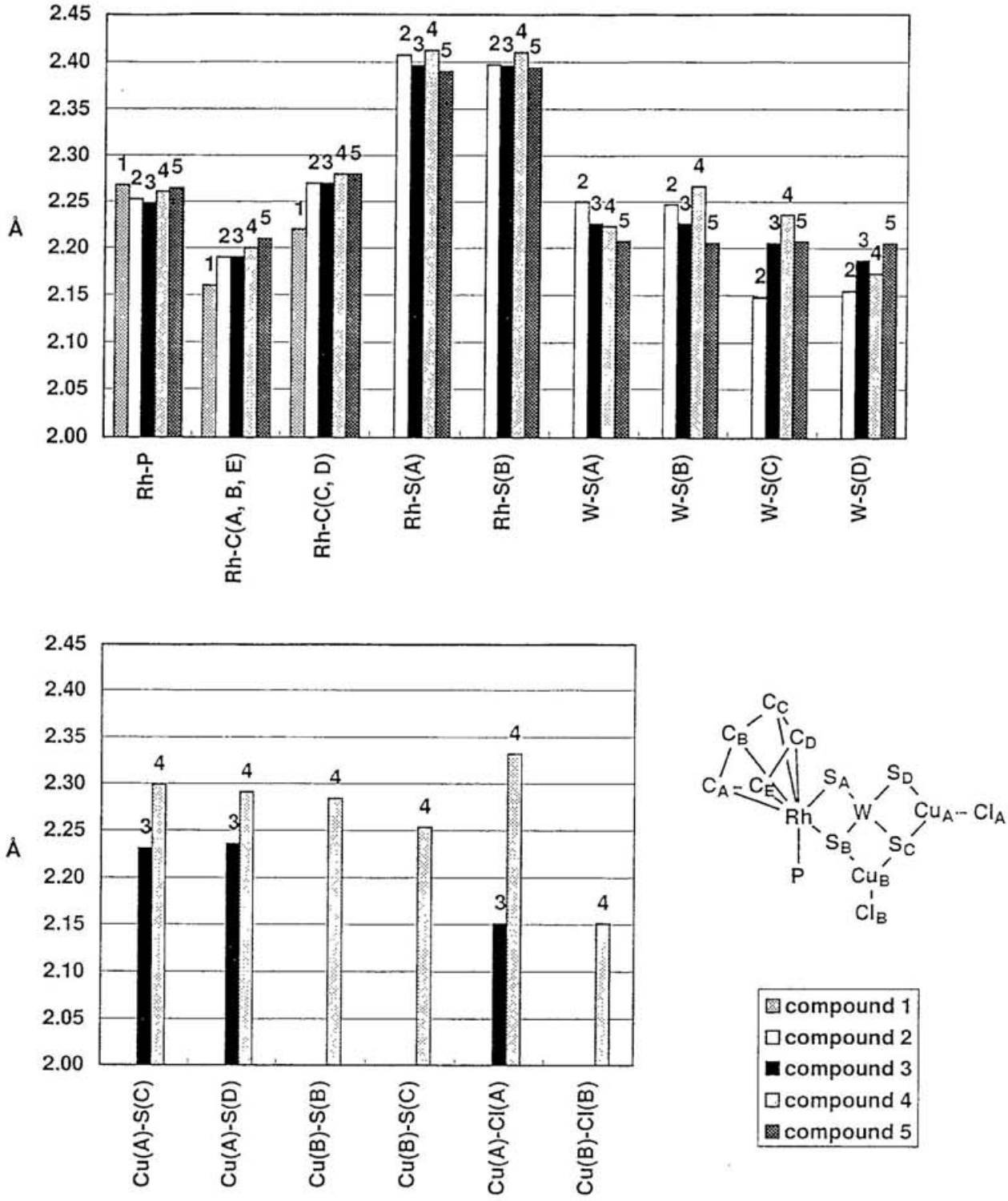

Figure 1-13. The bond distances (Å) between metal atoms and adjacent atoms of **1**, **2**, **3**, **4**, and **5**·$[BPh_4]_2$.

1-3-1-2 Infrared Spectroscopy

IR spectra in the ν_{W-S} regions of $[Cp^*RhP(OEt)_3Cl_2]$ (**1**), $[Cp^*RhP(OEt)_3WS_4]$ (**2**), $[Cp^*RhP(OEt)_3(\mu\text{-}WS_4)CuCl]$ (**3**), and $[\{Cp^*RhP(OEt)_3(\mu\text{-}WS_4)(CuCl)Cu\}_2(\mu\text{-}Cl)_2]$ (**4**) in mineral oil are shown in Figure 1-14. The IR spectrum of **2** exhibits two ν_{W-S} bands, one for W-S(terminal) (492 cm^{-1}) and the other for W-S(bridge) (430 cm^{-1}), and the similar patterns are found in $(Et_4N)_3[Rh(WS_4)_3]$ (ν_{W-S} = 486, 440 cm^{-1}),[59] $[(COD)PtWS_4]$ (499, 453 cm^{-1}),[60] [(*p*-cymene)$RuPPh_3WS_4$] (491, 435 cm^{-1}),[61] and $[(C_4Me_4)NiWS_4(PPhMe_2)]$ (491, 434 cm^{-1}).[62] The IR spectrum of **3** shows two bands at 466 cm^{-1} (W-S(Cu)) and 446 cm^{-1} (W-S(Rh)) which are downshifted and upshifted, respectively, from those of **2**. The three absorption bands of **4** at 478, 458, and 440 cm^{-1} are assigned to W-(μ_2-S(Cu)), W-(μ_2-S(Rh)), and W-(μ_3-S) stretching vibrations, respectively. Based on these assignments, an approximately linear relationship between ν_{W-S} and W-S bond distances obtained by the X-ray crystallographic analyses is given as shown in Figure 1-15.

1-3-1-3 X-ray photoelectron spectroscopy

Figure 1-16 shows binding energies from X-ray photoelectron spectra for $(PPh_4)_2WS_4$ (**B'**), **1**, **2**, **3**, and **4**. Although the values of binding energies of the Rh, W, and Cu atoms are not so much difference in the compounds to change the oxidation states, it can be regarded as significant, in fact, it refrects the diferences in the structures (and reactivity as seen in Chapter 2) of the clusters.

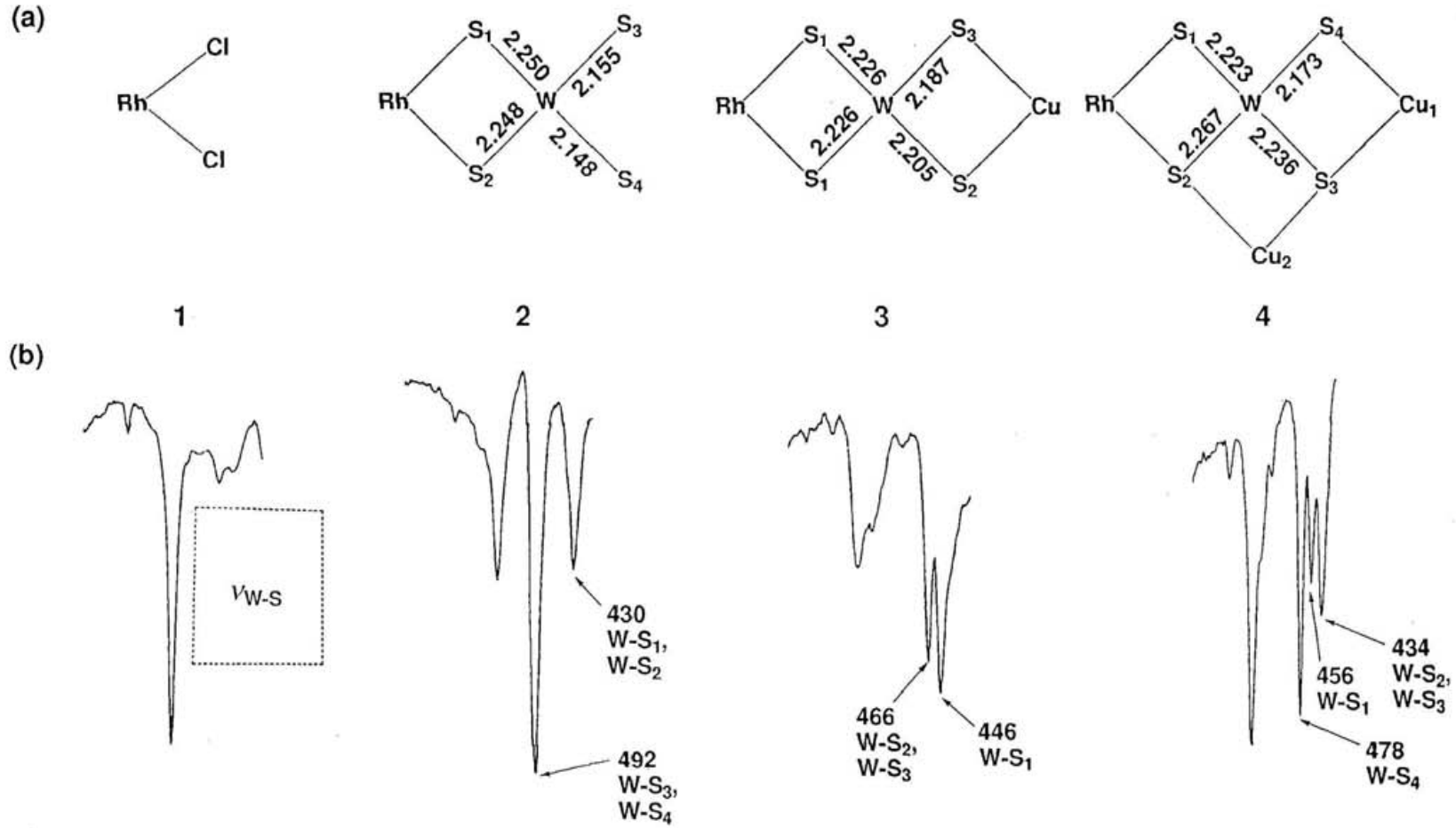

Figure 1-14. (a) W-S distances (Å) of **1**, **2**, **3**, and **4**.
(b) IR spectra (cm^{-1}) in the $\nu_{W\text{-}S}$ regions of **1**, **2**, **3**, and **4** in mineral oil.

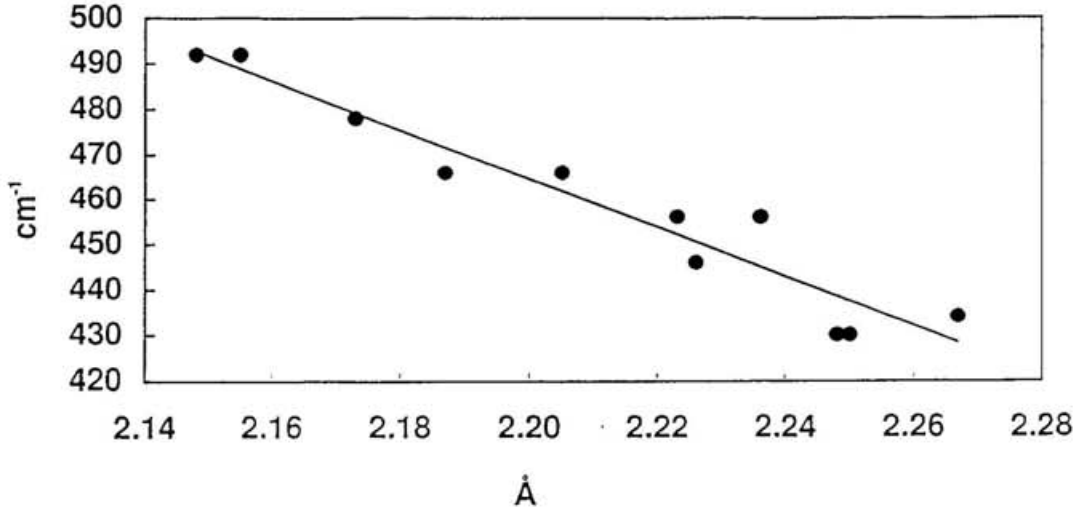

Figure 1-15. A plot of $\nu_{W\text{-}S}$ (cm^{-1}) vs. W-S bond distances (Å) for **1**, **2**, **3**, and **4** based on the assignments described in the text.

		B'	1	2	3	4	Ref.[63]
Rh	$3d_{5/2}$		308.8(1)	309.4(1)	309.1(1)	309.7(1)	Rh^{3+}: 308.5~310.0[a]
W	$4f_{7/2}$	32.5(1)		33.5(1)	33.3(1)	33.8(1)	W^{6+}: 32.5[b]
Cu	$2p_{3/2}$				932.3(1)	932.6(1)	Cu+: 931.8~932.8[c]

(a) $Rh(PPh_3)Cl_2(C_2H_4)$ and $Rh(PPh_3)_3Cl_3$; (b) $(Ph_4N)WS_4$;[64] (c) CuCl.

Figure 1-16. The binding energies (eV) from X-ray photoelectron spectra for $(PPh_4)_2WS_4$ (**B'**), **1**, **2**, **3**, and **4**. (These values are corrected by assuming C 1s binding energy in the compounds as 284.6 eV.)

1-3-2 Structures of 3 and 4 in dichloromethane and acetonitrile

1-3-2-1 Vapor Pressure Osmometry

Vapor pressure osmometry shows that the value of the molecular weight of **3** in dichloromethane is ca. 805, which corresponds to that of the undissociated molecule (calcd for **3** : 815.4). The observed molecular weight of **4** in dichloromethane is ca. 915, which is half the value of the molecular weight in the solid state (calcd for **4** : 1828.8).

1-3-2-2 Infrared Spectroscopy

As shown in Figure 1-17, The IR spectrum of **3** measured in dichloromethane shows two $\nu_{W\text{-}S}$ bands at 471 and 448 cm^{-1}, and in acetonitrile at 470 and 450 cm^{-1}; these values agree well to those obtained in the solid state as mentioned above. Therefore the linear-type framework of **3** is preserved in dichloromethane and acetonitrile.

The IR spectrum of a dichloromethane solution of **4** shows three $\nu_{W\text{-}S}$ bands at 478, 458, and 440 cm^{-1}; these values almost coincide with those in the solid state, however, of an acetonitrile solution at 470 and 450 cm^{-1}; these values correspond to those of **3** measured in acetonitrile. These results suggest that the coordination geometry around μ-WS_4^{2-} of **4** is preserved in dichloromethane, but Cu2Cl2 groups of **4** release from μ-WS_4^{2-} in acetonitrile. Judging from the consequences of both vapor pressure osmometry and infrared spectrometry of **4** in dichloromethane and acetonitrile, the cleavage in **4** occurs at the chloride bridges, and hence **4** exists as a tetranuclear complex, $[Cp^*RhP(OEt)_3(\mu\text{-}WS_4)(CuCl)_2]$, in dichloromethane, however, exists as **3** and CuCl moieties in acetonitrile.

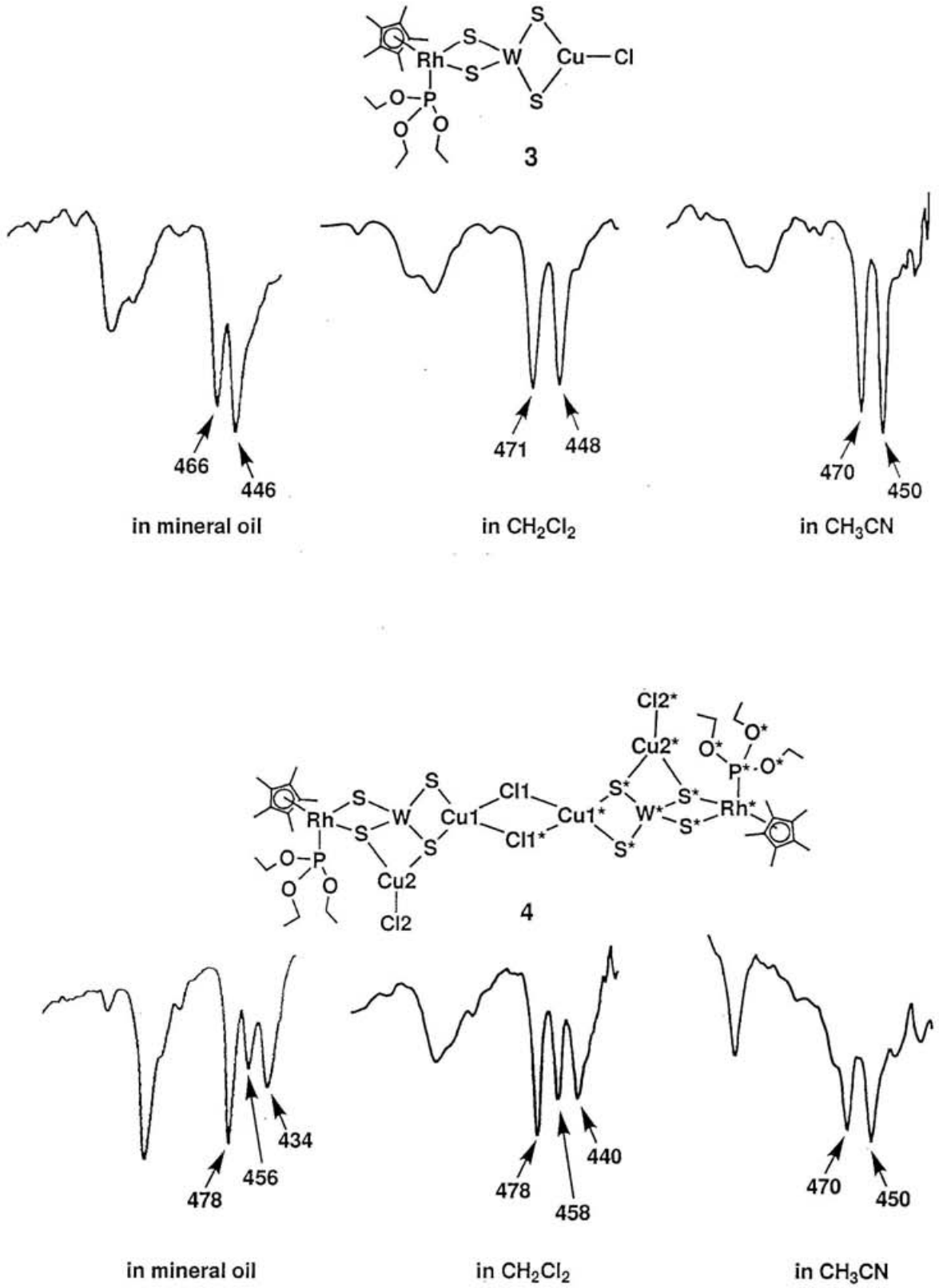

Figure 1-15. IR spectra (cm^{-1}) in the $\nu_{W\text{-}S}$ regions of **3** and **4** in mineral oil, CH_2Cl_2, and CH_3CN.

Chapter 2

A unique conversion of a $Rh(\mu\text{-}WS_4)Cu_2$ unit to a $Rh(\mu\text{-}WOS_3)Cu_2$ unit by the water saturated in dichloromethane

2-1 Introduction

Many enzymes and chemically synthesized clusters with the M-S-M' groups (M and M' = transition metal atoms) are oxidized by atmospheric oxygen or react with water to form oxo compounds or insoluble polymeric sulfide clusters.[65] It is interesting to investigate the mechanism of the oxidation reactions of the M-S-M' groups[66] and the resulting oxo compounds that have not been well-known because it is difficult to isolate discrete forms quantitatively without polymerizing.

In Chapter 2 a unique conversion of a bridging S atom in a $W(\mu_2\text{-}S)_2(\mu_3\text{-}S)_2$ group to a terminal O atom in a $WO(\mu_3\text{-}S)_3$ group is described. As shown in Figure 2-1 the cluster, $[\{Cp^*RhP(OEt)_3(\mu\text{-}WS_4)(CuCl)Cu\}_2(\mu\text{-}Cl)_2]$ (**4**) reacts with the water saturated in dichloromethane to give a linked incomplete cubane-type octanuclear cluster, $[Cp^*RhP(OEt)_3(\mu\text{-}WOS_3)(CuCl)Cu\}_2(\mu\text{-}Cl)_2]$ (**8**) at 51% yield for 60 days. This is the first example of the conversion of the bridging S atom in the M-S-M' groups into the terminal O atom without releasing of the constituent metal atoms. The use of the water saturated in dichloromethane is essential, because the several attempts to obtain **8** from **4** by using aqueous acetonitrile solution, basic conditions in common solvents, and two-phase conditions (water : dichloromethane = 1 : 1) which gave $[Cp^*RhP(OEt)_3Cl_2]$ (**1**), $[Cp^*RhP(OEt)_3(\mu\text{-}WS_4)CuCl]$ (**3**), $[Cp^*RhP(OEt)_3(\mu\text{-}WOS_3)(CuCl)]$ (**7**), and other unidentified products were not successful.

On the other hand, the clusters $[Cp^*RhP(OEt)_3WS_4]$ (**2**) and **3** are little reacted with the water saturated in dichloromethane or water under two-phase conditions of water and dichloromethane. It seems that the differences in the reactivity of the W-S-

(Cu) groups of clusters **2**, **3**, and **4** toward water are dependent on differences in the W atoms' electron densities, which are influenced by a strength of the π-electron donations from the S atoms.

A tentative mechanism of the transformation reaction (**4** → **8**) is as follows: water molecules saturated in dichloromethane interact with the W and S4 atoms of **4** to give an intermediary species that has W-O-H and Cu-S4-H groups, and then it is transformed to **8**.

Cluster **8** was also obtained by a stepwise synthesis using $[WOS_3]^{2-}$ as a tungsten source: **1** → $[Cp^*RhP(OEt)_3(\mu\text{-}S)_2WOS]$ (**6a**) → **7** → **8**. Cluster **6a** is one of two possible geometrical isomers of $[Cp^*RhP(OEt)_3(\mu\text{-}S)_2WOS]$ (see Section 2-2-2). The structures of **7** and **8** were determined by X-ray analysis. In addition the reactions of **4**, **7**, and **8** with hydrogen sulfide to give cluster **3** as the only major product are studied in Chapter 2.

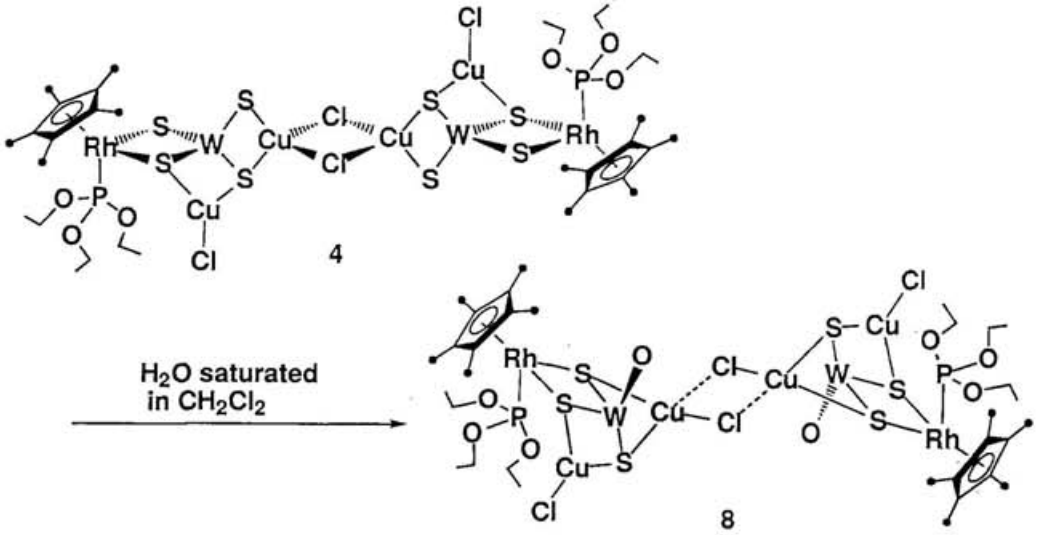

Figure 2-1. A unique conversion of a bridging S atom in a $(\mu_2\text{-}S)_2W(\mu_3\text{-}S)_2$ group of **4** to a terminal O atom in a $WO(\mu_3\text{-}S)_3$ group of **8** by the water saturated in dichloromethane.

2-2 Experimental section

2-2-1 Methods and materials

All preparative procedures were routinely carried out under an argon atmosphere. Hydrogen sulfide gas (99.99%) was purchased from NIPPON SANSO CORPORATION and was used without further purification. Hydrogen sulfide gas detector tube (the limited is 0.1 ppm for H_2S gas) was purchased from GASTEC CORPORATION. A thin-layer chromatoplate (Merck, silica gel 60 F_{254} pre-coated, No. 5717, 20 × 20 cm) was used for preparative thin-layer chromatography. Acetonitrile, dichloromethane, and DMF were distilled from calcium hydride. Diethyl ether was distilled from lithium aluminum hydride. The thiometalate, $(NH_4)_2[WOS_3]$, was prepared by the methods described in the literature.[67]

2-2-2 Preparations

The heterometallic sulfide complex, $[Cp^*RhP(OEt)_3(\mu\text{-}S)_2WOS]$, has two possible geometrical isomers, **6a** and **6b**, which are defined as follows, respectively. In this study **6a** was isolated but not **6b**.

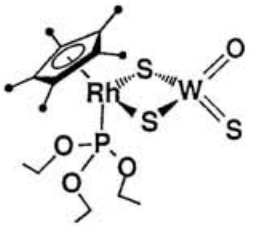

6a

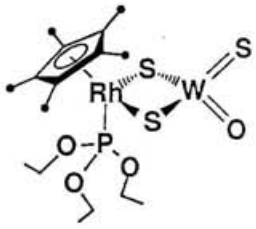

6b

2-2-2-1 Preparation of $[Cp^*RhP(OEt)_3(\mu\text{-}S)_2WOS]$ (6a)

The mixture of **6a** and **6b** was prepared by a reaction of $[Cp^*RhP(OEt)_3Cl_2]$ (**1**) (1.43 g, 3.01 mmol) and $(NH_4)_2[WOS_4]$ (1.00 g, 3.01 mmol) in water (50 cm^3) at room temperature. It was stirred for 12 h to yield an orange precipitate, which was collected by filtration, washed with water (3 × 10 cm^3). The precipitate was dissolved

in acetone (100 cm^3) and dried (Na_2SO_4), and then the solvent was removed to give a red solid. The crude product was purified by preparative thin-layer chromatography (SiO_2, 5% v/v MeOH / chloroform, R_f = 0.46) to afford **6a** (1.12 g, 53% yield).

Anal. Found: C, 27.25; H, 4.20%. Calcd for $C_{16}H_{30}O_4PRhS_3W$: C, 27.44; H, 4.32%. ^1H NMR : ($CDCl_3$, 23 °C, TMS) δ 1.29 (t, $^3J_{H,H}$=7.0 Hz, 9H, -CH_2CH_3), 1.94 (d, $^4J_{P,H}$=4.9 Hz, 15H, -CH_3(Cp^*)), 4.10 (dq, $^3J_{P,H}$=7.0 Hz, $^3J_{H,H}$=7.0 Hz, 6H, -CH_2-).

2-2-2-2 Preparation of [$Cp^*RhP(OEt)_3(\mu$-$WOS_3)CuCl$] (7)

The trinuclear sulfide cluster, [$Cp^*RhP(OEt)_3(\mu$-$WOS_3)CuCl$] (**7**), was obtained from a reaction of **6a** (1.00 g, 1.43 mmol) and CuCl (0.14 g, 1.43 mmol) in acetonitrile (50 cm^3). After stirring for 12 h at room temperature, the mixture was concentrated to 10 cm^3 giving red crystals, which were collected by filtration, washed with a small amount of diethyl ether, and dried in vacuo (0.91 g, 80% yield).

Anal. Found: C, 24.19; H, 4.01%. Calcd for $C_{16}H_{30}ClCuO_4PRhS_3W$: C, 24.04; H, 3.78%. ^1H NMR : (CD_2Cl_2, 23 °C, TMS) δ 1.29 (t, $^3J_{H,H}$=7.0 Hz, 9H, -CH_2CH_3), 1.98 (d, $^4J_{P,H}$=5.5 Hz, 15H, -CH_3(Cp^*)), 3.98 (dq, $^3J_{P,H}$=7.0 Hz, $^3J_{H,H}$=7.0 Hz, 6H, -CH_2-).

2-2-2-3 Preparation of [{$Cp^*RhP(OEt)_3(\mu$-$WOS_3)(CuCl)Cu\}_2(\mu$-$Cl)_2$] (8)

[Method I]

The sulfide cluster, [{$Cp^*RhP(OEt)_3(\mu$-$WS_4)(CuCl)Cu\}_2(\mu$-$Cl)_2$] (**4**) (1.00 g, 0.547 mmol) reacted slowly with the water saturated in dichloromethane (0.12 mol dm^{-3})[68] at room temperature, giving [{$Cp^*RhP(OEt)_3(\mu$-$WOS_3)(CuCl)Cu\}_2(\mu$-$Cl)_2$] (**8**). After 60 days the solvent was evaporated to give a mixture of **4** and **8** mainly. The desired cluster **8** is dissolved in chloroform but **4** is not. The cluster **8** was separated from the mixture by the difference in the solubility for chloroform and was recrystallized from acetonitrile (0.50 g, 51% yield). [{$Cp^*RhP(OEt)_3(\mu$-

$WOS_3)(CuCl)Cu\}_2(\mu\text{-}Cl)_2]\cdot(CH_3CN)_2$ was used for elemental analysis and NMR measurements. Anal. Found: C, 22.65; H, 3.40, N, 1.61%. Calcd for $C_{36}H_{66}Cl_4Cu_4N_2O_8P_2Rh_2S_6W_2$: C, 23.02; H, 3.54, N, 1.49%. ^1H NMR (CD_2Cl_2, 23°C): δ 1.36 (t, $^3J_{H,H}$ = 7.0 Hz, 18H, $-CH_2CH_3$), 2.05 (d, $^4J_{P,H}$ = 5.2 Hz, 30H, $-CH_3(Cp^*)$), 3.98 (dq, $^3J_{P,H}$ = 5.8 Hz, $^3J_{H,H}$ = 7.0 Hz, 12H, $-CH_2-$).

[Method II]

The octanuclear sulfide cluster **8** was prepared from the trinuclear cluster **6a** as follows. A reaction of **6a** with two equivalents of CuCl in acetonitrile at room temperature gave immediately a precipitate of **8**, which was recrystallized from acetonitrile to give red crystals (92% yield).

2-2-3 X-ray crystallographic studies of 7 and 8

Crystallographic data, experimental conditions, and refinement details of X-ray analysis for $[Cp^*RhP(OEt)_3(\mu\text{-}WOS_3)CuCl]$ (**7**) and $[\{Cp^*RhP(OEt)_3(\mu\text{-}WOS_3)(CuCl)Cu\}_2(\mu\text{-}Cl)_2](DMF)_2$ (**8**·$(DMF)_2$) are collected in Tables 2-1 and -2, respectively.

Table 2-1. Crystallographic data, experimental conditions, and refinement details of X-ray analysis for $[Cp^*RhP(OEt)_3(\mu\text{-}WOS_3)CuCl]$ (7)

Crystal data	
Compound	$[(\eta^5\text{-}C_5Me_5)Rh\{P(OC_2H_5)_3\}(\mu\text{-}WOS_3)CuCl]$
Chemical formula	$C_{16}H_{30}ClCuO_4PRhS_3W$
Formula weight	799.34
Solvent for crystallization	Dimethylformamide/diethyl ether
Color of crystal	Red
Shape of crystal	Prism
Size of specimen / mm^3	0.54 x 0.50 x 0.30
Crystal mount	Glass fiber
Crystal system	Orthorhombic
Laue group	*mmm*
Systematic absence	*h0l:* $h+l$ = odd, *hk0:* k = odd, *h00:* h = odd
Possible space group	$P2_1nb$
Space group (number)	$P2_1nb$ (No.33)
No. and range (/ °) of reflections used in the least-squares refinement of cell dimensions	25 and $28 < 2\theta < 30$
Lattice constants	
a / Å	14.515(2)
b / Å	17.225(3)
c / Å	10.261(3)
α / °	90
β / °	90
γ / °	90
V / $Å^3$	2565.4(7)
Z	4
D_x / g cm^{-3}	2.069
μ(Mo K_α) / cm^{-1}	63.6
F(000)	1544

Table 2-1. (Continued)

Data collection	
Instrument	AFC-5R
(voltage, current)	(50 kV, 120 mA)
X-ray tube	Normal-focus
Radiation (wave length, λ / Å)	Mo K_α (0.71073)
Monochromator	Graphite
Collimator diameter / mm	1.0
Temperature / °C	23
Scan method	$\theta - 2\theta$
Scan width / °	$1.3 + 0.5\tan\theta$
Scan speed (in θ) / ° min^{-1}	4
2θ range / °	$2\theta < 60$
Range of h, k, l	$0 \le h \le 20$
	$0 \le k \le 24$
	$0 \le l \le 14$
No. of reflections collected	4201
No. of independent reflections	3881
R_{int}	0
No. and frequency of standard reflections	3 and 150
Variation in standard reflections ($\Sigma(\lvert F_o \rvert / \lvert F_o \rvert_{initial})/n$)	1.000 - 0.997
Data reduction	
Lorentz and polarization corrections	Yes
Corrections for decay	No
Absorption corrections method	Gaussian[69]
Transmission factor, A	0.0597 - 0.1882

Table 2-1. (Continued)

Structure analysis	
Method used in structure solution	Patterson
Total no. of hydrogen atoms	30
No. of H atoms located in difference Fourier maps	30
Were these positions and thermal parameters refined?	Yes, both
No. of H atoms calculated	0
No. of parameters refined	372
2θ limit used for calculation / °	60
Cutoff criteria	$\|F_O\| > 3\sigma(\|F_O\|)$
No. of independent reflections used for calculation	3325
Atoms refined anisotropically	All non-H
Atoms refined isotropically	H
Weighting scheme	$w^{-1} = \sigma^2(\|F_O\|) + (0.015\|F_O\|)^2$
R[70]	0.054
R_w[71]	0.061
S[72]	2.389
Matrix type	Full
Final scale factor	1.939(4)
Extinction parameter refined ?	No
Anomalous dispersion corrections for which atoms	All
$(\Delta/\sigma)_{max}$ for non-hydrogen atoms	0.04915
$(\Delta/\sigma)_{av}$ for non-hydrogen atoms	0.001361
$(\Delta\rho)_{min}$, $(\Delta\rho)_{max}$ / eÅ^{-3}	-2.67, 3.00
Scattering factors used	Ref. [73]
Computer	Fujitsu S-4/IX
Computational program	*Xtal3.2*[74]

Table 2-2. Crystallographic data, experimental conditions, and refinement details of X-ray analysis for [{Cp*RhP(OEt)$_3$(μ-WOS$_3$)(CuCl)Cu}$_2$(μ-Cl)$_2$](DMF)$_2$ (**8**·(DMF)$_2$)

Crystal data	
Compound	[{η^5-C$_5$Me$_5$)RhP(OEt)$_3$(μ-WOS$_3$)(CuCl)Cu}$_2$(μ-Cl)$_2$](DMF)$_2$
Chemical formula	$C_{38}H_{74}Cl_4Cu_4N_2O_{10}P_2Rh_2S_6W_2$
Formula weight	1942.86
Solvent for crystallization	Dimethylformamide / diethyl ether
Color of crystal	Purple
Shape of crystal	Prism
Size of specimen / mm^3	0.40 × 0.22 × 0.16
Crystal mount	Glass fiber
Crystal system	Monoclinic
Laue group	*2/m*
Systematic absence	*h0l: l* = odd, *0k0: k* = odd
Possible space group	$P2_1/c$
Space group (number)	$P2_1/c$ (No.14)
No. and range (/ °) of reflections used in the least-squares refinement of cell dimensions	25 $29 < 2\theta < 30$
Lattice constants	
a / Å	10.011(3)
b / Å	17.115(3)
c / Å	18.678(3)
α/°	90
β/°	95.10(2)
γ/°	90
V / Å^3	3188(1)
Z	2
D_x / g cm^{-3}	2.02
μ(Mo K$_\alpha$) / cm^{-1}	58.5
F(000)	1888

Table 2-2. (Continued)

Data collection	
Instrument	AFC5R
(voltage, current)	(50 kV, 150 mA)
X-ray tube	Normal-focus
Radiation (wave length, λ / Å)	Mo K_α (0.71073)
Monochromator	Graphite
Collimator diameter / mm	1.0
Temperature / °C	23
Scan method	θ-2θ
Scan width / °	1.2 + 0.5tanθ
Scan speed (in θ) / ° min^{-1}	6
2θ range / °	$2\theta \leq 60$
Range of h, k, l	$0 \leq h \leq 14$, $0 \leq k \leq 24$, $-26 \leq l \leq 26$
No. of reflections collected	10082
No. of independent reflections	9290
R_{int}	0.037
No. and frequency of standard reflections	3 and 150
Variation in standard reflections ($\Sigma(\lvert F_o \rvert / \lvert F_o \rvert_{initial})/3$)	0.934 - 1.007
Data reduction	
Lorentz and polarization corrections	Yes
Corrections for decay	No
Absorption corrections method	Empirical Ψ scan[75]
Transmission factor, A	0.952 - 1.000

Table 2-2. (Continued)

Structure analysis	
Method used in structure solution	Usual heavy-atom method
Total no. of hydrogen atoms	37
No. of H atoms located in difference Fourier maps	37
Were these positions and thermal parameters refined?	Yes, both
No. of parameters refined	464
2θ limit used for calculation / °	60
Cutoff criteria	$\|F_o\| > 3\sigma(\|F_o\|)$
No. of independent reflections used for calculation	5670
Atoms refined anisotropically	All non-H
Atoms refined isotropically	H
Weighting scheme	$w^{-1} = \sigma^2(\|F_o\|) + (0.015\|F_o\|)^2$
R[76]	0.047
R_w[77]	0.051
S[78]	1.607
Matrix type	Full
Final scale factor	0.4421(6)
Extinction parameter refined ?	No
$(\Delta/\sigma)_{max}$ for non-hydrogen atoms	0.052
$(\Delta/\sigma)_{av}$ for non-hydrogen atoms	0.0025
$(\Delta\rho)_{min}$, $(\Delta\rho)_{max}$ / eÅ^{-3}	-3.47, 2.18
Scattering factors used	Ref. [79]
Computer	Fujitsu S-4 / IX
Computational program	*Xtal3.2*[80]

2-3 Results and discussion

2-3-1 Structures of 7 and 8

2-3-1-1 X-ray crystallography

The molecular structures of [$Cp^*RhP(OEt)_3(\mu$-$WOS_3)CuCl$] (7) and [{$Cp^*RhP(OEt)_3(\mu$-$WOS_3)(CuCl)Cu\}_2(\mu$-$Cl)_2$]$(DMF)_2$ (8·$(DMF)_2$) determined by single-crystal X-ray diffraction measurements are shown in Figures 2-2 and -3, respectively. The fractional coordinates and equivalent isotropic thermal parameters of non-hydrogen atoms of 7 and 8·$(DMF)_2$ are collected in Tables 2-3 and -5, respectively, and bond lengths and angles of 7 and 8·$(DMF)_2$ in Tables 2-4 and -6, respectively.

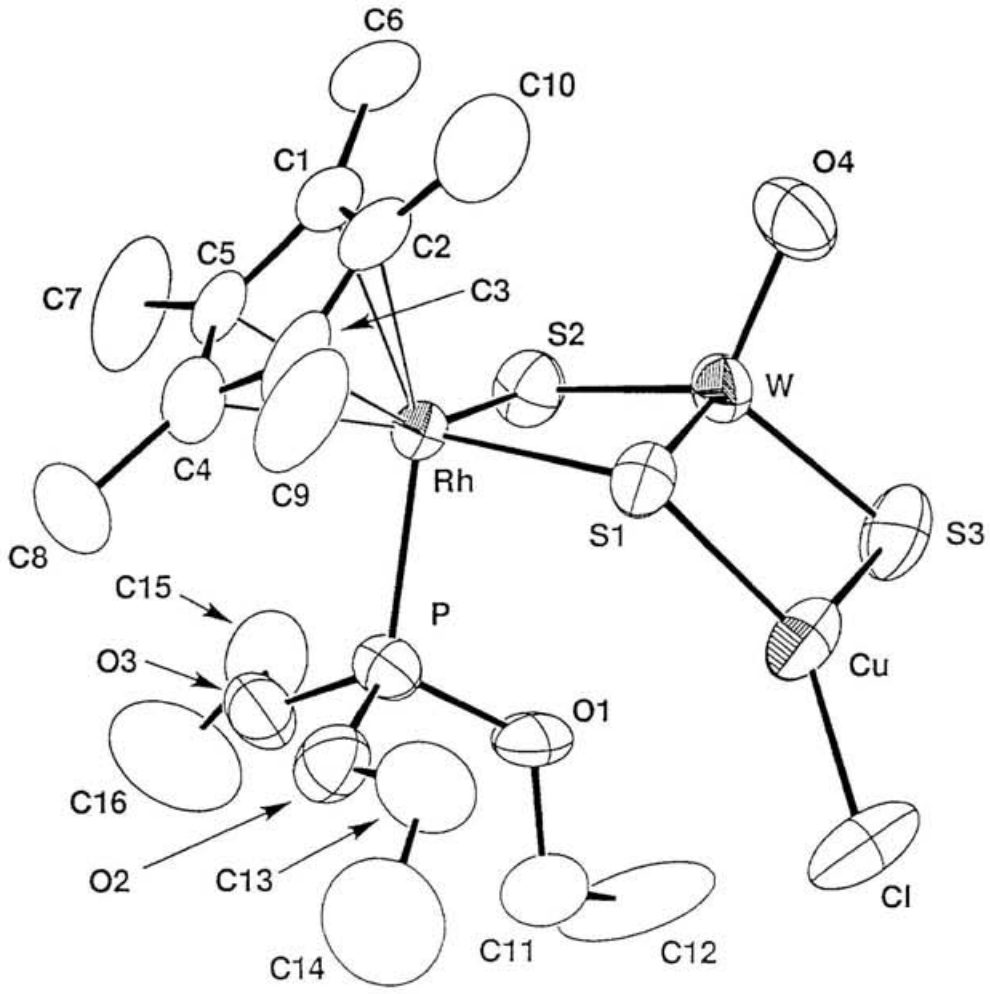

Figure 2-2. ORTEP drawing of [$Cp^*RhP(OEt)_3(\mu$-$WOS_3)CuCl$] (7)

Table 2-3. Fractional coordinates and equivalent isotropic thermal parameters (U_{eq}[81]/ Å^2) of non-hydrogen atoms for [Cp*RhP(OEt)$_3$(μ-WOS$_3$)CuCl] (**7**)

	x / *a*	y / *b*	z / *c*	U_{eq}
W	0.25000	0.40823(3)	0.58128(5)	0.0433(2)
Rh	0.28021(9)	0.52527(6)	0.38125(9)	0.0329(3)
Cu	0.3478(2)	0.4888(1)	0.7557(2)	0.0566(7)
Cl	0.4253(4)	0.5572(4)	0.8947(5)	0.084(2)
S(1)	0.3881(3)	0.4745(2)	0.5394(4)	0.044(1)
S(2)	0.1434(3)	0.4704(3)	0.4731(4)	0.046(1)
S(3)	0.2275(4)	0.4123(3)	0.7939(4)	0.066(2)
O(4)	0.265(1)	0.3133(6)	0.533(1)	0.063(4)
P	0.2639(3)	0.6358(2)	0.4986(3)	0.040(1)
O(1)	0.248(1)	0.6186(6)	0.6467(9)	0.053(3)
O(2)	0.3455(9)	0.6954(8)	0.491(1)	0.055(4)
O(3)	0.1850(9)	0.6947(7)	0.454(1)	0.055(4)
C(1)	0.259(2)	0.4572(9)	0.192(1)	0.052(5)
C(2)	0.354(2)	0.458(1)	0.217(1)	0.058(6)
C(3)	0.385(1)	0.537(1)	0.224(1)	0.057(6)
C(4)	0.307(1)	0.587(1)	0.195(2)	0.055(6)
C(5)	0.226(1)	0.538(1)	0.183(1)	0.044(5)
C(6)	0.195(2)	0.390(2)	0.172(2)	0.08(1)
C(7)	0.131(2)	0.564(2)	0.144(3)	0.09(1)
C(8)	0.312(2)	0.673(1)	0.169(3)	0.078(9)
C(9)	0.480(2)	0.558(2)	0.231(2)	0.09(1)
C(10)	0.409(3)	0.388(2)	0.230(3)	0.10(1)
C(11)	0.242(2)	0.678(1)	0.743(2)	0.061(6)
C(12)	0.173(3)	0.652(3)	0.834(3)	0.13(2)
C(13)	0.439(2)	0.676(1)	0.546(3)	0.079(9)
C(14)	0.489(4)	0.747(3)	0.578(6)	0.14(2)
C(16)	0.035(2)	0.740(2)	0.461(5)	0.11(2)
C(15)	0.089(1)	0.670(2)	0.457(2)	0.066(7)

Table 2-4. Bond lengths (l / Å), angles (ϕ / °), and selected contact distances (d / Å) of $[Cp^*RhP(OEt)_3(\mu\text{-}WOS_3)CuCl]$ (**7**)

Bond lengths	(l / Å)		
W-S1	2.346(4)	P-O1	1.57(1)
W-S2	2.185(4)	P-O2	1.57(1)
W-S3	2.207(4)	P-O3	1.60(1)
W-O4	1.72(1)	O1-C11	1.43(2)
Rh-S1	2.419(4)	O2-C13	1.50(3)
Rh-S2	2.393(4)	O3-C15	1.46(2)
Rh-P	2.264(4)	C1-C2	1.40(3)
Rh-C1	2.29(1)	C1-C5	1.48(2)
Rh-C2	2.31(2)	C1-C6	1.49(4)
Rh-C3	2.22(2)	C2-C3	1.44(3)
Rh-C4	2.22(2)	C2-C10	1.45(4)
Rh-C5	2.20(1)	C3-C4	1.44(3)
Cu-Cl	2.166(6)	C3-C9	1.42(3)
Cu-S1	2.308(4)	C4-C5	1.45(2)
Cu-S3	2.222(6)	C4-C8	1.50(3)
		C5-C7	1.50(3)
Bond Angles	(ϕ / °)		
S1-W-S2	105.9(1)	Rh-S1-Cu	116.2(2)
S1-W-S3	107.0(2)	W-S2-Rh	78.8(1)
S1-W-O4	107.5(5)	W-S3-Cu	74.2(2)
S2-W-S3	112.5(2)	Rh-P-O1	111.9(4)
S2-W-O4	114.2(5)	Rh-P-O2	116.5(5)
S3-W-O4	109.4(4)	Rh-P-O3	117.3(5)
S1-Rh-S2	97.5(1)	O1-P-O2	106.3(7)
S1-Rh-P	90.9(1)	O1-P-O3	106.9(7)
S2-Rh-P	92.1(1)	O2-P-O3	96.4(7)
Cl-Cu-S1	124.1(2)	P-O1-C11	123(1)
Cl-Cu-S3	127.9(2)	P-O2-C13	121(1)
S1-Cu-S3	107.8(2)	P-O3-C15	120(1)
W-S1-Rh	75.3(1)	O1-C11-C12	105(2)
W-S1-Cu	70.1(1)	O2-C13-C14	110(3)
		O3-C15-C16	106(2)

Table 2-4. (Continued)

Contact distances (d / Å)			
Rh-W	2.910(1)	W-Cu	2.672(2)

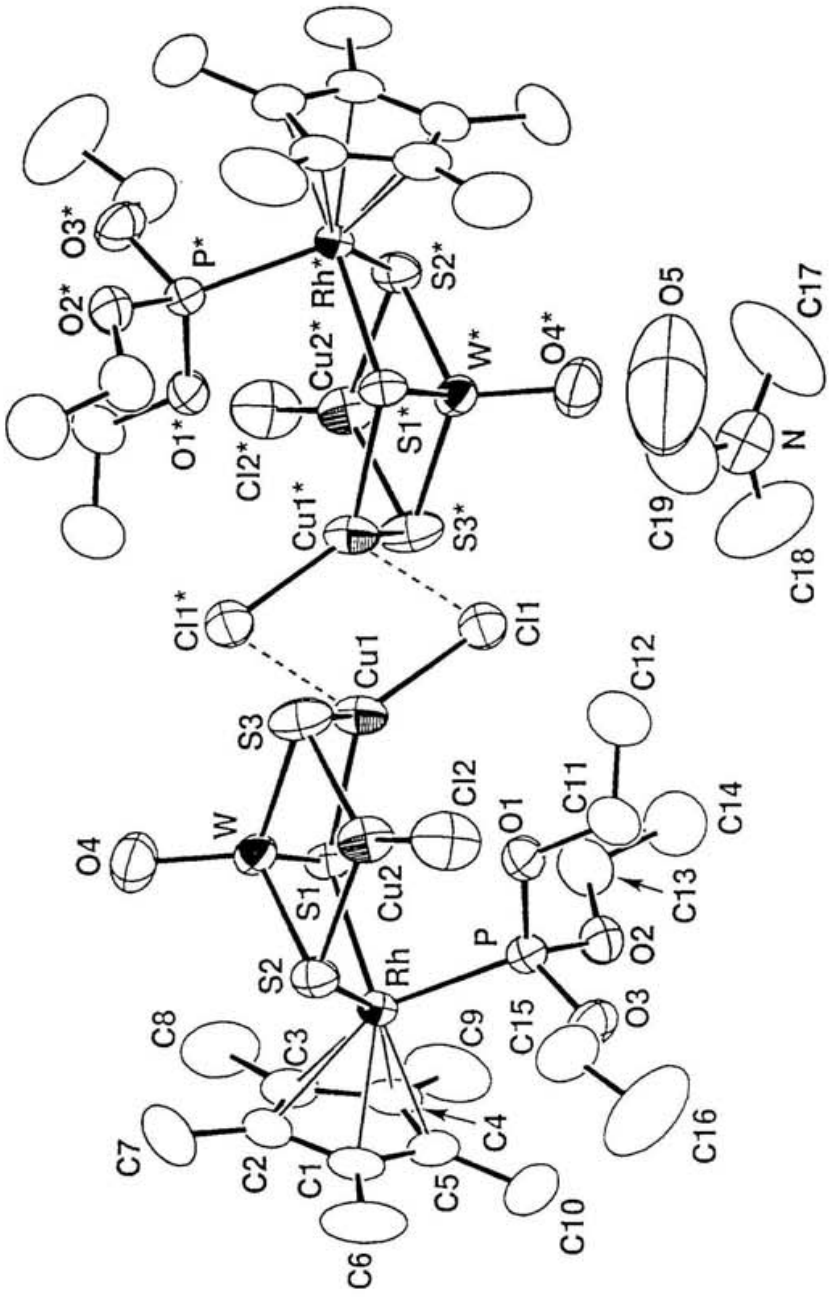

Figure 2-3. ORTEP drawing of $[\{Cp^*RhP(OEt)_3(\mu\text{-}WOS_3)(CuCl)Cu\}_2(\mu\text{-}Cl)_2]\cdot(DMF)_2$ (8·(DMF)$_2$)

Table 2-5. Fractional coordinates and equivalent isotropic thermal parameters (U_{eq}[82]/ Å^2) of non-hydrogen atoms for [{Cp*RhP(OEt)$_3$ (μ-WOS$_3$)(CuCl)Cu}$_2$(μ-Cl)$_2$](DMF)$_2$ (**8**·(DMF)$_2$)

	x / *a*	y / *b*	z / *c*	U_{eq}
W	1.13251(4)	1.12796(2)	0.33486(2)	0.0378(1)
Rh	1.35934(6)	1.03540(4)	0.29418(3)	0.0306(2)
Cu(1)	1.0381(1)	1.01875(8)	0.41964(6)	0.0497(4)
Cu(2)	0.9765(1)	1.06985(8)	0.22523(6)	0.0508(4)
S(1)	1.2605(2)	1.0454(1)	0.4069(1)	0.0379(7)
S(2)	1.1934(2)	1.1098(1)	0.2218(1)	0.0401(7)
S(3)	0.9143(3)	1.0934(2)	0.3355(2)	0.0568(9)
Cl(1)	0.9801(3)	0.9046(2)	0.4657(1)	0.0573(9)
Cl(2)	0.8603(3)	1.0324(2)	0.1288(2)	0.074(1)
P	1.2549(2)	0.9211(1)	0.2629(1)	0.0368(7)
O(1)	1.0986(6)	0.9250(4)	0.2663(4)	0.049(2)
O(2)	1.3084(7)	0.8459(4)	0.3065(3)	0.049(2)
O(3)	1.2784(7)	0.8882(4)	0.1860(3)	0.053(2)
O(4)	1.1559(8)	1.2227(4)	0.3603(4)	0.067(3)
C(1)	1.5185(9)	1.0698(6)	0.2267(5)	0.046(3)
C(2)	1.5177(9)	1.1281(6)	0.2819(6)	0.054(4)
C(3)	1.5493(9)	1.0904(7)	0.3483(6)	0.057(4)
C(4)	1.5655(8)	1.0083(6)	0.3346(5)	0.048(3)
C(5)	1.5528(8)	0.9970(6)	0.2586(5)	0.044(3)
C(6)	1.505(2)	1.087(1)	0.1460(8)	0.084(6)
C(7)	1.494(2)	1.2138(9)	0.271(2)	0.11(1)
C(8)	1.572(2)	1.127(2)	0.4212(9)	0.111(8)
C(9)	1.614(2)	0.947(1)	0.390(1)	0.089(7)
C(10)	1.586(1)	0.9256(9)	0.218(1)	0.077(6)
C(11)	1.010(1)	0.8598(8)	0.2350(7)	0.067(5)
C(12)	0.912(2)	0.842(1)	0.287(1)	0.105(8)
C(13)	1.291(2)	0.8374(7)	0.3842(7)	0.069(5)
C(14)	1.260(3)	0.758(1)	0.401(1)	0.12(1)
C(15)	1.229(1)	0.9284(9)	0.1195(6)	0.066(5)
C(16)	1.257(3)	0.879(2)	0.060(1)	0.12(1)

Table 2-5. (Continued)

N	0.761(1)	0.6822(6)	0.4890(5)	0.070(4)
C(17)	0.670(3)	0.644(2)	0.532(1)	0.16(1)
C(18)	0.901(3)	0.663(2)	0.492(1)	0.14(1)
C(19)	0.721(2)	0.745(1)	0.454(1)	0.109(8)
O(5)	0.598(2)	0.759(1)	0.453(1)	0.29(2)

Table 2-6. Bond lengths (l / Å), angles (ϕ / °), and selected contact distances (d / Å) of [{Cp*RhP(OEt)$_3$(μ-WOS$_3$)(CuCl)Cu}$_2$(μ-Cl)$_2$](DMF)$_2$ (**8**·(DMF)$_2$)

Bond lengths	**(l / Å)**		
Rh-P	2.270(2)	O1-C11	1.51(1)
Rh-S1	2.410(2)	O2-C13	1.48(2)
Rh-S2	2.411(2)	O3-C15	1.47(1)
Rh-C1	2.198(9)	C1-C2	1.43(1)
Rh-C2	2.27(1)	C1-C5	1.41(1)
Rh-C3	2.28(1)	C1-C6	1.53(2)
Rh-C4	2.184(8)	C2-C3	1.41(2)
Rh-C5	2.204(9)	C2-C7	1.50(2)
W-S1	2.267(2)	C3-C4	1.44(2)
W-S2	2.271(2)	C3-C8	1.50(2)
W-S3	2.264(3)	C4-C5	1.43(1)
W-O4	1.699(7)	C4-C9	1.52(2)
Cu1-Cl1	2.232(3)	C5-C10	1.49(2)
Cu1-Cl1*	2.531(3)	C11-C12	1.47(3)
Cu1-S1	2.305(3)	C13-C14	1.44(2)
Cu1-S3	2.301(3)	C15-C16	1.45(3)
Cu2-Cl2	2.152(3)	N-C17	1.42(3)
Cu2-S2	2.283(3)	N-C18	1.43(3)
Cu2-S3	2.240(3)	N-C19	1.30(2)
P-O1	1.573(7)	C19-O5	1.25(3)
P-O2	1.591(7)		
P-O3	1.579(7)		

Table 2-6. (Continued)

Bond Angles	(ϕ / °)		
S1-W-S2	106.40(8)	W-S2-Cu2	71.35(8)
S1-W-S3	109.2(1)	Rh-S2-Cu2	115.8(1)
S1-W-O4	111.8(2)	W-S3-Cu1	71.76(8)
S2-W-S3	107.92(9)	W-S3-Cu2	72.27(9)
S2-W-O4	110.4(3)	Cu1-S3-Cu2	110.6(1)
S3-W-O4	110.9(3)	Rh-P-O1	112.9(3)
S1-Rh-S2	97.81(8)	Rh-P-O2	116.1(3)
S1-Rh-P	94.07(8)	Rh-P-O3	116.1(3)
S2-Rh-P	91.86(8)	P-O1-C11	120.5(7)
S1-Cu1-S3	106.6(1)	P-O2-C13	121.2(7)
S1-Cu1-Cl1	120.0(1)	P-O3-C15	122.5(7)
S3-Cu1-Cl1	127.3(1)	O1-C11-C12	107(1)
S2-Cu2-S3	108.3(1)	O2-C13-C14	111(1)
S2-Cu2-Cl2	120.7(1)	O3-C15-C16	108(1)
S3-Cu2-Cl2	130.5(1)	C17-N-C18	122(2)
W-S1-Rh	77.33(7)	C17-N-C19	119(2)
W-S1-Cu1	71.64(7)	C18-N-C19	118(2)
Rh-S1-Cu1	123.48(9)	N-C19-O5	115(2)
W-S2-Rh	77.25(7)		
Contact distances	(d / Å)		
Rh-W	2.9241(9)	W-Cu1	2.676(1)
W-Cu2	2.656(1)	Cu1-Cu1*	3.227(2)

As shown in Figure 2-2 [$Cp^*RhP(OEt)_3(\mu$-$WOS_3)CuCl$] (**7**), in which the three metal atoms are arranged in a right-angled fashion (Rh-W-Cu = 91.87°) and the S1 atom has a μ_3-coordination mode, has a butterfly-type framework:

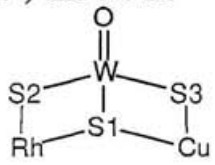

The W-O bond distance (1.72(1) Å) is in the normal double bond distance range.[83]

As depicted in Figure 2-3 [{$Cp^*RhP(OEt)_3(\mu$-$WOS_3)(CuCl)Cu\}_2(\mu$-$Cl)_2$] (**8**) has the linked incomplete cubane-type octanuclear framework in which the two incomplete cuboidal subunits, $M_4(\mu_3\text{-}S)_3$ (M = Rh, W, and Cu), are linked by the two Cu-(μ_2-Cl)···Cu bridges. The W atom has a distorted tetrahedral coordination geometry with one terminal O and three μ_3-S atoms. Although both Cu1 and Cu2 have a trigonal planar coordination geometry with two S and one Cl atoms, Cu1 has a weak interaction with the neighboring Cl* atom in the

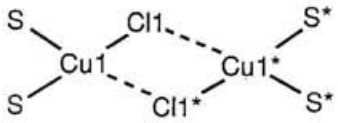

system, in which distances of Cu1-Cl1 and Cu1-Cl1* are 2.232(3) and 2.531(3) Å, respectively.[84] A steric hindrance of the $P(OEt)_3$ groups prevents from the Cu1 (or Cu1*) atom's having a tetrahedral coordination geometry, and reflecting the week interaction between Cu1Cl1 and Cu1*Cl1* in cluster **8**.

In addition the structure of **8** is intriguing in comparison with the geometrical structure[85] of the Fe/Mo/S units in nitrogenase as shown in Figure 2-4 because such linked incomplete cubane-type structures with the $M_4(\mu_3\text{-}S)_3$ frameworks are rare. In cluster **8** the $[WOS_3]^{2-}$ unit forms a framework of a half cubane with the oxygen ligand exhibiting less affinity toward the Rh or Cu atoms than the sulfur ligands.

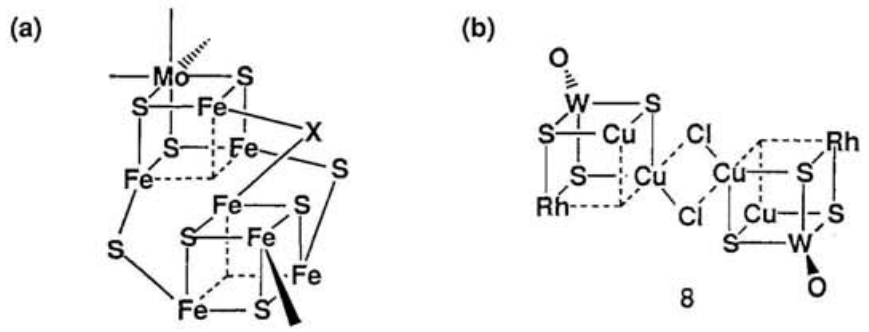

Figure 2-4. (a) Possible structure of the Fe/Mo/S units in nitrogenase based on X-ray structure determination. (X = a light atom N, O, ?).
(b) The simplified expression of the framework of [{Cp*RhP(OEt)$_3$(μ-WOS$_3$)(CuCl)Cu}$_2$(μ-Cl)$_2$] (**8**).

2-3-1-2 Infrared spectroscopy

As shown in Figure 2-5 the IR spectrum in the ν_{W-S} region of [Cp*RhP(OEt)$_3$(μ-WOS$_3$)CuCl] (**7**) measured in dichloromethane shows two ν_{W-S} bands at 466 and 445 cm^{-1}, and in acetonitrile at 465 and 446 cm^{-1}; these values agree well with those obtained in the solid state (in mineral oil) at 460 and 444 cm^{-1}. Therefore, the butterfly-type framework of **7** is preserved in dichloromethane and acetonitrile.

The IR spectrum of a dichloromethane solution of [{Cp*RhP(OEt)$_3$(μ-WOS$_3$)(CuCl)Cu}$_2$(μ-Cl)$_2$] (**8**) shows one strong ν_{W-S} band at 442 cm^{-1}; this agrees well with that obtained in the solid state at 440 cm^{-1}, however, of an acetonitrile solution at 465 and 444 cm^{-1}; these values correspond to those of **7** measured in acetonitrile. These results suggest that the coordination geometry around [μ-WOS$_3$]$^{2-}$ of **8** is preserved in dichloromethane, but one CuCl group releases from one [μ-WOS$_3$]$^{2-}$ unit of **8** in acetonitrile.

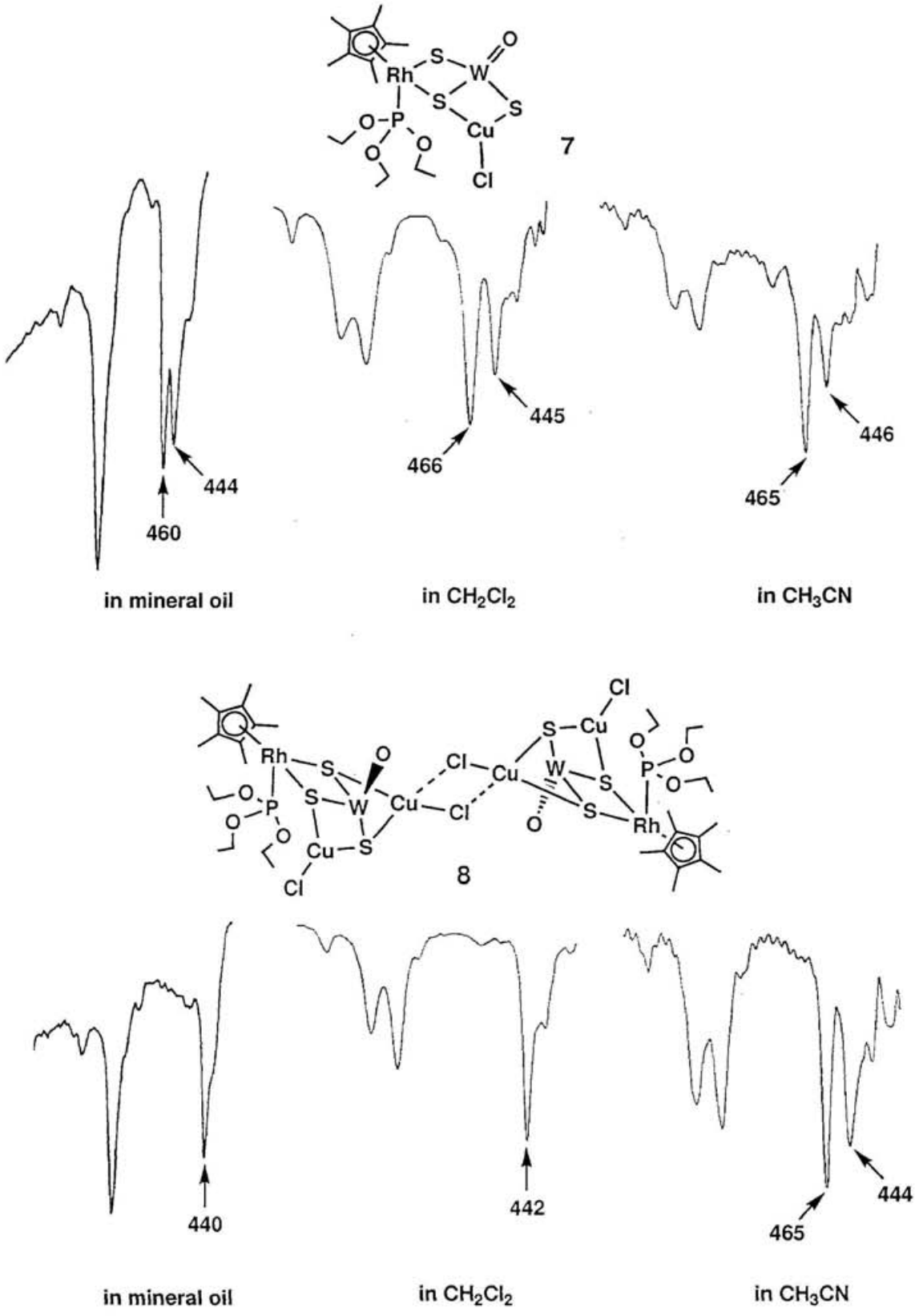

Figure 2-5. IR spectra (cm^{-1}) in the ν_{W-S} regions of **7** and **8** in mineral oil, CH_2Cl_2, and CH_3CN.

2-3-1-3 Vapor pressure osmometry

Vapor pressure osmometry shows that the value of the molecular weight of **7** in dichloromethane is ca. 810, which agrees well with that of the undissociated molecule (calcd for **7** : 799.3). The observed molecular weight of **8** in dichloromethane is ca. 903, which corresponds to half of the molecular weight of **8** in the solid state (calcd for **8** : 1796.7).

Judging from the consequences of both vapor pressure osmometry and infrared spectroscopy of **8** in dichloromethane and acetonitrile, the cleavage in **8** occurs at the chloride bridges, and hence **8** exists in a tetranuclear species, $[Cp^*RhP(OEt)_3(\mu\text{-}WOS_3)(CuCl)_2]$, in dichloromethane, however, exists as $[Cp^*RhP(OEt)_3(\mu\text{-}WOS_3)CuCl]$ (**7**) and CuCl moieties in acetonitrile, similarly to **4**.

2-3-2 Reactivity of 2, 3, and 4 toward water and reactivity of 3, 4, 7, and 8 toward hydrogen sulfide

2-3-2-1 Reactivity of 2, 3, and 4 toward water

The cluster $[\{Cp^*RhP(OEt)_3(\mu\text{-}WS_4)(CuCl)Cu\}_2(\mu\text{-}Cl)_2]$ (**4**) reacts with the water saturated in dichloromethane to give the cluster $[Cp^*RhP(OEt)_3(\mu\text{-}WOS_3)(CuCl)Cu\}_2(\mu\text{-}Cl)_2]$ (**8**) (eq. 2-1). As the reaction proceeds the amount of H_2O in the reaction system decreases, and it was confirmed by ^1H NMR as shown in Figure 2-6 (a). H_2S was not detected by ^1H NMR or by an H_2S gas detector tube.

$$[\{Cp^*RhP(OEt)_3(\mu\text{-}WS_4)(CuCl)Cu\}_2(\mu\text{-}Cl)_2] + 2\,H_2O \rightarrow [\{Cp^*RhP(OEt)_3(\mu\text{-}WOS_3)(CuCl)Cu\}_2(\mu\text{-}Cl)_2] + 4\,H^+ + 2\,S^{2-} \quad \text{(eq. 2-1)}$$

A tentative mechanism of the transformation reaction, **4** → **8**, is shown in Figure 2-6 (b). The water molecules saturated in dichloromethane interact with the W and S4 atoms of **4** to give an intermediary species that has W-O-H and Cu-S4-H groups, and then it is transformed to **8**. The reasons the H_2O molecule specifically interacts the S4 atom in the four S atoms of $[\mu\text{-}WS_4]^{2-}$ group in cluster **4** are that the S1 and S2 atoms are covered with the balky Cp* and $P(OEt)_3$ groups to prevent from the

H_2O molecules' approaching, and the S4 atom has more lone pairs of electrons to easily interact with the H_2O molecule than the S3 atom.

The reaction of **4** with water under two-phase conditions (water : dichloromethane = 1 :1) for 48 hours at room temperature gave peaks due to **3** (ca. 50%, calculated by ^1H NMR based on the signal intensity of Cp*), **7** (ca. 28%), **1** (ca. 9%), and uncharacterized products.

On the other hand, clusters **2** and **3** are little reacted with the water saturated in dichloromethane or water under two-phase conditions (water : dichloromethane = 1 :1).[86] It seems that the differences in the reactivity of the W-S-(Cu) groups of clusters **2**, **3**, and **4** toward water are dependent on the differences in the W atoms' electron densities, which are influenced by the strength of the π-electron donations from the S atoms. The W atoms of cluster **4** have the less electron density than ones of **2** and **3**, and therefore easily attract the water molecules. This view is supported by the investigation of binding energies for X-ray photoelectron spectra of them (see Figure 1-16).

2-3-2-3 Reactivity of 3, 4, 7, and 8 toward hydrogen sulfide

Although **3** does not react with H_2S in dichloromethane, the clusters of **4**, **7**, and **8** does within 15 minutes at room temperature to form **3** as the only major product. These reactions are based on a specific reactivity of the CuCl group(s) in **3**, **4**, **7**, and **8** towards excess H_2S. For example, the reaction (**8** → **3**, eq. 2-2) indicates that one of the two CuCl moieties in **8** and the CuCl moiety in **3** are inert toward excess H_2S.

$$1/2\ [\{Cp^*RhP(OEt)_3(\mu\text{-}WOS_3)(CuCl)Cu\}_2(\mu\text{-}Cl)_2] + 3/2\ H_2S \rightarrow$$
$$[Cp^*RhP(OEt)_3(\mu\text{-}WS_4)CuCl] + 1/2\ Cu_2S + H^+ + Cl^- + H_2O \quad \text{(eq. 2-2)}$$

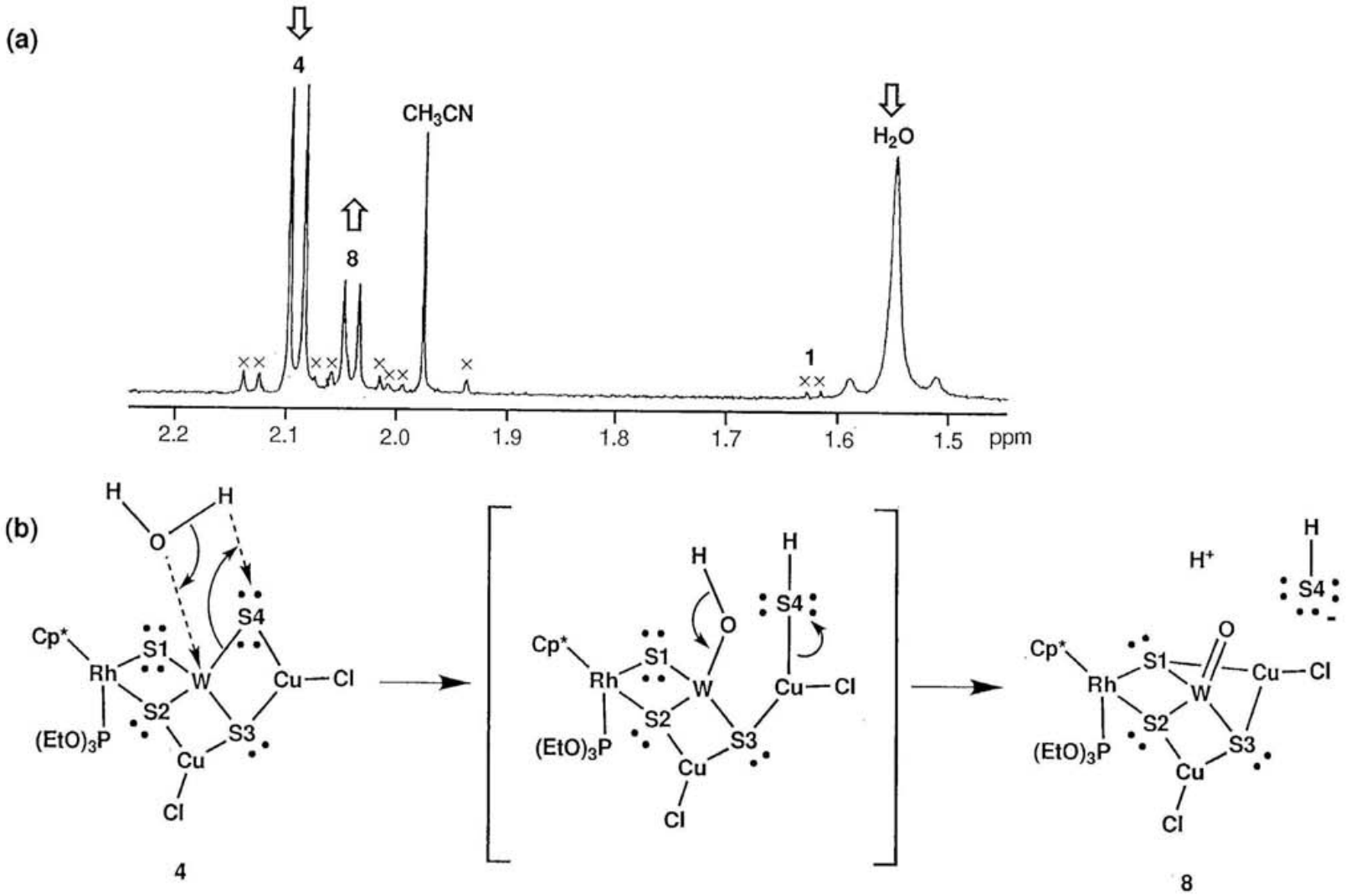

Figure 2-6. (a) A ^{1}H NMR spectrum of a reaction **4** with the water saturated in dichlorometane.
(b) A possible mecanism of a reaction **4** with the water saturated in dichloromethane.

Chapter 3

Synthesis of a linear-type pentanuclear (Rh^{III}-W^{VI}-Cu^{I}-W^{VI}-Rh^{III}) sulfide cluster predicted by fast atom bombardment mass spectrometry

3-1 Introduction

Although single-crystal X-ray analysis plays an important role in the structural characterization of higher-nuclearity sulfide clusters, the technique is limited by the availability of suitable crystals. Extended X-ray absorption fine structure (EXAFS)[87] and fast atom bombardment mass spectrometry (FAB-MS)[88] are useful tools for structural characterization of non-crystalline compounds. In FAB-MS target compounds sometimes produce several ions that are heavier than the molecular ions but these have been neglected in many cases.[89] As shown in the chemistry of fullerenes,[90] however, the heavier ions occasionally give important information on higher-nuclearity clusters that might be synthesized. In Chapter 3, the effectiveness of FAB-MS is examined by the direct synthesis of predicted sulfide clusters.

The positive ion FAB mass spectrum of [Cp*RhP(OEt)$_3$(μ-WS_4)CuCl] (**3**), whose structure is preserved in *m*-nitrobenzylalcohol (NBA) used as a matrix, shows the existence of many ions heavier than the molecular ion. The second highest envelope at m/z 1497 corresponds to an interesting pentanuclear cationic cluster, [{Cp*RhP(OEt)$_3$(μ-WS_4)}$_2$Cu]$^+$ ([**B**]$^+$, Figure 3-1), which is probably produced by the recombination of two [Cp*RhP(OEt)$_3$$WS_4$] fragment ions and a chloride-free Cu^+ ion in the ionization chamber. Hence, it was synthesized by the reaction between [Cp*RhP(OEt)$_3$$WS_4$] (**2**) and Cu^+ in a 2:1 molar ratio to yield [{Cp*RhP(OEt)$_3$(μ-WS_4)}$_2$Cu][PF_6] (**9**·[PF_6]). The structure was determined by a combination of single-crystal X-ray diffraction analysis, Extended X-ray absorption fine structure (EXAFS), and IR measurements. The FAB mass spectrum of **9**·[PF_6] showed that the cationic

cluster $[\mathbf{9}]^+$ is identical with $[\mathbf{B}]^+$ found in the FAB mass spectrum of **3**.

3-2 Experimental section

3-2-1 Methods and materials

Compounds **3** and **9**·$[PF_6]$ are stable to air, but not to moisture. All preparative procedures were routinely carried out under an argon atmosphere. **9**·$[PF_6]$ is unstable to heat, for example, reflux of an acetonitrile solution brings about decomposition gradually. Acetonitrile, 1,2-dichloroethane and ethyl acetate were distilled from calcium hydride. Diethyl ether was distilled from lithium aluminum hydride. The copper complex, $[Cu(CH_3CN)_4][PF_6]$, was purchased from Aldrich Chemicals.

3-2-2 Physical measurements

FAB-MS

Fast atom bombardment (FAB) mass spectra in a positive ion mode were obtained from a SHIMADZU/KRATOS CONCEPT I S mass spectrometer operating at an accelerating potential of 8 kV. Xenon was used to generate the primary ionizing beam. The FAB gun was operated at 7-8 kV and a current of 1 mA. The compound was dissolved in *m*-nitrobenzylalcohol (NBA) and placed on a stainless steel FAB probe tip. The analytical mass range was generally from *m/z* 100 to 1900 with a scan time of 3 sec / decade. The MS system was tuned and calibrated with perfluoroalkyl phosphazine (Ultramark). Daughter ions were determined by linked scans (B / E method).

A conventional $R(I)$ factor,[91] $R(I) = (\Sigma \| \|I_o\| - \|I_c\| \|) / \Sigma |I_o|$, in which I_o and I_c are the observed and calculated intensities, respectively, at a given mass number, was calculated to provide a quantitative measure of the fit between the observed spectrum and calculated isotopomers of the proposed compound. Peaks at least 9 mass units in

each observed envelope were used in this calculation.

EXAFS Analysis

The EXAFS spectra of the Rh-K, Cu-K, and W-L_3 edges were measured in a transmission mode on a BL-10B station of Photon Factory, the National Laboratory for High Energy Physics (KEK-PF), using synchrotron radiation at 70 K for Cu-K and W-L_3 edges and 296 K for Rh-K edge. X-Ray was monochromatized with a Si(311) channel-cut crystal. The storage ring was operated at 2.5 GeV and the ring current was in the range 100-300 mA. The intensity of the incident beam, I_0, and that of the transmitted beam, I, were measured with the ionization chambers, which were placed before and after the sample, respectively. N_2 and N_2 / Ar (75:25) gases were used in the I_0 and I ionization chambers for both Cu-K and W-L_3 edges, while Kr gas was used in the I_0 and I ionization chambers for the Rh-K edge. The lengths of I_0 and I ionization chambers were 17 cm and 34 cm, respectively. The samples were ground to fine powder and mixed with wheat flour to make homogeneous self-supported disks by pressing them up to 400 kgf / cm^2.

The data analyses were carried out by using the EXAFS analysis program package "*REX ver. 2.04*" kindly supplied by Rigaku Co.[92] The EXAFS oscillations were subtracted from the absorption coefficient by using spline smoothing method and normalized by the edge height. The energy dependence of edge height was taken into account by using McMaster equation.[93] The threshold energy (E_0) was determined by the inflection point of absorption edge. The k^3-weighted EXAFS oscillation were Fourier transformed over photoelectron wavenumber (k) range of 3.0 - 16.6 $Å^{-1}$, 3.0 - 15.5 $Å^{-1}$, 3.0 - 18.0 $Å^{-1}$ for Cu-K, Rh-K, and W-L_3 edges with the Hanning window functions.[94] For the present work we only paid attention to the second coordination shell. Thus the interatomic distance (r) space data were Fourier filtered in k-space over 2.2-3.1Å, 2.3-3.2Å, and 2.1-3.0Å for Cu, Rh, and W data, respectively. Curve fitting analysis was carried out using reference compounds. The total numbers of freedom

(defined as $2\Delta k\Delta r / \pi$) should be about 8, 7, and 8.6. The reference compounds were [Cp*RhP(OEt)$_3$(μ-WS$_4$)CuCl] (**3**) and [{Cp*RhP(OEt)$_3$(μ-S$_2$)}$_2$W][BPh$_4$]$_2$ (**5**·[BPh$_4$]$_2$). The Fourier transformations of these reference compounds were carried out in the same range as the unknown compounds. The non-linear least square fitting was carried out using Newton method. A $R(\chi)$ factor defined as the equation, $R(\chi) = \{\Sigma(\chi_{obs} - \chi_{cal})^2 / \Sigma\chi_{obs}^2\}^{1/2}$, was used to estimate the degree of fitting.

Fitting parameters were interatomic distance (r), coordination number (N), shift of E_0 and Debye-Waller factor (σ). Error estimation was carried out by changing the analytical procedure (k-range and k-weight). Curve fitting analyses were carried out using reference compounds. The effect of multiple scattering can be neglected because the angles of Cu-S-W and W-S-Rh are less than 100 deg.[95]

3-2-3 Preparation of [{Cp*RhP(OEt)$_3$(μ-WS$_4$)}$_2$Cu][PF$_6$] (**9**·[PF$_6$])

To an acetonitrile solution (120 cm^3) of [Cp*RhP(OEt)$_3$WS$_4$] (**2**) (1.00 g, 1.40 mmol) was added an acetonitrile solution (30 cm^3) of [Cu(CH$_3$CN)$_4$][PF$_6$] (0.26 g, 0.70 mmol) at room temperature. After stirring for 10 h, the red solution was concentrated to 50 cm^3 under a reduced pressure. Diethyl ether (200 cm^3) was added to the concentrate to give a red precipitate of **9**·[PF$_6$], which was collected by filtration, washed with diethyl ether (10 cm^3) and dried *in vacuo* (1.05 g, 91% yield). Anal. Found: C, 23.25; H, 3.41%. Calcd for $C_{32}H_{60}CuF_6O_6P_3Rh_2S_8W_2$: C, 23.42; H, 3.68%. ^{1}H NMR : (CD_2Cl_2, 23 °C, TMS) δ 1.33 (t, $^3J_{H,H}$ = 7.0 Hz, 18H, -CH$_2$C*H*$_3$), 2.06 (d, $^4J_{P,H}$ = 5.2 Hz, 30H, -C*H*$_3$(Cp*)), 4.05 (dq, $^3J_{P,H}$ = 7.0 Hz, $^3J_{H,H}$ = 7.0 Hz, 12H, -C*H*$_2$-). IR (mineral oil): ν_{W-S} = 470, 444 cm^{-1}, (CH_2Cl_2): 476, 446 cm^{-1}.

3-2-4 X-ray crystallographic study of 9·[PF_6]

Crystallographic data, experimental conditions, and refinement details of X-ray analysis for 9·[PF_6] are collected in Tables 3-1.

Table 3-1. Crystallographic data, experimental conditions, and refinement details of X-ray analysis for [{Cp*RhP(OEt)$_3$(μ-WS_4)}$_2$Cu][PF_6] (9·[PF_6])

Crystal data	
Compound	[{(η^5-C_5Me_5)RhP(OEt)$_3$(μ-WS_4)}$_2$Cu][PF_6]
Chemical formula	$C_{32}H_{60}CuF_6O_6P_3Rh_2S_8W_2$
Formula weight	1641.27
Solvent for crystallization	1,2-Dichloroethane / ethyl acetate
Color of crystal	Red
Shape of crystal	Plate
Size of specimen / mm^3	0.40 × 0.40 × 0.10
Crystal mount	Glass fiber
Crystal system	Triclinic
Laue group	$\bar{1}$
Systematic absence	None
Possible space group	$P1$, $P\bar{1}$
Space group (number)	$P\bar{1}$ (No. 2)
No. and range (/ °) of reflections used in the least-squares refinement of cell dimensions	24 $20 < 2\theta < 25$
Lattice constants	
a / Å	14.63(1)
b / Å	19.43(2)
c / Å	10.337(7)
α / °	102.28(6)
β / °	99.49(6)
γ / °	100.47(7)
V / Å^3	2760(4)
Z	2
D_x / g cm^{-3}	1.975
μ(Mo Kα) / cm^{-1}	56.3
F(000)	1588

Table 3-1. (Continued)

Data collection	
Instrument	AFC-5R
(voltage, current)	(50 kV, 120 mA)
X-ray tube	Normal-focus
Radiation (wave length, λ / Å)	Mo K_α (0.71073)
Monochromator	Graphite
Collimator diameter / mm	1.0
Temperature / °C	23
Scan method	$\theta - 2\theta$
Scan width / °	$1.9 + 0.5\tan\theta$
Scan speed (in θ) / ° min^{-1}	16
2θ range / °	$2\theta \leq 55$
Range of h, k, l	$0 \leq h \leq 21$, $-27 \leq k \leq 27$, $-15 \leq l \leq 15$,
No. of reflections collected	11131
No. of independent reflections	10749
R_{int}	0.059
No. and frequency of standard reflections	3 and 150
Variation in standard reflections ($\Sigma(\lvert F_o \rvert / \lvert F_o \rvert_{initial})/n$)	1.004 - 0.995
Data reduction	
Lorentz and polarization corrections	Yes
Corrections for decay	No
Absorption corrections method	Empirical Ψ scan[96]
Transmission factor, A	0.6366 - 1

Table 3-1. (Continued)

Structure analysis	
Method used in structure solution	Usual heavy-atom method
Total no. of hydrogen atoms	60
Treatment of hydrogen atoms	Not included in the structural factor calculation
No. of parameters refined	541
2θ limit used for calculation / °	55
Cutoff criteria	$\|F_o\| > 3\sigma(\|F_o\|)$
No. of independent reflections used for calculation	4551
Atoms refined anisotropically	All non-H
Atoms refined isotropically	None
Weighting scheme	$w^{-1} = \sigma^2(\|F_o\|) + (0.015\|F_o\|)^2$
R[97]	0.135
R_w[98]	0.146
S[99]	3.883
Matrix type	Full
Final scale factor	0.537(2)
Extinction parameter refined ?	No
$(\Delta/\sigma)_{max}$ for non-hydrogen atoms	4.533
$(\Delta/\sigma)_{av}$ for non-hydrogen atoms	0.4949
$(\Delta\rho)_{min}$, $(\Delta\rho)_{max}$ / eÅ^{-3}	-6.74, 10.79[100]
Scattering factors used	Ref. [101]
Computer	Fujitsu S-4/IX
Computational program	*Xtal3.2*[102]

3-3 Results and discussion

3-3-1 FAB mass spectrum of 3

It was determined that the structure of **3** is preserved in *m*-nitrobenzylalcohol (NBA) by ^{1}H NMR measurement. The positive ion FAB mass spectrum of **3** is shown in Figures 3-1 and -2. In the spectrum each envelope gives a wide distribution of isotopomers due to isotopes of W (^{180}W (0.13%), ^{182}W (26.30%), ^{183}W (14.30%), ^{184}W (30.67%), ^{186}W (28.60%)), Cu (^{63}Cu (69.17%), ^{65}Cu (30.83%)) and Cl (^{35}Cl (75.77%), ^{37}Cl (24.23%)). The characteristic isotopic distribution of each envelope was employed to assign it to a specific fragment (Table 3-2). For example, an observed envelope at *m/z* 816 matches well ($R(I) = 0.060$) the calculated isotopic distribution for the molecular ion, $[\mathbf{3}]^+$, as illustrated in Figure 3-3. The spectrum of **3** (Figures 3-1 and -2) shows the existence of higher mass ions in the FAB-MS chamber. The highest mass envelope at *m/z* 1595 and the second one at 1497 correspond to $[2\ (\mathbf{3})$ - Cl$]^+$ (denoted by $[\mathbf{A}]^+$, $R(I) = 0.158$) and $[2\ (\mathbf{3})$ - 2 (Cl) -Cu$]^+$ (denoted by $[\mathbf{B}]^+$, $R(I) = 0.157$, Figure 3-4 (a)), respectively. $[\mathbf{A}]^+$ is a hexanuclear ion which is produced by the recombination of $[\mathbf{3}$ - Cl$]^+$ (*m/z* 781) and **3**. $[\mathbf{B}]^+$ is a pentanuclear ion that probably contains a chloride-free Cu^+ ion and two $[Cp^*RhP(OEt)_3WS_4]$ units. As shown in Figure 3-5 a linked scan (B / E method) of $[\mathbf{A}]^+$ gives the intense daughter envelopes at *m/z* 1429 ($[\mathbf{A}$ - **P**$]^+$) and 1263 ($[\mathbf{A}$ - 2**P**$]^+$), and that of $[\mathbf{B}]^+$ at 1331 ($[\mathbf{B}$ - **P**$]^+$) and 1165 ($[\mathbf{B}$ - 2**P**$]^+$; **P** = $P(OEt)_3$).

3-3-2 Synthesis, FAB mass spectrum, and structure of 9·[PF_6]

3-3-2-1 Synthesis of 9·[PF_6]

The $[\mathbf{A}]^+$ ion is not a suitable target for synthesis because it has too many possible geometrical isomers. On the other hand, the $[\mathbf{B}]^+$ ion has fewer possible isomers and the most reasonable structure is a linear Rh-W-Cu-W-Rh pentanuclear framework. Hence, we have tried to prepare the predicted linear pentanuclear cluster

ion, $[\mathbf{B}]^+$, in a laboratory scale using $[Cp^*RhP(OEt)_3WS_4]$ and Cu^+ as building blocks. From a reaction mixture of $[Cp^*RhP(OEt)_3WS_4]$ and $[Cu(CH_3CN)_4][PF_6]$ in a 2:1 molar ratio a red precipitate of $[\{Cp^*RhP(OEt)_3(\mu\text{-}WS_4)\}_2Cu][PF_6]$ ($\mathbf{9}\cdot[PF_6]$) was obtained by addition of diethyl ether. The precipitate is analytically pure, and the elemental analysis gives the expected composition, that is, the hexafluorophosphate salt of the pentanuclear sulfide cluster.

3-3-2-2 FAB mass spectrum of $\mathbf{9}\cdot[PF_6]$

A positive ion FAB mass spectrum of $\mathbf{9}\cdot[PF_6]$ is shown in Figure 3-6. The highest mass envelope (*m/z* 1497) corresponds to the molecular ion $[\mathbf{B}]^+$ ($R(I) = 0.052$, Fig. 3-4 (b)), whose isotopic distribution is identical with that of $[\mathbf{B}]^+$ in the spectrum of **3**. Thus, $[\mathbf{9}]^+$ obtained from the chemical synthesis is the same as $[\mathbf{B}]^+$ found in FAB-MS study of **3**. Of course, $\mathbf{9}\cdot[PF_6]$ does not produce the ion peaks derived from $[\mathbf{A}]^+$ found in the spectrum of **3**.

3-3-2-3 Structure of $\mathbf{9}\cdot[PF_6]$

Recrystallization of $\mathbf{9}\cdot[PF_6]$ from common organic solvents gave only thin plate crystals. A red plate crystal ($0.40 \times 0.40 \times 0.10$ mm^3) obtained from a mixture of 1,2-dichloroethane and ethyl acetate was used for X-ray diffraction. The structural factor calculation did not give a satisfied convergence, which may be due to the poor quality of the crystal. The obtained pentanuclear structure is, however, correct because the other structural data (EXAFS and IR; *vide infra*) support the structure indicated by the X-ray diffraction.

The structure of the pentanuclear cluster in $\mathbf{9}\cdot[PF_6]$ determined by single-crystal X-ray diffraction measurement is given in Figure 3-7 (a) together with the atom numbering scheme. The fractional coordinates and equivalent isotropic thermal parameters of non-hydrogen atoms of $\mathbf{9}\cdot[PF_6]$ are collected in Tables 3-3, and bond lengths and angles in Tables 3-4. In this cluster the five metal atoms (Rh1-W1-Cu-W2-Rh2) are arranged in an approximately linear configuration, and all of S atoms have a

μ_2-coordination mode. The coordination geometries around Rh and W atoms are similar to those of **3**, and the Cu atom in **9**·[PF_6] is coordinated with four S atoms tetrahedrally. As shown in a polyhedral model in Figure 3-7 (b), the two coordination geometries around the Rh atoms are twisted at ca. 90° to each other through the Rh···W···Cu···W···Rh axis. Due to the different coordination geometries around Cu atoms in **3** and **9**·[PF_6], the W···Cu distances in **9**·[PF_6] (av. 2.743 Å) are relatively longer than that in **3** (2.631(1) Å).

The infrared spectrum of **9**·[PF_6] confirms an arrangement around the WS_4 unit which is similar to that in **3**. The values of $\nu_{W\text{-}S}$ bands of **9**·[PF_6] (in mineral oil; 470 and 444 cm^{-1} and in dichloromethane; 476 and 446 cm^{-1}) corresponded closely to those of **3** (in mineral oil; 466 and 446 cm^{-1} and in dichloromethane; 471 and 448 cm^{-1}), suggesting the presence of the $(\mu\text{-S})_2W(\mu\text{-S})_2$ moiety.

Figure 3-8 shows the k^3-weighted Fourier transforms of Cu-K edge EXAFS of **9**·[PF_6]. The most intense peak at about 1.7-2.3 Å in the Fourier transform is due to Cu-S bonds, whereas the second intense peak at about 2.3-3.0 Å in the Fourier transform is due to Cu···W interaction. Curve-fitting analysis on the second Fourier-transformed peak was carried out using the Fourier filtering method. The curve-fitting analysis over several different k regions revealed that the Cu···W distance is 2.75(3) Å, and the coordination number of W is 1.8(5). These values are similar to the X-ray crystallographic data (av. 2.743 Å and 2, respectively) shown in Table 3-5. This result indicates that the coordination number of W is larger than unity and close to 2 within the range of error and it confirms that the cluster **9**·[PF_6] includes a **W···Cu···W** sequence. Similarly the analyses of W-L_3 and Rh-K edge EXAFS support the X-ray crystallographic data (Table 3-5).

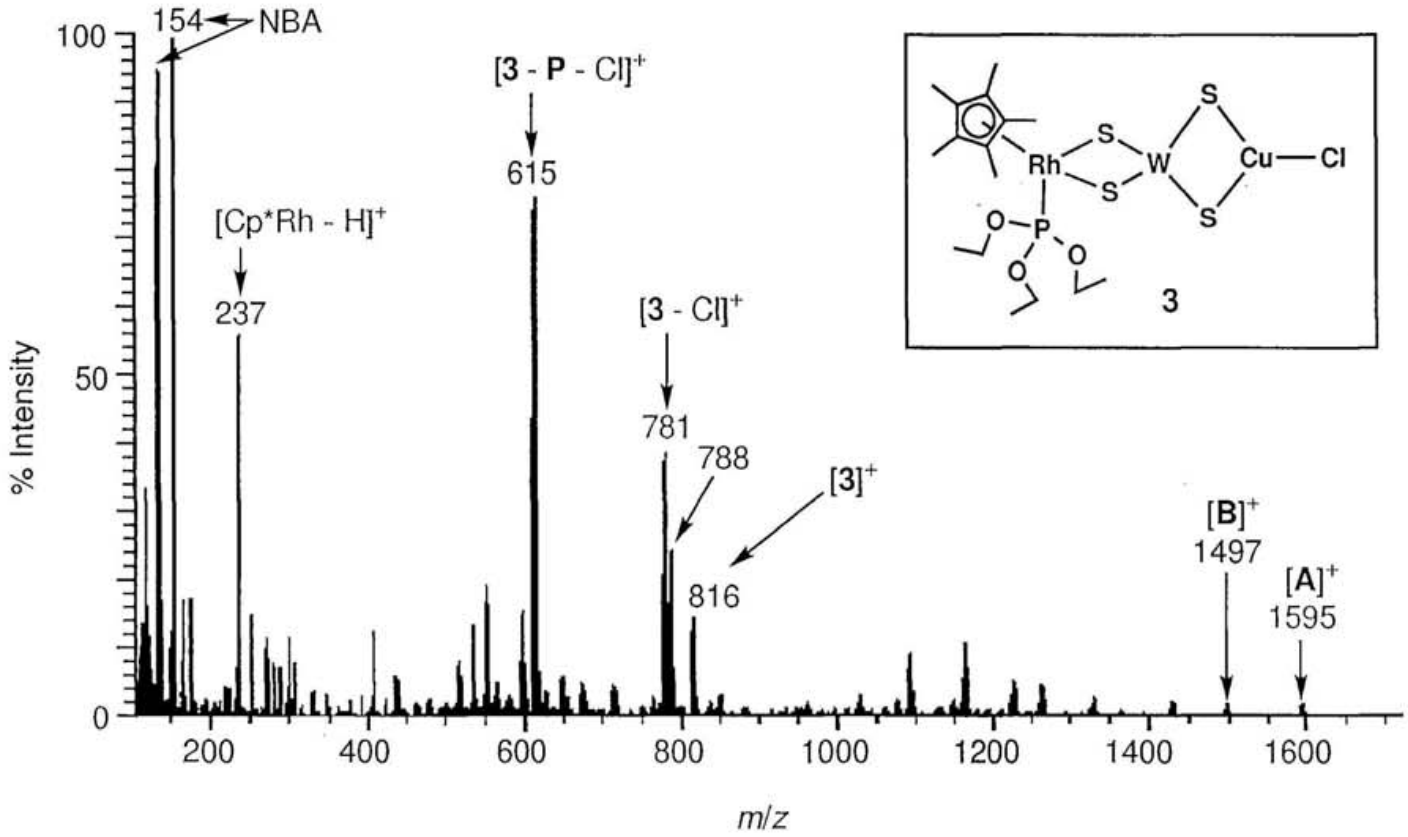

Figure 3-1. Positive ion FAB mass spectrum of $[Cp^*RhP(OEt)_3(\mu\text{-}WS_4)CuCl]$ (**3**).
Abbreviations in this figure: $[\mathbf{3}]^+ = [Cp^*RhP(OEt)_3(\mu\text{-}WS_4)CuCl]^+$, $[\mathbf{A}]^+ = [2\ (\mathbf{3})\ -\ Cl]^+$, $[\mathbf{B}]^+ = [2\ (\mathbf{3})\ -\ 2\ (Cl)\ -\ Cu]^+$, $\mathbf{P} = P(OEt)_3$. Mass envelopes at m/z 788 is unidentified.

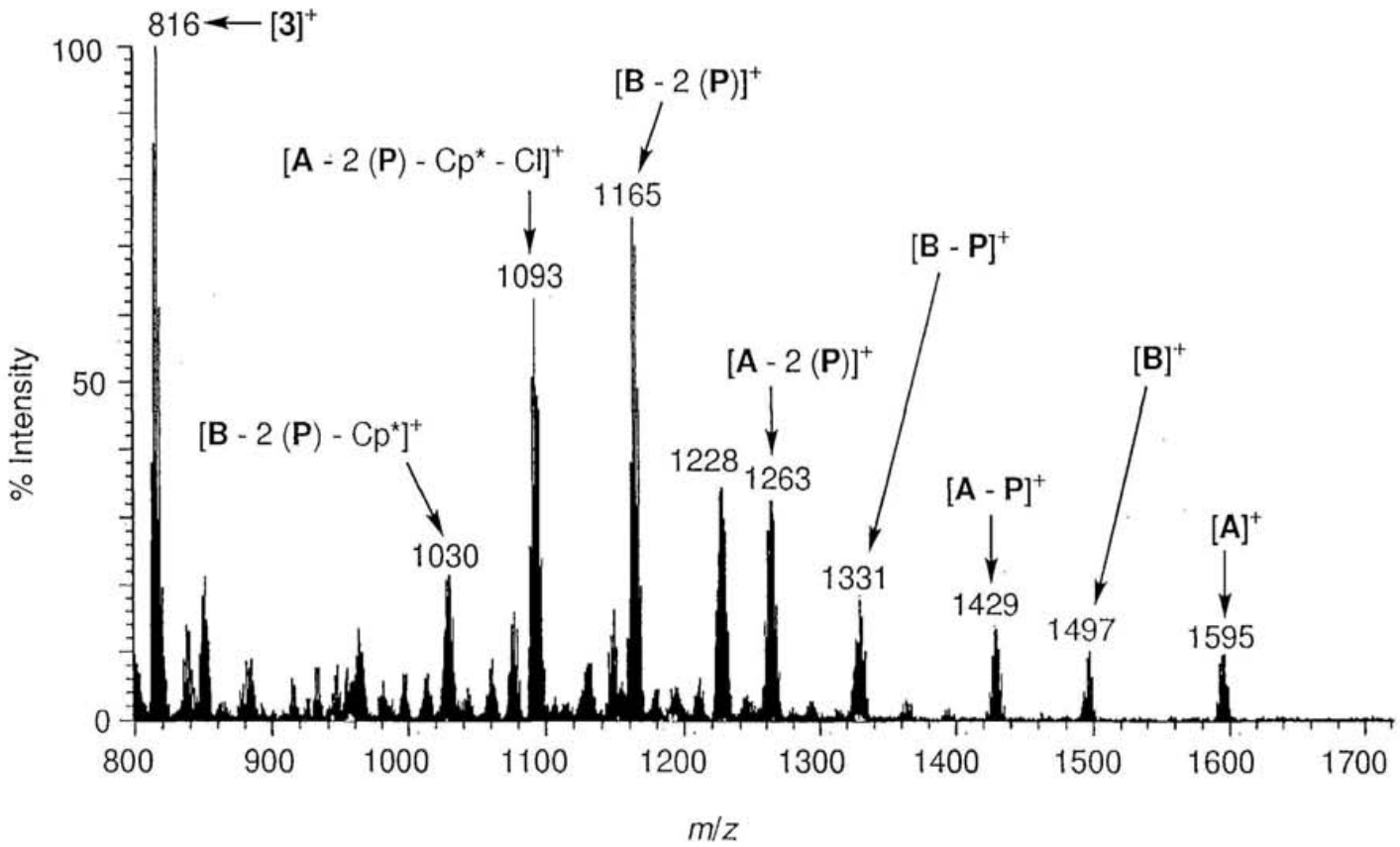

Figure 3-2. An enlargement of positive ion FAB mass spectrum of [Cp*RhP(OEt)$_3$(μ-WS$_4$)CuCl] (**3**). Abbreviations in this figure: [**3**]$^+$ = [Cp*RhP(OEt)$_3$(μ-WS$_4$)CuCl]$^+$, [A]$^+$ = [2 (**3**) - Cl]$^+$, [**B**]$^+$ = [2 (**3**) - 2 (Cl) - Cu]$^+$, **P** = P(OEt)$_3$. Mass envelopes at m/z 1228 is unidentified.

Table3-2. Selected Ions Detected in the FAB Mass Spectra of **3** and **9**·[PF_6][a]

	3			**9**·[PF_6]		
m/z	identification	*R* (*I*) factor[b]	used mass units[c]	identification	*R* (*I*) factor[b]	used mass units[c]
1595	[**A**]$^+$	0.158	11	-	-	-
1497	[**B**]$^+$	0.157	12	[**9**]$^+$	0.052	12
1429	[**A** - **P**]$^+$	0.142	9	-	-	-
1331	[**B** - **P**]$^+$	0.154	9	[**9** - **P**]$^+$	0.118	9
1263	[**A** - 2 (**P**)]$^+$	0.073	11	-	-	-
1165	[**B** - 2 (**P**)]$^+$	0.029	11	[**9** - 2 (**P**)]$^+$	0.024	11
1093	[**A** - 2 (**P**) - Cp* - Cl]$^+$	0.073	11	-	-	-
1030	[**B** - 2 (**P**) - Cp*]$^+$	0.146	9	[**9** - 2 (**P**) - Cp*]$^+$	0.112	9
816	[**3**]$^+$	0.060	9	-	-	-

[a] [**A**]$^+$ = [2 (**3**) - Cl]$^+$, [**B**]$^+$ = [2 (**3**) - 2 (Cl) - Cu]$^+$, **P** = $P(OEt)_3$.

[b] $R(I) = (\Sigma \| |I_o| - |I_c| |) / \Sigma |I_o|$, in which I_o is the observed intensity and I_c is the calculated intensity.

[c] Number of mass units used in the calculations of *R* (*I*) factors.

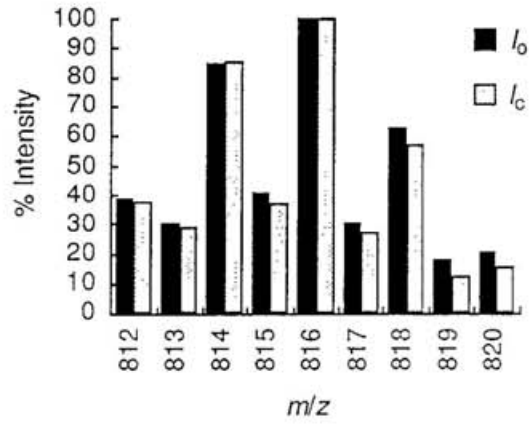

Figure 3-3. Comparison of observed (I_o) and calculated (I_c) FAB mass spectrum in the molecular ion region of [Cp*RhP(OEt)$_3$(μ-WS$_4$)CuCl] (**3**).

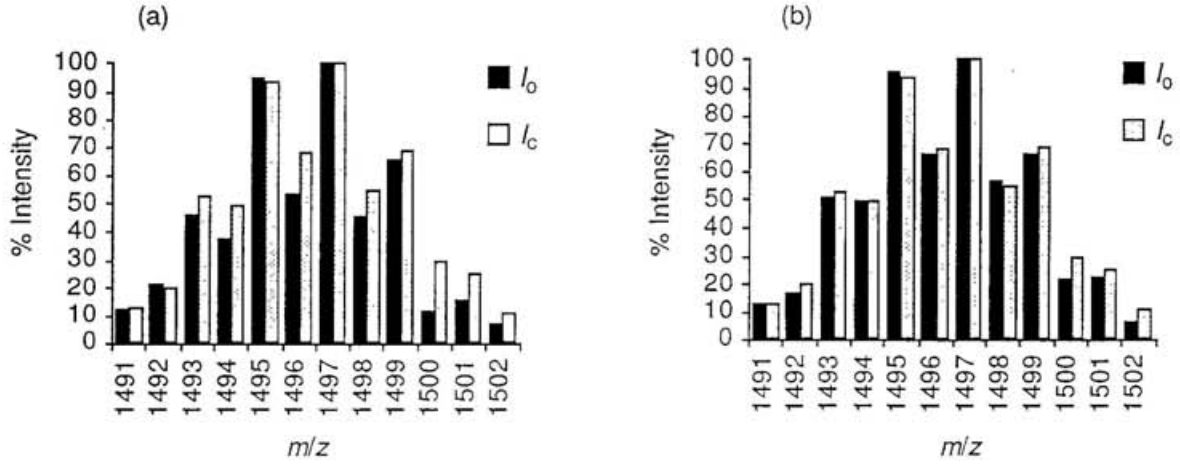

Figure 3-4. (**a**) Comparison of observed (I_o) and calculated (I_c) FAB mass spectrum of [**B**]$^+$.
(**b**) Comparison of observed (I_o)) and calculated (I_c) FAB mass spectrum of [**9**]$^+$.

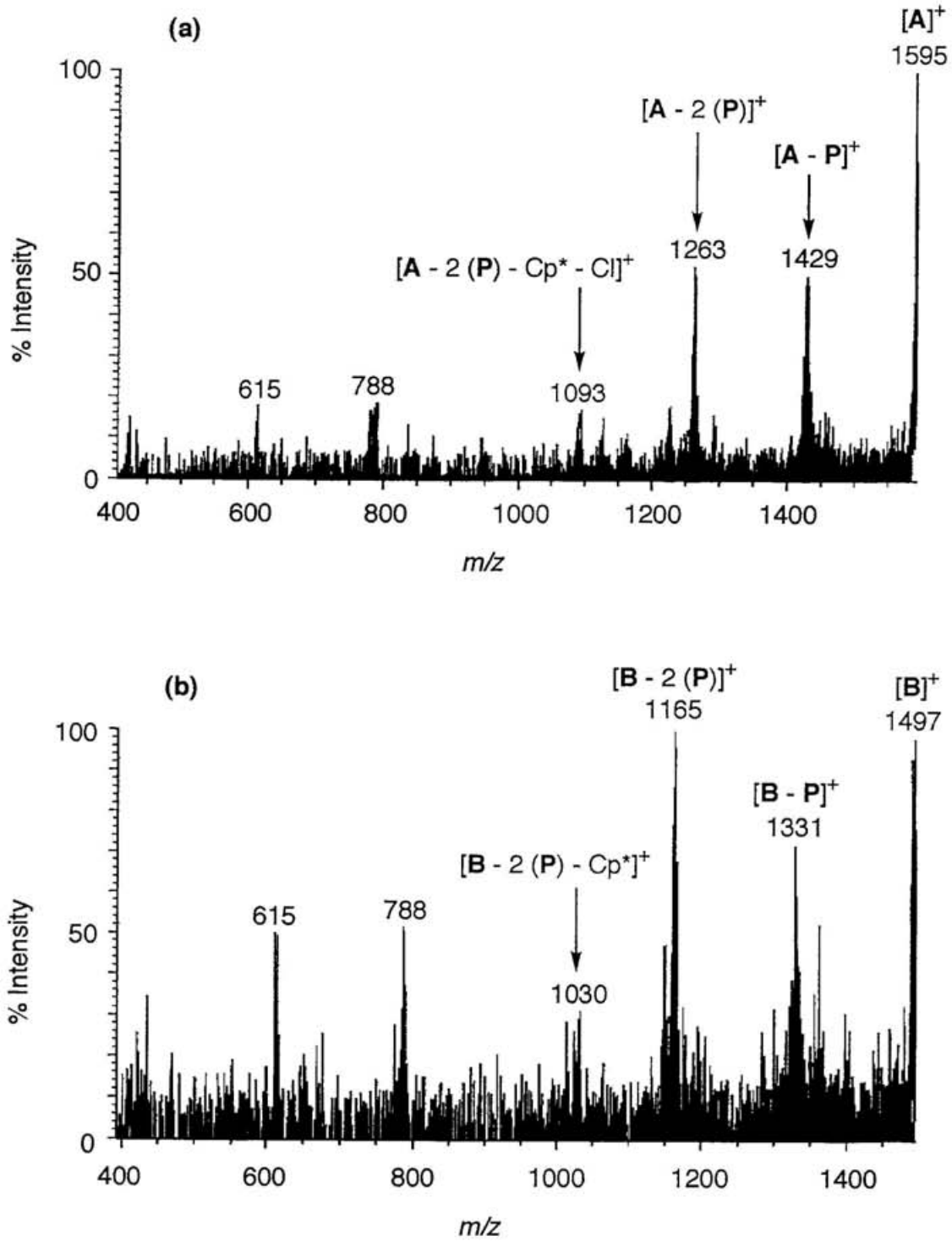

Figure 3-5. **(a)** A linked scan (B/E method) spectrum of $[\mathbf{A}]^+ = [2\ (\mathbf{3})\ -\ Cl]^+$ observed in the FAB mass spectrum of $[Cp^*RhP(OEt)_3(\mu\text{-}WS_4)CuCl]$ (**3**).
(b) One of $[\mathbf{B}]^+ = [2\ (\mathbf{3})\ -\ 2\ (Cl)\ -\ Cu]^+$. Abbreviation: $\mathbf{P} = P(OEt)_3$.

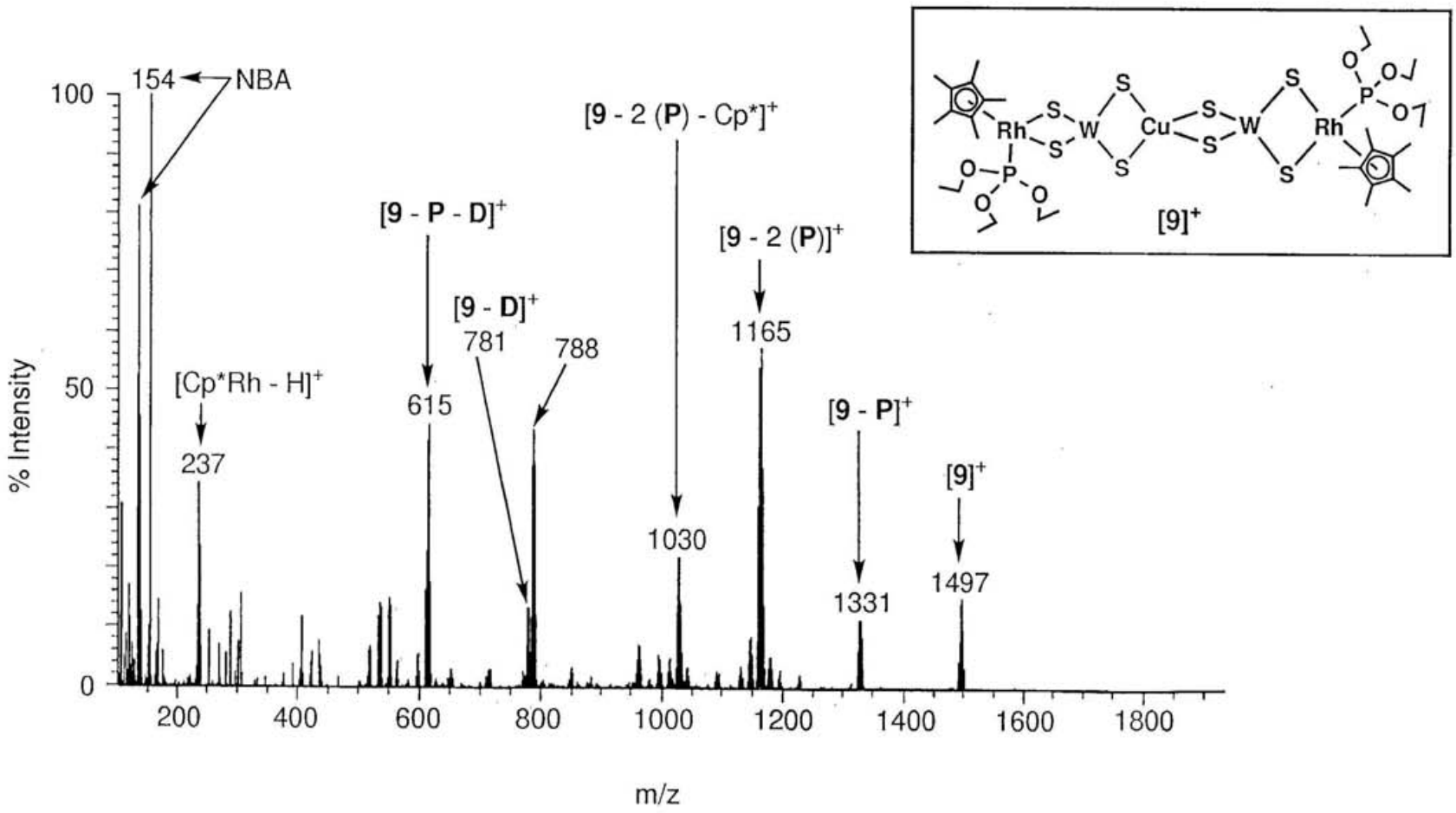

Figure 3-6. Positive ion FAB mass spectrum of $[\{Cp^*RhP(OEt)_3(\mu\text{-}WS_4)\}_2Cu][PF_6]$ ($\mathbf{9}\cdot PF_6$). Abbreviations in this figure: $[\mathbf{9}]^+ = [\{Cp^*RhP(OEt)_3(\mu\text{-}WS_4)\}_2Cu]^+$, **D** = $[Cp^*RhP(OEt)_3WS_4]$, **P** = P(OEt)3. Mass envelope at m/z 788 is unidentified.

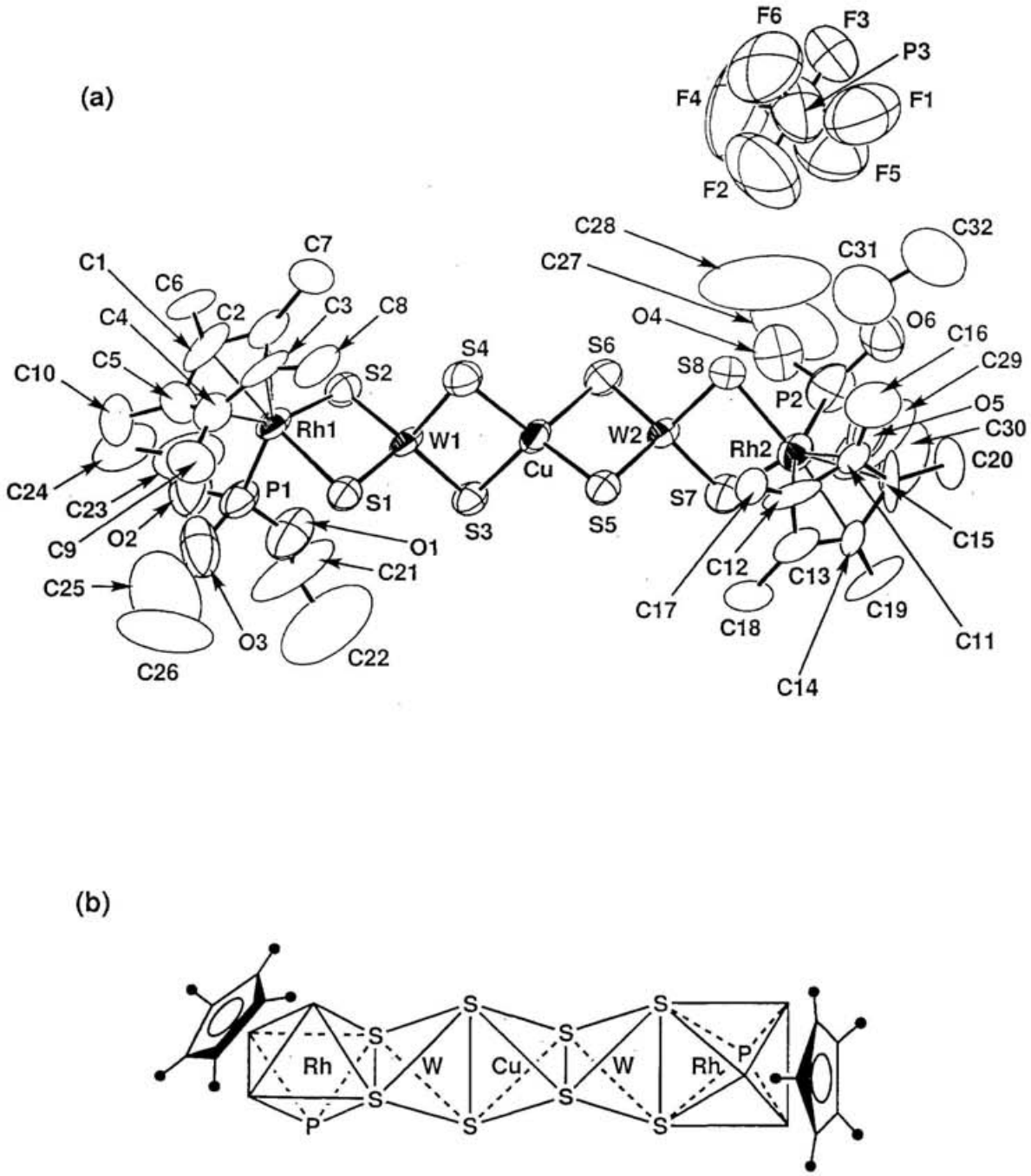

Figure 3-7. (a) ORTEP drawing of $[\{Cp^*RhP(OEt)_3(\mu\text{-}WS_4)\}_2Cu][PF_6]$ (**9**·$[PF_6]$). (b) A polyhedral model of $[\mathbf{9}]^+$.

Table 3-3. Fractional coordinates and equivalent isotropic thermal parameters (U_{eq}[103]/ Å^2) of non-hydrogen atoms for [{Cp*RhP(OEt)$_3$(μ-WS$_4$)}$_2$Cu][PF$_6$] (**9**·[PF$_6$])

	x / *a*	y / *b*	z / *c*	U_{eq}
W1	0.2701(2)	-0.0355(1)	0.6615(2)	0.049(1)
W2	0.1889(2)	0.1757(1)	1.0408(2)	0.047(1)
Rh1	0.2827(4)	-0.1364(3)	0.4189(4)	0.061(2)
Rh2	0.1204(4)	0.2614(3)	1.2543(4)	0.064(2)
Cu	0.2289(6)	0.0705(5)	0.8495(7)	0.060(3)
S1	0.195(1)	-0.1460(9)	0.589(1)	0.061(7)
S2	0.385(1)	-0.0243(9)	0.546(1)	0.063(8)
S3	0.333(1)	-0.0049(9)	0.880(1)	0.058(7)
S4	0.173(1)	0.035(1)	0.619(2)	0.072(9)
S5	0.110(1)	0.0634(9)	0.972(1)	0.060(7)
S6	0.302(1)	0.1913(9)	0.925(2)	0.065(8)
S7	0.251(1)	0.201(1)	1.262(2)	0.073(9)
S8	0.093(1)	0.2517(9)	1.017(1)	0.062(7)
P1	0.377(2)	-0.198(1)	0.514(2)	0.08(1)
P2	0.226(2)	0.365(1)	1.284(2)	0.10(1)
O1	0.418(3)	-0.167(3)	0.669(4)	0.11(3)
O2	0.456(5)	-0.213(4)	0.459(5)	0.13(4)
O3	0.329(6)	-0.279(4)	0.487(5)	0.15(4)
O4	0.296(4)	0.362(3)	1.184(6)	0.12(3)
O5	0.289(4)	0.388(4)	1.435(5)	0.14(3)
O6	0.177(4)	0.435(3)	1.276(5)	0.11(3)
C1	0.301(6)	-0.136(6)	0.212(5)	0.11(5)
C2	0.232(5)	-0.085(5)	0.255(5)	0.08(4)
C3	0.153(5)	-0.137(5)	0.261(5)	0.08(4)
C4	0.173(5)	-0.209(4)	0.243(6)	0.06(3)
C5	0.257(7)	-0.211(4)	0.216(6)	0.09(4)
C6	0.408(5)	-0.091(4)	0.185(6)	0.09(4)
C7	0.233(5)	-0.009(4)	0.259(6)	0.10(4)
C8	0.061(4)	-0.112(4)	0.297(5)	0.09(4)
C9	0.112(5)	-0.279(4)	0.240(6)	0.10(4)
C10	0.313(5)	-0.264(4)	0.165(5)	0.09(3)
C11	-0.028(4)	0.271(4)	1.282(5)	0.06(3)

Table 3-3. (Continued)

C12	-0.029(4)	0.190(5)	1.227(6)	0.09(4)
C13	0.038(4)	0.174(4)	1.339(6)	0.07(3)
C14	0.076(4)	0.238(3)	1.446(5)	0.06(3)
C15	0.042(4)	0.304(4)	1.414(6)	0.09(3)
C16	-0.093(4)	0.310(4)	1.208(7)	0.10(4)
C17	-0.095(4)	0.144(3)	1.112(5)	0.06(2)
C18	0.050(4)	0.098(4)	1.333(6)	0.08(3)
C19	0.148(4)	0.246(4)	1.574(5)	0.10(4)
C20	0.060(5)	0.374(3)	1.499(7)	0.09(3)
C21	0.493(7)	-0.173(8)	0.763(9)	0.2(1)
C22	0.456(8)	-0.19(1)	0.87(1)	0.3(1)
C23	0.54(1)	-0.169(5)	0.459(9)	0.20(8)
C24	0.601(7)	-0.204(6)	0.37(1)	0.17(7)
C25	0.33(1)	-0.34(1)	0.50(2)	0.3(1)
C26	0.28(2)	-0.384(9)	0.51(2)	0.3(2)
C27	0.37(1)	0.413(8)	1.22(2)	0.3(1)
C28	0.38(2)	0.42(1)	1.11(2)	0.4(2)
C29	0.360(7)	0.424(6)	1.60(1)	0.18(7)
C31	0.111(7)	0.432(6)	1.15(1)	0.15(7)
C32	0.104(7)	0.519(6)	1.22(1)	0.18(7)
P3	0.238(5)	0.541(3)	0.857(4)	0.21(3)
F1	0.176(6)	0.578(5)	0.940(8)	0.26(6)
F2	0.187(9)	0.452(5)	0.855(9)	0.34(8)
F3	0.286(6)	0.623(4)	0.864(7)	0.21(5)
F4	0.317(7)	0.512(9)	0.795(9)	0.4(1)
F5	0.301(5)	0.557(4)	1.003(7)	0.23(5)
F6	0.179(6)	0.527(4)	0.714(6)	0.27(6)

Table 3-4. Selected bond lengths (l / Å) and angles (ϕ / °) of $[\{Cp^*RhP(OEt)_3(\mu\text{-}WS_4)\}_2Cu][PF_6]$ (**9**·$[PF_6]$)

Bond lengths	**(l / Å)**		
W1-S1	2.14(2)	W2-S5	2.18(2)
W1-S2	2.22(2)	W2-S6	2.21(2)
W1-S3	2.20(1)	W2-S7	2.22(2)
W1-S4	2.20(2)	W2-S8	2.23(2)
Rh1-S1	2.35(2)	Rh2-S7	2.41(2)
Rh1-S2	2.38(1)	Rh2-S8	2.38(2)
Rh1-P1	2.22(3)	Rh2-P2	2.23(3)
Cu-S3	2.32(2)	Cu-S5	2.32(2)
Cu-S4	2.30(2)	Cu-S6	2.30(2)
Bond Angles	**(ϕ / °)**		
S1-W1-S2	105.0(6)	S5-W2-S6	108.7(6)
S1-W1-S3	113.2(6)	S5-W2-S7	109.6(7)
S1-W1-S4	109.6(6)	S5-W2-S8	111.3(6)
S2-W1-S3	109.7(6)	S6-W2-S7	110.9(6)
S2-W1-S4	110.5(7)	S6-W2-S8	110.8(7)
S3-W1-S4	108.8(6)	S7-W2-S8	105.5(6)
S1-Rh1-S2	93.9(6)	S7-Rh2-S8	95.7(6)
S1-Rh1-P1	87.2(8)	S7-Rh2-P2	88.0(8)
S2-Rh1-P1	91.4(7)	S8-Rh2-P2	88.2(8)
S3-Cu-S4	101.6(7)	S4-Cu-S5	113.6(7)
S3-Cu-S5	115.2(7)	S4-Cu-S6	112.6(7)
S3-Cu-S6	113.1(6)	S5-Cu-S6	101.2(7)
W1-S1-Rh1	80.0(6)	W2-S7-Rh2	77.5(6)
W1-S2-Rh1	77.8(5)	W2-S8-Rh2	77.9(6)
W1-S3-Cu	74.5(5)	W2-S5-Cu	75.1(5)
W1-S4-Cu	75.1(6)	W2-S6-Cu	74.9(6)

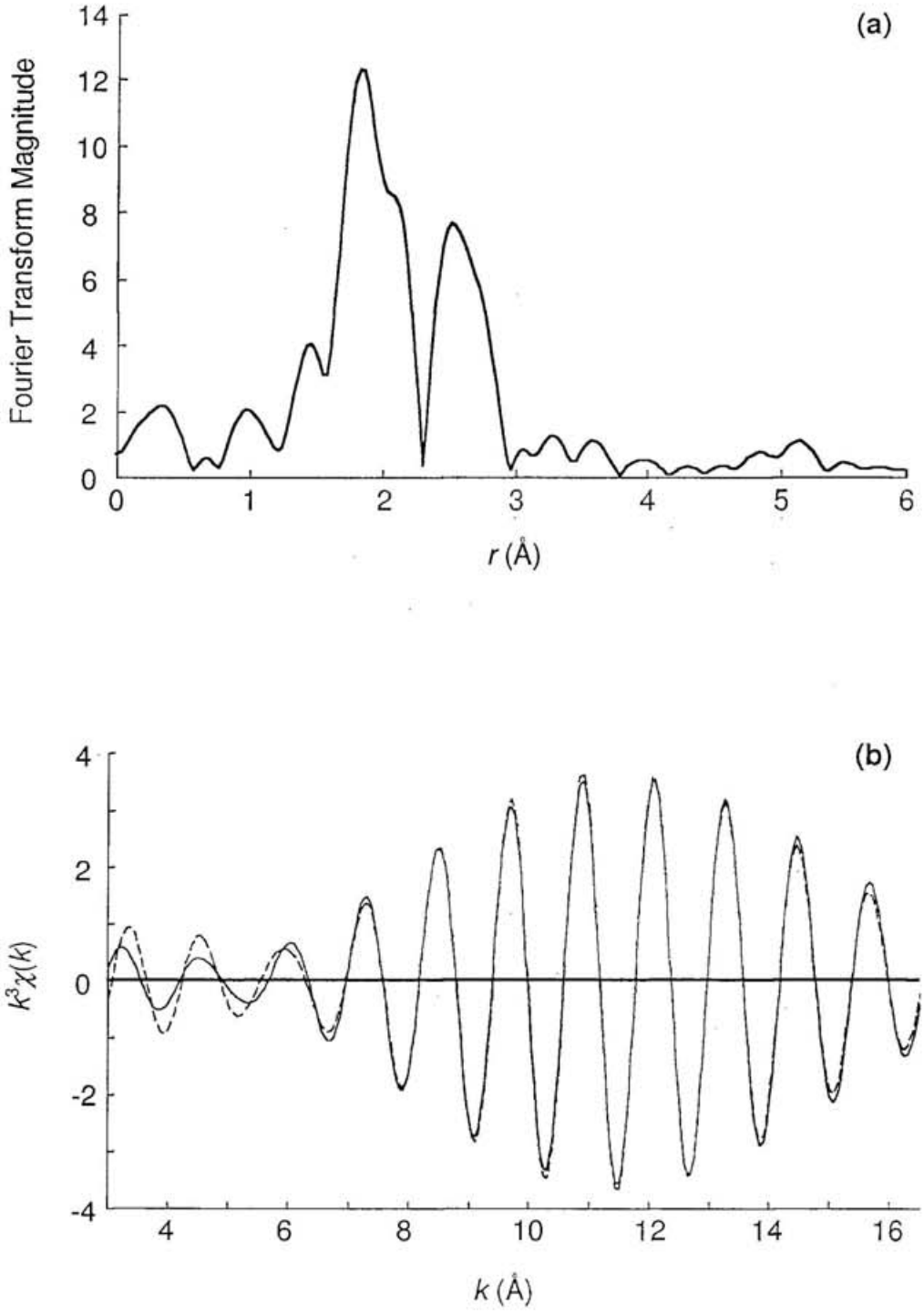

Figure 3-8. (a) Fourier transform of k^3-weighted EXAFS for **9**·[PF_6]. (b) The fitting curve for the second coordination shell: —, observed; ···, calculated.

Table 3-5. Curve-Fitting Analyses of EXAFS Data for **9**·[PF_6]

edge		r^a / Å		N^b	ΔE^c / eV	σ^d / Å	$R(\chi)^e$
		EXAFS	X-ray				
Cu - K	Cu ··· W	2.75(3)	av. 2.743	1.8 (5)	5(3)	0.07(1)	0.007
W - L_3	W ··· Cu	2.75(3)		1.0 (4)	2(2)	0.05(1)	0.007
Rh - K	Rh ··· W	2.91(4)	av. 2.897	1.2 (4)	4(3)	0.07(1)	0.03
W - L_3	W ··· Rh	2.91(3)		0.9 (4)	14(2)	0.07(1)	0.007

[a] interatomic distance.
[b] coordination number.
[c] shift of E_0.
[d] Debye-Waller factor.
[e] $R(\chi)= \{\Sigma(\chi_{obs} - \chi_{cal})^2 / \Sigma\chi_{obs}^2\}^{1/2}$.

Chapter 4

Conclusion

The goals of this research are to develop a systematically synthetic method of higher-nuclearity heterometallic sulfide clusters, to investigate interactions of M-S-M' (M and M' = Rh, W, or Cu) groups in the newly prepared clusters, and to find an interesting reactivity of the M-S-M' groups in the clusters toward small molecules (e. g. H_2O and H_2S) from view points of a basic cluster chemistry.

First, the new building-block method was developed in this resarch by use of the Cp*RhP(OEt)$_3$ group that plays an important role to prevent from polymerizing of the products and to construct the higher-nuclearity heterometallic sulfide clusters soluble in common organic solvents. The stepwise synthesis, [Cp*RhP(OEt)$_3$Cl$_2$] (**1**) $\rightarrow$ [Cp*RhP(OEt)$_3$WS$_4$] (**2**) $\rightarrow$ [Cp*RhP(OEt)$_3$(μ-WS$_4$)CuCl] (**3**) $\rightarrow$ [{Cp*RhP(OEt)$_3$(μ-WS$_4$)(CuCl)Cu}$_2$(μ-Cl)$_2$] (**4**), was demonstrated and the interactions of the M-S-M' groups were examined. It is concluded that the building method is useful to systematically synthesize the higher-nuclearity heterometallic sulfide clusters whose structures are constructed by the regiospecific interactions of M-S-M' groups with other building blocks.

Second, the unique conversion of the bridging S atom in the W(μ_2-S)$_2$(μ_3-S)$_2$ group to the terminal O atom in the WO(μ_3-S)$_3$ group by the water saturated in dichloromethane was found. This is the first example of the conversion of the bridging S atom in the M-S-M' groups into the terminal O atom without releasing of the constituent metal atoms. That the use of the water saturated in dichloromethane is essential to obtain **8** from **4**, and it seems that the specific reactivity of the W-S-Cu groups of **4** is dependent on differences in the electron density of S atoms and the steric effects of the Cp* and P(OEt)$_3$ groups of **4**.

Third, the unique idea of the synthesis of the higher-nuclearity heterometallic

sulfide clusters by using the information of FAB-MS was introduced. The FAB mass spectrum of **3** shows many ions heavier than the molecular ion, and one envelope corresponds to $[\{Cp^*RhP(OEt)_3(\mu\text{-}WS_4)\}_2Cu]^+$ ($[\mathbf{9}]^+$), which was synthesized by the reaction between complex **2** and Cu^+ in the 2:1 molar ratio in the laboratory scale. It is concluded that this is a representative example to show the FAB-MS technique provides the useful guiding principal for the synthesis of the higher-nuclearity clusters.

References and notes

1 For example, (a) Kim, J.; Rees, D. C. *Science* **1992**, *257*, 1677; *Nature* **1992**, *360*, 553. (b) Chan, M. K.; Kim, J.; Rees, D. C. *Science* **1993**, *260*, 792. (c) Sellmann, D. *Angew. Chem. Int. Ed. Engl.* **1993**, *32*, 64. (d) Du, S.; Zhu, N.; Chen, P.; Wu, X. *Angew. Chem. Int. Ed. Engl.* **1992**, *31*, 1085. (e) Nordlander, E.; Lee, S. C.; Cen, W.; Wu, Z. Y.; Natoli, C. R.; Cicco, A. D.; Filipponi, A.; Hedman, B.; Hodgson, K. O.; Holm, R. H. *J. Am. Chem. Soc.* **1993**, *115*, 5549.

2 For example, (a) Howard, K. E.; Lockemeyer, J. R.; Massa, M. A.; Rauchfuss, T. B.; Wilson, S. R.; Yang, X. *Inorg. Chem.* **1990**, *29*, 4385. (b) Rauchfuss, T. B. *Prog. Inorg. Chem.* **1991**, *39*, 259. (c) Curtis, M. D. *Appl. Organomet. Chem.* **1992**, *6*, 429.

3 Cattle raised on Mo-rich and Cu-poor soil develops severe copper deficiencies that are responsible for a weakening of connective tissue in animals. The resulting disorders can be counteracted by supplementing copper compounds to the animals' feed. This interaction is caused by high tendency of Cu^{I} atom to form Cu-S bonds, that is, copper atoms are tightly bound to thiomolybdate, $[MoO_mS_{4-m}]^{2-}$ (m = 0, 1, or 2) which are formed from molybdenum and sulfur containing substances in the digestive tract of ruminants. For example, (a) Sarkar, S.; Mishra, S. B. S. *Coord. Chem. Rev.* **1984**, *59*, 239. (b) Müller, A.; Diemann, E.; Jostes, R.; Bögge, H. *Angew. Chem. Int. Ed. Engl.* **1981**, *20*, 934. (c) Mills, C. F. *Phil. Trans. R. Soc. Lond.* **1979**, *288*, 51.

4 For example, Harmer, M. A.; Sykes, A. G. *Inorg. Chem.* **1980**, *19*, 2881.

5 (a) The discoveries of vast majority of metal clusters that are known were mere accident. For example, Holm, R. H. *Chem. Soc. Rev.* **1981**, *10*, 455. (b) The many research groups attempted to make the analog of FeMo-cofactor of

nitrogenase, but it is obviously not formed by single strict self-assembly process. For example, Müller, A. and Krahn, E. *Angew. Chem. Int. Ed. Engl.* **1995**, *34*, 1071. (c) Ibers, J. A.; Holm, R. H. *Science* **1980**, *209*, 223. (d) Hagen, K. S.; Reynolds, J. G.; Holm, R. H. *J. Am. Chem. Soc.* **1981**, *103*, 4054.

6 Ogo, S.; Chen, H.; Olmstead, M. M.; Fish, R. H. submitted for publication.

7 For example, (a) Yamamoto, A. Organotransition Metal Chemistry, John Wiley & Sons, Inc., **1996**. (b) Dobbs, D. A.; Bergman, R. G. *Inorg. Chem.* **1994**, *33*, 5329.

8 For example, Yamamoto, A. Organotransition Metal Chemistry, John Wiley & Sons, Inc., **1996**.

9 Wilkinson, G. (Editor-in-chief) Comprehensive Coordination Chemistry, Pergamon Press, **1987**.

10 $[\{Cp^*RhP(OEt)_3\}_2(\mu\text{-}WS_4)](BPh_4)_2$ (**5**·$[BPh_4]_2$) is an authentic sample which has Rh-W-Rh framework for EXAFS measurements described in Chapter 3.

11 White, C.; Yates, A. and Maitlis, P. M. *Inorg. Synth.*, **1992**, *29*, 228.

12 Hadjikyriacou, A. I. and Coucouvanis, D. *Inorg. Synth.*, **1990**, *27*, 39.

13 Mullenberg, G. E. (Editor), Handbook of X-ray Photoelectron Spectroscopy, Perkin-Elmer Corporation, **1979**.

14 Busing, W. R. & Levy, H. A. *Acta Crystallogr.*, **1957**, *10*, 180.

15 $R = \Sigma||F_o|-|F_c||/\Sigma|F_o|$.

16 $R_w = (\Sigma w(|F_o|-|F_c|)^2/\Sigma w|F_o|^2)^{1/2}$.

17 $S = (\Sigma w(|F_o|-|F_c|)^2)^{1/2}/(n_{data}-n_{par})$.

18 "International Tables for X-ray Crystallography", Kynoch Press, Birmingham **1974**, Vol. 4.

19 Hall, S. R., Flack, H. D. & J. M. Stewart, ***Xtal3.2***, Program for X-ray crystal

structure analysis, Universities of Western Australia, Geneva & Maryland, **1992**.

20 A set of ψ scan was employed.

21 $R = \Sigma\,||F_o|-|F_c||/\Sigma|F_o|$.

22 $R_w = (\Sigma w(|F_o|-|F_c|)^2/\Sigma w|F_o|^2)^{1/2}$.

23 $S = (\Sigma w(|F_o|-|F_c|)^2)^{1/2}/(n_{data}-n_{par})$.

24 "International Tables for X-ray Crystallography", Kynoch Press, Birmingham **1974**, Vol. 4.

25 Sakurai, T., Kobayashi, K., *Rikagaku Kenkyusho Hokoku*, **1979**, *55*, 69.

26 Busing, W. R. & Levy, H. A. *Acta Crystallogr.*, **1957**, *10*, 180.

27 $R = \Sigma\,||F_o|-|F_c||/\Sigma|F_o|$.

28 $R_w = (\Sigma w(|F_o|-|F_c|)^2/\Sigma w|F_o|^2)^{1/2}$.

29 $S = (\Sigma w(|F_o|-|F_c|)^2)^{1/2}/(n_{data}-n_{par})$.

30 "International Tables for X-ray Crystallography", Kynoch Press, Birmingham **1974**, Vol. 4.

31 Hall, S. R., Flack, H. D. & J. M. Stewart, ***Xtal3.2***, Program for X-ray crystal structure analysis, Universities of Western Australia, Geneva & Maryland, **1992**.

32 A set of ψ scan was employed.

33 $R = \Sigma\,||F_o|-|F_c||/\Sigma|F_o|$.

34 $R_w = (\Sigma w(|F_o|-|F_c|)^2/\Sigma w|F_o|^2)^{1/2}$.

35 $S = (\Sigma w(|F_o|-|F_c|)^2)^{1/2}/(n_{data}-n_{par})$.

36 "International Tables for X-ray Crystallography", Kynoch Press, Birmingham **1974**, Vol. 4.

37 Hall, S. R., Flack, H. D. & J. M. Stewart, ***Xtal3.2***, Program for X-ray crystal structure analysis, Universities of Western Australia, Geneva & Maryland,

1992.

38 Busing, W. R. & Levy, H. A. *Acta Crystallogr.*, **1957**, *10*, 180.

39 $R = \Sigma \| |F_O| - |F_C| | / \Sigma |F_O|$.

40 $R_w = (\Sigma w(|F_O| - |F_C|)^2 / \Sigma w |F_O|^2)^{1/2}$.

41 $S = (\Sigma w(|F_O| - |F_C|)^2)^{1/2} / (n_{data} - n_{par})$.

42 "International Tables for X-ray Crystallography", Kynoch Press, Birmingham **1974**, Vol. 4.

43 Hall, S. R., Flack, H. D. & J. M. Stewart, ***Xtal3.2***, Program for X-ray crystal structure analysis, Universities of Western Australia, Geneva & Maryland, **1992.**

44 $U_{eq} = (1/3)\Sigma_i\Sigma_j U_{ij} a_i^* a_j^* \mathbf{a_i \cdot a_j}$

45 The x coordinates of the atoms were fixed in the refinements.

46 $B_{eq} = (8\pi^2/3)\Sigma_i\Sigma_j U_{ij} a_i^* a_j^* \mathbf{a_i \cdot a_j}$

47 $U_{eq} = (1/3)\Sigma_i\Sigma_j U_{ij} a_i^* a_j^* \mathbf{a_i \cdot a_j}$

48 The y coordinates of the atoms were fixed in the refinements.

49 $U_{eq} = (1/3)\Sigma_i\Sigma_j U_{ij} a_i^* a_j^* \mathbf{a_i \cdot a_j}$

50 $U_{eq} = (1/3)\Sigma_i\Sigma_j U_{ij} a_i^* a_j^* \mathbf{a_i \cdot a_j}$

51 The x coordinates of the atoms were fixed in the refinements.

52 The z coordinates of the atoms were fixed in the refinements.

53 The W-S(terminal) bond distances lie between those for a single and double bonds, and thus suggest the involvement of π bonds. For example, (a) Müller, A.; Diemann, E.; Jostes, R.; Bögge, H. *Angew. Chem. Int. Ed. Engl.* **1981**, *20*, 934. (b) Belton, P. S.; Cox, I. J.; Harris, R. K.; and O'Connor, M. *J. Aust. J. Chem.* **1986**, *39*, 943.

54 Howard, K. E.; Lockemeyer, J. R.; Massa, M. A.; Rauchfuss, T. B.; Wilson, S. R.; Yang, X. *Inorg. Chem.* **1990**, *29*, 4385.

55 Sécheresse, F.; Salis, M.; Potvin, C; and Manoli, J. M. *Inorg. Chim. Acta* **1986**, *114*, L19.

56 Clegg, W.; Scattergood, C. D.; Garner, C. D. *Acta Crystallogr., Sect. C* **1987**, *43*, 786.

57 Sécheresse, F.; Bernés, S.; Robert, F.; Jeannin, Y. *J. Chem. Soc., Dalton Trans.* **1991**, 2875.

58 Howard, K. E.; Rauchfuss, T. B.; Wilson, S. R. *Inorg. Chem.* **1988**, *27*, 3561.

59 Howard, K. E.; Rauchfuss, T. B.; Wilson, S. R. *Inorg. Chem.* **1988**, *27*, 3561.

60 Howard, K. E.; Rauchfuss, T. B.; Wilson, S. R. *Inorg. Chem.* **1988**, *27*, 3561.

61 Howard, K. E.; Lockemeyer, J. R.; Massa, M. A.; Rauchfuss, T. B.; Wilson, S. R.; Yang, X. *Inorg. Chem.* **1990**, *29*, 4385.

62 Howard, K. E.; Lockemeyer, J. R.; Massa, M. A.; Rauchfuss, T. B.; Wilson, S. R.; Yang, X. *Inorg. Chem.* **1990**, *29*, 4385.

63 Mullenberg, G. E. (Editor), Handbook of X-ray Photoelectron Spectroscopy, Perkin-Elmer Corporation, **1979**.

64 Ozawa, Y; Hayashi, Y.; and Isobe, K. *Chem. Lett.*, **1990**, 249.

65 For example, W. E. Newton et al. reported the oxidation reactions of the iron-molybdenum cofactor (FeMoco) of *Azotobactor vinelandii nitrogenase* to yield either $[MoS_4]^{2-}$ or $[MoOS_3]^{2-}$, depending on the reaction conditions. Newton, W. E.; Gheller, S. P.; Hedman, B.; Hodgson, K. O.; Lough, S. M.; McDonald, J. W. *Eur. J. Biochem.* **1986**, *159*, 111.

66 The kinetic study of the conversion of $[MoS_4]^{2-}$ to $[MoOS_3]^{2-}$ in an aqueous solution was reported by Harmer and Sykes: Harmer, M. A.; Sykes, A. G.

Inorg. Chem. **1980**, *19*, 2881. The $t_{1/2}$ of conversion of $[MoS_4]^{2-}$ to $[MoOS_3]^{2-}$ at pH 8.2-9.8 is ca. 50 h. Although a similar aspect of the conversion from $[WoS_4]^{2-}$ have not been studied, $[WoOS_3]^{2-}$ are formed more slowly than $[MoOS_3]^{2-}$.

67 McDonald, J. W.; Friesen, G. D.; Rosenhein, L. D.; Newton, W. E. *Inorg. Chim. Acta* **1983**, *72*, 205.

68 The water content of dichloromethane was determined by Karl Fischer method.

69 Busing, W. R. & Levy, H. A. *Acta Crystallogr.*, **1957**, *10*, 180.

70 $R = \Sigma||F_o|-|F_c||/\Sigma|F_o|$.

71 $R_w = (\Sigma w(|F_o|-|F_c|)^2/\Sigma w|F_o|^2)^{1/2}$.

72 $S = (\Sigma w(|F_o|-|F_c|)^2)^{1/2}/(n_{data}-n_{par})$.

73 "International Tables for X-ray Crystallography", Kynoch Press, Birmingham **1974**, Vol. 4.

74 Hall, S. R., Flack, H. D. & J. M. Stewart, ***Xtal3.2***, Program for X-ray crystal structure analysis, Universities of Western Australia, Geneva & Maryland, **1992**.

75 A set of ψ scan was employed.

76 $R = \Sigma||F_o|-|F_c||/\Sigma|F_o|$.

77 $R_w = (\Sigma w(|F_o|-|F_c|)^2/\Sigma w|F_o|^2)^{1/2}$.

78 $S = (\Sigma w(|F_o|-|F_c|)^2)^{1/2}/(n_{data}-n_{par})$.

79 "International Tables for X-ray Crystallography", Kynoch Press, Birmingham **1974**, Vol. 4.

80 Hall, S. R., Flack, H. D. & J. M. Stewart, ***Xtal3.2***, Program for X-ray crystal structure analysis, Universities of Western Australia, Geneva & Maryland, **1992**.

81 $U_{eq} = (1/3)\Sigma_i\Sigma_j U_{ij} a_i^* a_j^* \mathbf{a_i \cdot a_j}$

82 $U_{eq} = (1/3)\Sigma_i\Sigma_j U_{ij} a_i^* a_j^* \mathbf{a_i \cdot a_j}$

83 For example, Müller, A.; Diemann, E.; Jostes, R.; Bögge, H. *Angew. Chem. Int. Ed. Engl.* **1981**, *20*, 934.

84 The distances of Cu1-Cl1 and Cu1-Cl1* are in a normal range of the Cu-Cl single bond. The distances Cu1-(S1S3Cl1) and Cu2-(S2S3Cl2) are 0.323 and 0.092 Å, respectively.

85 (a) Kim, J.; Rees, D. C. *Science* **1992**, *257*, 1677; *Nature* **1992**, *360*, 553. (b) Chan, M. K.; Kim, J.; Rees, D. C. *Science* **1993**, *260*, 792. (c) Sellmann, D. *Angew. Chem. Int. Ed. Engl.* **1993**, *32*, 64. (d) Du, S.; Zhu, N.; Chen, P.; Wu, X. *Angew. Chem. Int. Ed. Engl.* **1992**, *31*, 1085. (e) Nordlander, E.; Lee, S. C.; Cen, W.; Wu, Z. Y.; Natoli, C. R.; Cicco, A. D.; Filipponi, A.; Hedman, B.; Hodgson, K. O.; Holm, R. H. *J. Am. Chem. Soc.* **1993**, *115*, 5549.

86 The reaction of **2** with water gave very small peaks due to **6a** and uncharacterized products around the ethyl of $P(OEt)_3$ and the methyl of Cp* regions in the ^1H NMR spectrum. In the reaction of **7** with water very small peaks due to **7** and uncharacterized products were observed by ^1H NMR.

87 For example, (a) Asakura, K.; Kitamura-Bando, K.; Isobe, K.; Arakawa, H.; Iwasawa Y. *J. Am. Chem. Soc.* **1990**, *112*, 3242; (b) Asakura, K.; Kitamura-Bando, K.; Iwasawa Y.; Arakawa, H.; Isobe, K. *J. Am. Chem. Soc.* **1990**, *112*, 9096 (c) Chen, J.; Christiansen, J.; Tittsworth, R. C.; Hales, B. J.; George, S. J.; Coucouvanis, D.; Cramer, S. P. *J. Am. Chem. Soc.* **1993**, *115*, 5509; (d) Nordlander, E.; Lee, S. C.; Cen, W.; Wu, Z. Y.; Natoli, C. R.; Cicco, A. D.; Filipponi, A.; Hedman, B.; Hodgson, K. O.; Holm, R. H. *J. Am. Chem. Soc.* **1993**, *115*, 5549; (e) Teranishi, T.; Harada, M.; Asakura, K.; Asanuma, H.; Saito, Y.; Toshima, N. *J. Phys. Chem.* **1994**, *98*, 7967.

88 For example, (a) Trovarelli, A.; Finke, R. G. *Inorg. Chem.* **1993**, *32*, 6034; (b) Carlson, J. B.; Davies, G.; Vouros, P. *Inorg. Chem.* **1994**, *33*, 2334; (c) Reynolds, J. D.; Burn, J. L. E.; Boggess, B.; Cook, K. D.; Woods, C. *Inorg. Chem.* **1993**, *32*, 5517.

89 For example, Branan, D. M.; Hoffman, N. W.; McElroy, E. A.; Ramage, D. L.; Robbins, M. J.; Eyler, J. R.; Watson, C. H.; deFur, P.; Leary, J. A. *Inorg. Chem.* **1990**, *29*, 1915.

90 (a) Kroto, H. W.; Heath, J. R.; O'Brien, S. C.; Curl, R. F.; Smalley, R. E. *Nature* **1985**, *318*, 162; Krätschmer, W.; Lamb, L. D.; Fostiropoulos, K.; Huffman, D. R. *Nature* **1990**, *347*, 354.

91 (a) Andrews, M. A.; Kirtley, S. W.; Kaesz, H. D. *Inorg. Chem.* **1977**, *16*, 1556; (b) Voss, E. J.; Stern, C. L.; Shriver, D. F. *Inorg. Chem.* **1994**, *33*, 1087.

92 EXAFS analysis program package "*REX ver. 2.04*" (Rigaku Industrial Corporation, **1993**).

93 McMaster, W. H.; Grande, N. del; Mallett, J. H.; Hubbell, J. H. *Compilation of X-ray Cross Sections* (National Technical Information Service, Springfield, **1969**).

94 Teo, B.-K *EXAFS: Basic Principles and Data Analysis* (Springer-Verlag, New York, **1986**).

95 (a) Teo, B.-K *J. Am. Chem. Soc.* **1981**, *103*, 3990; (b) O'Day, P. A.;Rehr, J. J. ; Zabinsky, S. I.; Brown, G. E. Jr. *J. Am. Chem. Soc.* **1994**, *116*, 2938.

96 A set of ψ scan was employed.

97 $R = \Sigma | |F_O| - |F_C| | / \Sigma |F_O|$.

98 $R_W = (\Sigma w(|F_O| - |F_C|)^2 / \Sigma w |F_O|^2)^{1/2}$.

99 $S = (\Sigma w(|F_O| - |F_C|)^2)^{1/2} / (n_{data} - n_{par})$.

100 The final difference Fourier map shows some ghost peaks, but they are close to W, Rh, or Cu atoms.

101 "International Tables for X-ray Crystallography", Kynoch Press, Birmingham **1974**, Vol. 4.

102 Hall, S. R., Flack, H. D. & J. M. Stewart, ***Xtal3.2***, Program for X-ray crystal structure analysis, Universities of Western Australia, Geneva & Maryland, **1992**.

103 $U_{eq} = (1/3)\Sigma_i\Sigma_j U_{ij} a_i^* a_j^* \mathbf{a_i \cdot a_j}$

Acknowledgment

This study at Department of Structural Molecular Science, The Graduate University for Advanced Studies was generously supported by Institute for Molecular Science, and carried out under the supervision of Prof. Kiyoshi Isobe. The author would like to express his gratitude to Prof. Kiyoshi Isobe. S.O. really appreciates his instructive directions and continuous encouragement.

S.O. wishes to thank Dr. Takayoshi Suzuki for his kindness of heart and instruction in the art of X-ray analysis. S.O. would like to thank Dr. Masaaki Abe, Dr. Hiroshi Shimomura, Dr. Takanori Nishioka, Dr. Yuichi Kaneko, Dr. Rimo Xi, and Prof. Hee Kwon Chae for their useful suggestions for this thesis.

S.O. thanks Dr. Yoshiki Ozawa, Prof. Kiyotaka Asakura, and Ms. Sachiyo Nomura for their helps in measurements. S.O. is grateful to Prof. Takeshi Yamamura for a basic discipline at Science University of Tokyo.

S.O. wishes to thank The Japan Scholarship Foundation for funds supporting a research with Prof. Richard H. Fish in Lawrence Berkeley National Laboratory, University of California. S.O. is grateful to R.H.F. for the new projects in LBNL and his daily discussions about them. S.O. thanks Dr. Hong Chen, Dr. Jozsef Devenyi, and Dr. Wei Lee for big helps to enjoy a life in US. S.O. would like to thank Ms. Diane Tosse and Mr. Lloyd Tosse for the wonderful time and space in Berkeley.

Finally, Seiji Ogo wishes to thank parents and sister for their patient and warm affection, which gave S.O. the strength to go on with everything.

Okazaki, November 20, 1995

Seiji Ogo

A list of publications

(1) A Heterotrimetallic Sulfide Cluster Having a Linear $Rh^{III}...W^{VI}...Cu^{I}$ Framework of an Octahedral - Tetrahedral - Trigonal Planar Sequence

Seiji Ogo, Takayoshi Suzuki, Yoshiki Ozawa, and Kiyoshi Isobe

Chemistry Letters **1994**, 1235-1238.

(2) A Unique Three-Step Cyclic Reaction Sequence of Heterotrimetallic Sulfide Clusters. Structures and Properties of $[\{Cp^*RhP(OEt)_3(\mu\text{-}WS_4)(CuCl)Cu\}_2(\mu\text{-}Cl)_2]$ ($Cp^* = \eta^5\text{-}C_5Me_5$) with a Branched Structure and $[\{Cp^*RhP(OEt)_3(\mu\text{-}WOS_3)(CuCl)Cu\}_2(\mu\text{-}Cl)_2]$ with a Linked Incomplete Cubane-Type Structure

Seiji Ogo, Takayoshi Suzuki, and Kiyoshi Isobe

Inorganic Chemistry **1995**, *34*, 1304-1305.

(3) Synthesis of a Linear-Type Pentanuclear (Rh^{III}-W^{VI}-Cu^{I}-W^{VI}-Rh^{III}) Sulfide Cluster Predicted by Fast Atom Bombardment Mass Spectrometry

Seiji Ogo, Takayoshi Suzuki, Sachiyo Nomura, Kiyotaka Asakura, and Kiyoshi Isobe

Journal of Cluster Science **1995**, *6*, 421-436.

Other publications

(1) Aqueous Organometallic Chemistry 2. ^1H NMR Spectroscopy, Synthetic, and Structural Study of the Chemo- and Diastereoselective Reactions of $[Cp^*Rh(\eta^1\text{-}H_2O)_3]^{2+}$ with Nitrogen Ligands as a Function of pH

Seiji Ogo, Hong Chen, Marilyn M. Olmstead, and Richard H. Fish

Organometallics In Press

(2) Bioorganometallic Chemistry. 8. The Molecular Recognition of Aromatic and Aliphatic Amino Acids and Substituted Aromatic and Aliphatic Carboxylic Acid Guests with Supramolecular (η^5-Pentamethylcyclopentadienyl)rhodium-Nucleobase, Nucleoside, and Nucleotide Cyclic Trimer Host via Non-Covalent π-π and Hydrophobic Interactions in Water: Steric, Electronic, and Conformational Parameters

Hong Chen, Seiji Ogo, and Richard H. Fish

Submitted for *Journal of the American Chemical Society*

(3) Unique Reactivity of M-S-M' (M and M' = Rh, W, and Cu) Groups of Higher-nuclearity Heterometallic Sulfide Clusters toward Water and Hydrogen Sulfide: Drastic Structural Changes in the Cluster Frameworks

Seiji Ogo, Takayoshi Suzuki, and Kiyoshi Isobe

Submitted for *Inorganic Chemistry*

(4) A Unique Conversion of a Linear-Type Pentanuclear (Rh^{III}-W^{VI}-Cu^{I}-W^{VI}-Rh^{III}) Sulfide Cluster into Form a Linear-Type Trinuclear (Rh^{III}-W^{VI}-Rh^{III}) Sulfide Cluster Predicted by Fast Atom Bombardment Mass Spectrometry

Seiji Ogo, Sachiyo Nomura, Takayoshi Suzuki, and Kiyoshi Isobe

In Preparation

(5) Selective Removal and Recovery of Metal-Dye Complexes From Aqueous Solution by Utilization of Novel Polymer Pendant Ligands

Wei Li, Seiji Ogo, Louis E. Lavely, Jr., and Richard H. Fish

In Preparation

(6) A New Model for High Potential Iron Sulfur Proteins. Synthesis and Electrochemistry of an Iron Sulfur Cluster Encapsulated in Calix[4]arene Dithiol Derivatives

Seiji Ogo and Takeshi Yamamura

In Preparation